REPORT DOCUMENTATION PAGE

AFRL-SR-BL-TR-01-

0302

1. AGENCY USE ONLY *(Leave blank)*	2. REPORT DATE	3. REPORT TYPE AND DATES
	19 Apr 01	Final Report: 01 Jun 95 TO 31 May 98

4. TITLE AND SUBTITLE
A MICROMECHANICAL INVESTIGATION OF INSTABILITY IN PARTICULATE MATERIALS AND HIGHER ORDER CONTINUUM THEORY ASSUMPTIONS

5. FUNDING NUMBERS
F49620-95-1-0420

6. AUTHOR(S)
Dr. Jean-Pierr Bardet

7. PERFORMING ORGANIZATION NAME(S) AND ADDRESS(ES)
UNIVERSITY OF SOUTHERN CALIFORNIA
LOS ANGELES
CALIFORNIA 90089-2531

8. PERFORMING ORGANIZATION REPORT NUMBER

9. SPONSORING/MONITORING AGENCY NAME(S) AND ADDRESS(ES)
AFOSR/NA
801 N. RANDOLPH ST. RM 732
ARLINGTON VA 22203

10. SPONSORING/MONITORING AGENCY REPORT NUMBER

11. SUPPLEMENTARY NOTES

12a. DISTRIBUTION AVAILABILITY STATEMENT
APPROVED FOR PUBLIC RELEASE: DISTRIBUTION UNLIMITED

12b. DISTRIBUTION CODE

13. ABSTRACT *(Maximum 200 words)*

The micropolar theory (Eringen, 1966, 1968) is a continuum version of the structural theory of Cosserat (1909). It enriches the kinematics and kinetics of continua by adding material rotations and couple stresses. Using a micropolar approach similar to Kanatani (1979), Muhlhaus and Vardoulakis (1986) explained the emergence, orientation and thickness of shear bands in granular materials. Bardet and Proubet (1992a) used a similar linear stability analysis and micropolar description, and investigated the structure of persistent shear bands in idealized granular media. They successfully described the thickness of shear bands and the relation between particle rotation and displacement within persistent shear bands. However, the coefficients of their micropolar models, based on the flow or deformation theory of plasticity, had to be set to unrealistic values to reproduce the observations.

Chang et al. (1990, 1991, 1992) developed micropolar theories for granular materials based on microscopic models. They derived the micropolar constants in terms of the inter-particle stiffness, and investigated the micropolar effects on the solution of selected boundary value problems. Chang derived stress-strain relationships without examining their effects on material instability. He did not investigate the problem of strain localization as De Borst and Sluys (1992).

14. SUBJECT TERMS	15. NUMBER OF PAGES
MICROMECHANICAL INVESTIGATION OF ISNTABILITY IN PARTICULATE MATERIALS	16. PRICE CODE

17. SECURITY CLASSIFICATION OF REPORT	18. SECURITY CLASSIFICATION OF THIS PAGE	19. SECURITY CLASSIFICATION OF ABSTRACT	20. LIMITATION OF ABSTRACT
UNCLASSIFIED	UNCLASSIFIED	UNCLASSIFIED	UL

UNIVERSITY OF SOUTHERN CALIFORNIA

Department of Civil Engineering

A Micromechanical Investigation of Instability in Particulate Materials and Higher Order Continuum Theory Assumptions

By

Jean-Pierre Bardet and Julie Young

Report to The Air Force Office of Scientific Research

Grant F49620-93-1-0235 and AASERT Grant F49620-95-1-0420

August 31, 1998

Research is needed to determine the microscopic origins of material instability. A microscopic investigation becomes the rational means to examine shear band instability which has a thickness of several grains (i.e., microscopic dimension).

Research objectives and report organization

Many continuum theories and numerical simulations have been proposed to describe shear band instability; however they rely on semi-intuitive arguments not always founded on physical observations on particulate media. The main research objective is to investigate the physical origins of shear band instability in particulate media, and the assumptions of higher-order continuum theories proposed to account for instabilities in granular media. The particular research objectives were (1) to review the work in computational granular mechanics relevant to the formation of shear bands in granular media, (2) to explore a critical micro-macro transition relevant to material instability (i.e., stress symmetry), and (3) to devise laboratory experiments for generating useful experimental data sets relevant to material instability.

This document is organized in three sections. Following the introduction and research background, the first section reviews past work on computational granular mechanics. The second section investigates the transition between discrete and continuous fields, and especially the symmetry of stress tensors in granular media. The third and last section summarizes the experimental work on discrete models.

PART I. GRANULAR MECHANICS

Introduction

The first discrete modeling of soils can be traced to Hertz (1882) who formulated a contact law between spheres, and Reynolds (1885) who proposed a dilatancy theory. Dantu (1957) and Schneebli (1955) idealized real soils as assemblies of rigid rods, and noticed some striking similarities between the mechanical responses of these mechanical analogs and real soils. Duffy and Mindlin (1957), Deresiewicz (1958), and Thurston and Deresiewicz (1959) examined the response of soil models made of spheres. Biarez (1962) used glass beads and duralumium rods to examine the elastic and limit response of soils, and applied his observations to analyze practical problems in geotechnical engineering. These pioneer works were later followed by photoelastic investigations (e.g., Drescher, 1976; and Descher and Josselin de Jong, 1972) to visualize stresses within granular media.

The discrete modeling of soils benefited substantially from the development of computers in the 1970's. The computational discrete modeling of soils can be attributed to Cundall, who developed the computer code BALL (Cundall and Strack, 1978-79). At this time, computers had very limited capabilities, comparable to those of today's hand-held calculators. They were slow, and had limited memory and storage capacity. Yet, Cundall developed BALL, a program which many researchers still use. The program is fully documented in a two-volume report to the US National Science Foundation (Cundall and Strack, 1978-79). Since 1978, many researchers have adapted the original version of BALL to solve specific problems. Researchers have realized the power of computer simulations to understand the mechanics of granular materials. The major advantage of computations over real experiments is the generation of abundant information on particle displacements, contact forces and other physical quantities, which can be processed rapidly to comprehend the physics of granular assemblages.

This chapter reviews the basics of the discrete modeling of granular media, with the intent of providing readers with some understanding of granular material behavior based

on the first principles in mechanics and computational methods. Three particular aspects of computational granular mechanics will be covered: (1) physical modeling of granular media, (2) numerical methods for computational granular mechanics, and (3) transitions from discrete to continuous media. Before going into these subjects, we will first try to answer the following questions. What exactly is discrete modeling? What are the applications of discrete modeling? Has discrete modeling any advantages over continuum mechanics? What are the limitations of discrete modeling? What are the main computational tools in discrete modeling?

Examples of discrete modeling in soil mechanics

Discrete modeling can best be described by considering two particular examples: one is relevant to the study of constitutive behavior, and the other to the failure of foundations.

Example 1

As shown in Fig. 1, the sample was constructed with 1848 cylindrical rods of diameter 4, 6 and 8 mm. There are 1040 particles of 4-mm diameter, 532 of 6-mm diameter, and 266 of 8-mm diameter. The sample slenderness ratio is 2.43. The rods were made of identical transparent acrylic material, which has an average density of 1.30 g/cm^3, and were cut to a 10-cm length. Their front ends were half painted in black to visualize their rotation and displacement simultaneously. Figures 1 and 2 show the experimental setup. The sample is enclosed in a 0.15-mm thick transparent latex membrane with two circular loading platens at the top and bottom. The membrane is clamped to the platens with compression rings. During the sample fabrication, the membrane is stretched on a rectangular mold, and the rods are manually positioned inside the mold with their axis parallel to one another. During the test, the specimen is subjected to a vacuum inside the membrane, which is equivalent to applying an external constant confining pressure equal to 95 kPa. The axial compression is applied by raising the lower platen at the constant rate of 5.6 mm/min, while the upper platen remains fixed. Figure 2 shows a side view of the experimental setup. The photograph of Fig.1 was obtained by using a 35-mm camera positioned approximately one meter in front of the sample, with its aim perpendicular to the front of the sample. The particles were lighted from behind by using a light box. The

sample was tested by increasing the axial strain while keeping the confining pressure constant. The stress-strain curve is shown in Fig. 3. The axial strain ε is

$$\varepsilon = \Delta h/h_0 \tag{1.1}$$

where Δh is the vertical displacement of the lower platen, and h_o is the initial sample height. The axial stress σ is

$$\sigma = F/A_0 \tag{1.2}$$

where F is the measured axial load, and A_o is the initial cross-sectional area. The Initial Young's modulus was 300 MPa, and the peak friction angle was 18.4 deg.

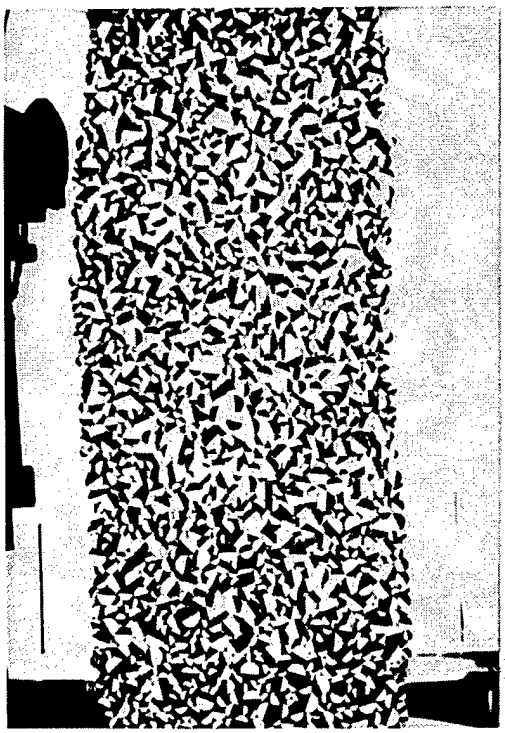

Figure 1. An assembly of cylindrical rods subjected to axial compression.

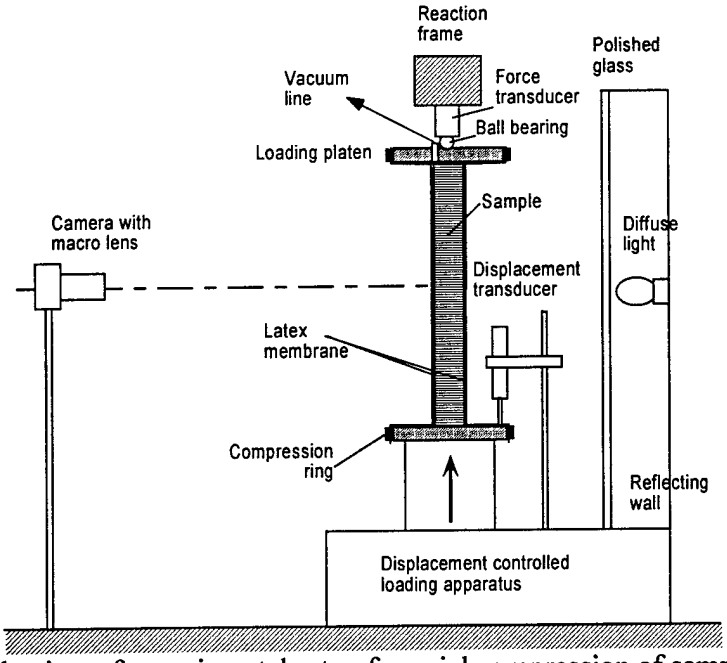

Figure 2. Side view of experimental setup for axial compression of sample in Fig. 1.

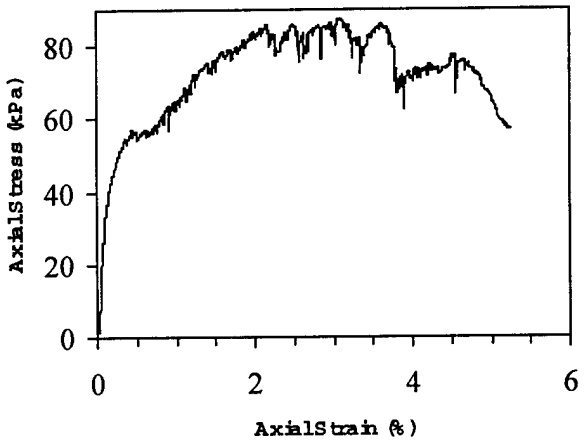

Figure 3. Stress-strain response of sample shown in Fig. 1 (the confining pressure is 95 kPa).

Example 2

Figure 4 shows an early example of the application of discrete modeling for understanding the failure mechanism under shallow footing (Lambe and Whitman, 1979). This photograph was taken by using a slow shutter speed, which blurs the moving

particles. It shows the pattern of motion at failure within a stack of duralumium rods loaded by a rigid punch. The rods are 150-mm long and are of two shapes and sizes (round, 3 mm and 6 mm diameter; and hexagonal 4.8 and 7,9 mm across flats) to simulate the interlocking which occurs in actual soils. Additional examples of discrete models for understanding the failures of foundations and retaining walls can be found in (Biarez, 1962).

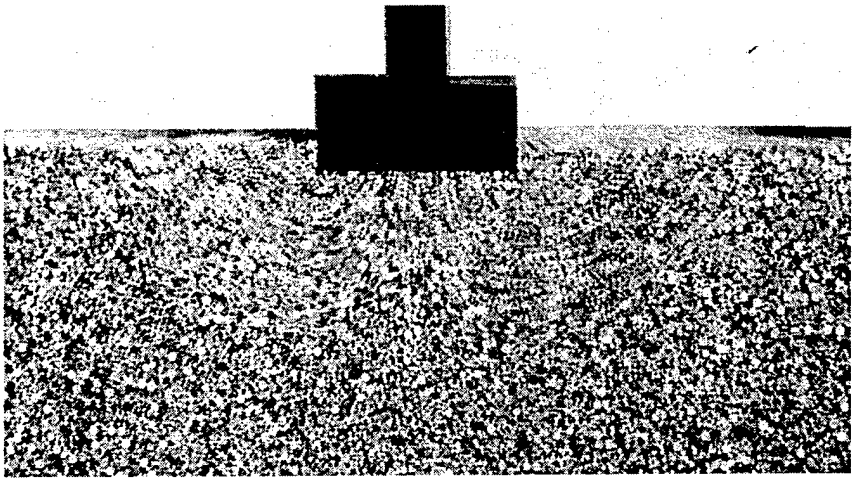

Figure 4. Failure zone under a shallow foundation (Lambe and Whitman, 1979).

Applications of discrete modeling in engineering and applied sciences

One may attempt to survey the applications of discrete modeling in engineering and applied sciences by consulting the proceedings of the following conferences:

(1) the 1st International Conference on Powders and Grains (Biarez and Gourves, 1989);

(2) the 2nd International Conference on Powders and Grains (Thornton, 1993);

(3) the 3rd International Conference on Powders and Grains (Behringer and Jenkins, 1997);

(4) the 1st US Conference on Discrete Element Methods (Mustoe et al., 1989); and

(5) the 2nd International Conference on Powders and Grains (Wiliams and Mustoe, 1993).

Discrete modeling is used for many applications in engineering and applied sciences. A review of the literature on discrete modeling, which is by no means exhaustive, indicates that past work can be sorted in the following general categories:

- *Experimental studies of granular media*: (e.g., Biarez, 1962; Dantu, 1957; Drescher, 1976; Drescher and Josselin de Jong, 1972; Meakin and Skeltorp, 1993; Nakase et al., 1992; Oda, 1972-1973; Subbash et al., 1991; Sukla and Rossmanith, 1982; and Supel, 1985).

- *Studies of contact between particles*: (e.g., Anandarajah, 1994; Azarkhin, 1988; Bardet and Huang, 1992; Bentall and Johnson, 1967; Carter, 1926; Deresiewicz, 1958; Doménech et al., 1987; Fabrikant, 1986, 1988; Foerster et al., 1994; Goodman, 1962; Hertz, 1882; Jagota et a., 1997; Johnson et al., 1997; Johnson, 1958, 1985; Kalker, 1979, Lecornu, 1905; Lee, 1966; Lesbur et al., 1997; Mindlin, 1949, Mindlin and Deresiewicz, 1953; Misra, 1995; Reynolds, 1885, 1895; tabor, 1955; Vermeulen and Johnson, 1964; Wells, 1997; Witters and Duymelinck, 1986).

- *Numerical techniques for discrete modeling*: (e.g., Bardet and Proubet, 1991; Bashir and Goddard, 1991; Borja and Wren, 1995; Chang and Misra, 1989; Cundall, 1988, 1989; Cundall and Strack, 1979; Ghaboussi and Barbosa, 1990; Goddard et al., 1993; Hahn, 1988; Hart et al., 1988; Jean, 1995; Jean and Moreau, 1996; Kishino, 1988; LaBudde and Greenspan, 1976; Meakin and Skeltorp, 1993; Moreau, 1966, 1988, 1994, 1995; Mujinza et al, 1993; O'connor et al., 1993; Papadrakakis, 1981; Park and Underwood, 1980; Ting, 1992; Ting and Corkum, 1992; Ting et al., 1989, 1993; Trent and Margolin, 1992; Underwood, 1983; Underwood and Park, 1980; Walton, 1980, 1983; Walton and Braun, 1986; Walton et al., 1988; Williams and Mustoe, 1987; Zhuang and Goddard, 1993; Zhuang et al., 1995).

- *Elastic behavior of granular media*: (e.g., Bathurst and Rothenburg, 1988; Chang et al., 1990; Changet al., 1995; Dubujet etal., 1997; Horne, 1965, 1969; Johnson et al., 1997).

- *Failure of granular media*: (e.g., Chang, 1993; Sun and Thornton, 1994; Thornton, 1979).

- *Stress-strain behavior of granular media*: (e.g., Bardet, 1994; Bathurst and Rothenburg, 1990; Chang, 1993; Chang and Liao, 1990; Chang and Misra, 1990; Chang et al., 1992; Christoffersen et al., 1981; Cundall et al., 1982; Daudon et al., 1997; Deresiewicz, 1958; Dobry and Ng, 1992; Duffy and Mindlin, 1957; Houlsby, 1981; Ke and Bray, 1995; Koenders, 1987; Krawietz 1982; Laalai et al., 1995; Lun and Bent, 1993; Matsuoka and Yamamoto, 1994; Mehrabadi et al., 1993; Nemat-Nasser and Mehrabadi, 1984; Ng and Dobry, 1994; Ng, 1992; Reynolds, 1895; Rothenburg and Bathurst, 1989, 1991, 1992; Rowe, 1962; Tatsuoka et al., 1990; Thornton, 1979, 1994; Thornton and Randall, 1988; Thornton and Sun, 1994; Thurston and Deresiewicz, 1959; Weber, 1996).

- *Higher-order continuum theories:*

  - *Second order gradient continuum*: (e.g., Chang and Gao, 1995).

  - *Micropolar continuum*: (e.g., Bardet and Proubet, 1992; Bardet and Huang, 1992; Chang and Ma, 1991; Diepolder et al., 1991; Kanatani, 1979; Sternberg, 1968).

- *Strain localization and shear bands*: (e.g., Bardet and Proubet, 1991, 1992; Cundall, 1989, Desrues, 1984, Desrues and Duthilleul, 1984; Desrues et al., 1985; Moreau, 1996; Mühlhaus and Vardoulakis, 1987; Nakase et al., 1992; Oda, 1993; Oda et al., 1997).

- *Powders and sintering processes*: (e.g., Aizawa et al., 1993; Greening et al., 1997; Hong, 1997; Lian et al., 1997; Tamura and Aizawa, 1993).

- *Suspension:* (e.g., Goddard, 1977, 1986).

- *Granular Flow*: (e.g., Foerster et al., 1994; Campbell and Brennen, 1985; Savage and Jeffrey, 1981).

- *Fluid and solid mixtures, including fluidized beds*: (e.g., Kawaguchi et al., 1995; Sudji et al, 1992, 1993; Tsuji, 1997).

- *Rock mechanics*: (e.g., Bardet and Scott, 1985; Cundall, 1971, 1981, 1988; Shi, 1993; Shi and Goodman, 1988, 1989).

- *Physics of granular media:* (e.g., Clément et al., 1992; Knight et al., 1993; Manna and Herrmann, 1991; Meakin and Skeltorp, 1993; Meftah et al., 1993; Radjai et al., 1996).

Discrete and continuous modeling

Continuum mechanics is a powerful approach to solve scientific and engineering problems. It is based on mathematical assumptions, which are well described in the continuum mechanics literature (e.g., Eringen, 1967; Truesdell, 1985). It formulates engineering problems as mathematical boundary value problems (BVP). The main components are the governing equilibrium equations (i.e., partial differential equations translating basic physical balances, such as stress equilibrium); the boundary conditions (prescribed values of the unknown quantities or their derivatives on external surfaces); and the constitutive equations (generalized relation between stress and strain, or their respective rates). In the past 20 years, the continuum approach has been implemented using finite elements and finite differences, and has successfully been applied to solve engineering problems (e.g., Zienkiewicz and Taylor, 1991).

One of the major assumptions of continuum mechanics is that the material properties can be scaled from small laboratory samples to large material masses using constitutive relations. Researchers have now produced a myriad of constitutive relations for various types of engineering materials. Many constitutive models are clever fittings of experimental results in the laboratory. Unfortunately, most models are not based on physics.

Through the use of bifurcation theory, the continuum approach was discovered to exhibit problems, especially associated with the loss of uniqueness of boundary value problems. The problems mainly result from local material instability and limitations of constitutive

equations (e.g., Vardoulakis and Graf, 1985). These findings questioned some applications of continuum mechanics to soil mechanics, and pointed out the need for seeking a fundamental understanding of material behavior. Discrete modeling can be of great help to continuum mechanics, for not only developing constitutive models based on physics, but also for understanding the physical origins of material instability, and the limitations of continuum mechanics.

Limitations of discrete modeling in soil mechanics

Discrete modeling has obvious limitations in soil mechanics. The sheer number of individual soil particles, especially those with smaller diameters, within soil masses of practical interest to engineering, prohibits the simulation of their overall response even with the most advanced computers. For instance, in a cubic centimeter of soil, there may be as many as $5x10^{12}$ clay particles, when those are assumed to be identical square platelets (1-μm x 1-μm x 0.1-μm), and the void ratio is equal to one. Therefore, the largest computers yet built would not be sufficient to handle 1 cm^3 of fine-grained soils, which is quite irrelevant for engineering purposes. The number of soil particles in a volume decreases roughly with the cube of the particle size. In a cubic centimeter, there may be as many as 1,000 particles of coarse sand, when those are assumed rounded with 1-mm diameter and the void ratio is still equal to one. Yet again, the most powerful computers of today, with numerous parallel processors, would have extreme difficulty handling 1 m^3 of coarse sand, which corresponds to $1x10^9$ particles.

In view of the excessively large number of particles in soils, it seems more feasible to combine the advantages of discrete modeling and continuum mechanics to solve engineering problems. In summary, discrete and continuum mechanics should be perceived as complementary, not adversary, tools in soil mechanics to understand the mechanics and physics of soil behavior.

Numerical methods for discrete modeling

The main numerical tool of discrete modeling is the *discrete element method* (Cundall and Strack, 1979). Cundall (1989) proposed that this appellation apply to a computer program only if it (a) allows finite displacements and rotations of discrete bodies,

including detachment, and (b) recognizes new contacts automatically as the calculation progresses. To my knowledge, there are eight main classes of numerical methods corresponding to this definition.

1. *Distinct element methods (DEM).* These methods use explicit and time-marching algorithms to solve the equation of motion. Bodies may be rigid or deformable, but contacts are always deformable. Examples of DEM codes are TRUBAL (Cundall, 1988); UDEC (Cundall, 1980); 3DEC (Hart et al., 1988); DIBS (Walton, 1980); 3DSHEAR (Walton et al., 1988); and JP2 (Bardet and Proubet, 1989). In granular statics, DEM calculates the equilibrium states of particle systems by using dynamic transitions, the convergence of which are generally accelerated and optimized by introducing an artificial viscous damping. Such optimizations include density scaling (Cundalll, 1982) and adaptative dynamic relaxation (Bardet and Proubet, 1991).

2. *Modal methods.* These methods, which are similar to DEM in the case of rigid bodies, use modal superposition for deformable bodies, (e.g., Williams and Mustoe, 1987). A representative code is CICE (Hocking et al., 1985).

3. *Discontinuous deformation analysis (DDA).* In DDA (Shi, 1993), contacts are rigid, and bodies may be rigid or deformable. The condition of no-interpenetration is achieved by an iteration scheme; the body deformability comes from superposition of strain modes.

4. *Momentum-exchange methods.* The contacts and bodies are both rigid: momentum is exchanged between two contacting bodies during an instantaneous collision. Frictional sliding can be represented (e.g., Campbell and Brennen, 1985; Hahn, 1988).

5. *Multibody Dynamics methods (MDM).* Moreau (1966) treats the problem of non-penetrability by using *Convex Analysis*. The unilateral mechanical constraints of frictional non-penetrability are mathematically formulated in (Brogliato, 1996; Delassus, 1917; Moreau, 1966, 1988, 1993, 1994, 1995; Pfeiffer and Glocker, 1966). MDM was implemented in (Jean, 1995) using an implicit algorithm, and was applied

by several investigators to examine various aspects of particulate behavior (e.g., Daudon et al., 1997). MDM considers only purely rigid bodies, and ignores the deformability of individual grains and contacts.

6. *Structural Mechanics methods (SMM).* These methods derive from the numerical techniques used in computational mechanics, especially finite element methods for continuum plasticity and contact mechanics (e.g., Borja and Wren, 1995; Kishino, 1988; Zienkiewicz and Taylor, 1991). The equilibrium equations for the system of particles are solved quasi-statically, and not dynamically, which eliminates the spurious oscillations of dynamic relaxation. SMM obtain the incremental transition between equilibrium states by relying on a tangential stiffness matrix, which is determined from the local contact stiffness between particles. Unfortunately, this tangential operator consumes a large amount of computer memory, rendering it inapplicable to large numbers of particles, and often becomes singular and causes numerical problems. However, SMM guarantees a strict convergence, when the physical problem has a solution, and is capable of detecting bifurcation points. This approach, which benefits from the progress in finite element methods for structural and continuum mechanics (e.g., Bathe, 1996; Zienkiewicz and Taylor, 1991), reveals that there are many similarities between the numerical techniques in finite and discrete element methods.

7. *Mean Field method* (e.g., Bashir and Goddard, 1991; Zhuang et al., 1995). The transitions between static states are calculated by imposing a mean field of displacement and rotation to the particles, and by restoring a new equilibrium configuration by means of incremental motions or "*fluctuations*" of each particle about the mean. The fluctuating motions of individual particles are determined statically by a global stiffness matrix, which is determined from the local contact stiffness between particles, as in structural mechanics. The problems arising from the matrix singularity are overcome by solving the linear equations with the well-known relaxation method (Southwell, 1940).

8. *Energy minimization method* (e.g., Chichili et al., 1993). The transition between static states is obtained by incorporating the geometric constraints of non-penetrability, Mohr-Coulomb friction criterion for relative sliding, and a minimization function that translates the energy dissipated at the contacts due to internal friction. The interparticle forces are calculated at each time step by using an explicit finite difference scheme based on linear programming technique.

Following the classification in (Cundall, 1989), Fig. 5 summarizes the attributes, advantages and shortcomings of the methods listed above, which include:

- contact and body stiffness
- number and shapes of bodies
- capabilities of fracturing individual particles
- packing density
- amplitude of displacement and strain, and
- static and dynamic capabilities.

A shown in Fig. 5, the method performances are grouped in three categories, ranging from good to not applicable. At the present, it is difficult to conclude on the superiority of a particular method, due to a lack of in-depth comparative studies. In this chapter, we will not cover all these methods, but will only introduce the basics of discrete element methods.

Physical modeling of granular media

Geometry of grains

As described in soil mechanics textbooks (e.g., Bardet, 1997; Lambe and Whitman, 1979), soil grains have irregular and various shapes including spheres, ellipsoids, platelets, cylinders, and tubes, when they are observed with the naked eye and microscopes. Their wide range of grain sizes vary from colloids (<1 μm) to boulders

(>100 cm). The diversity of grain shape, size, distribution, and structures are one of the major causes of the multiplicity of soil behavior observed in the laboratory and the field.

For the sake of simplification, hereafter we idealize soil grains as two-dimensional rods. This convenient assumption obviously departs from reality. However, it is sustainable as long as it provides us with some useful hints about material response. Some researchers have already moved to 3D geometry, and are getting new insights into material behavior (e.g., Thornton and Sun, 1994). 2D models are educational for a first hands-on experience of granular mechanics. Many 2D concepts can readily be extended to 3D modeling.

Particles

As shown in Fig. 6, the set B represents a generic assembly of N rigid particles with nonlinear interaction at contacts, i.e., $B = \{1,...,N\}$. The particles, which are subjected to external forces and moments excluding body forces, belong to the set $B_E = \{N_I,...,N\}$, and the remaining ones belong to the set B_I. The sets B_I and B_E are complementary, i.e., $B = B_I \cup B_E$.

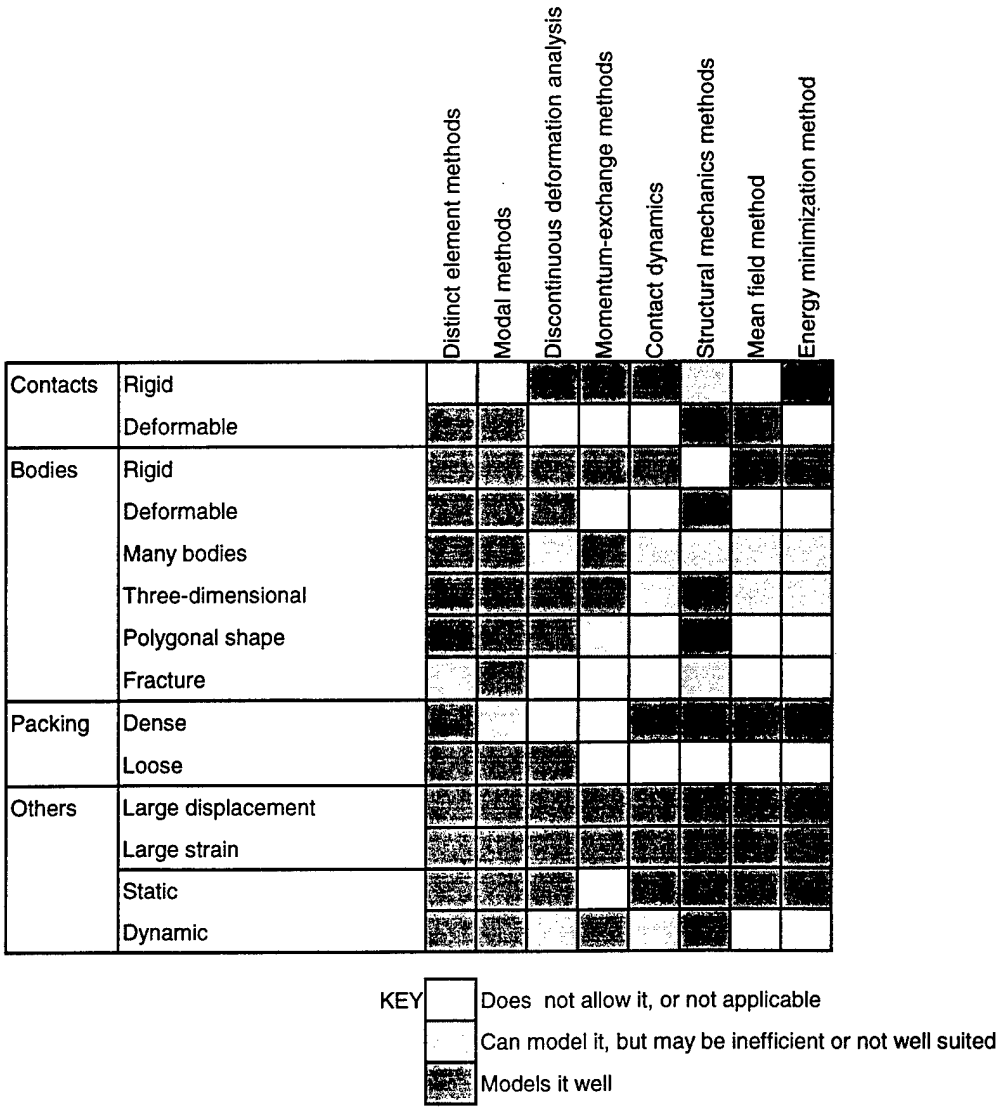

Figure 5. Attributes of the various classes of discrete element methods (adapted from Cundall, 1989).

The particles are assumed rigid (i.e., they cannot deform). The assumption of rigid particles will be discussed later. The conservation of mass implies that B is constant, i.e., no rigid particle should be lost. Some particles of B_I may become part of B_E forces/displacement. However B_I and B_E can vary, provided that they remain complementary.

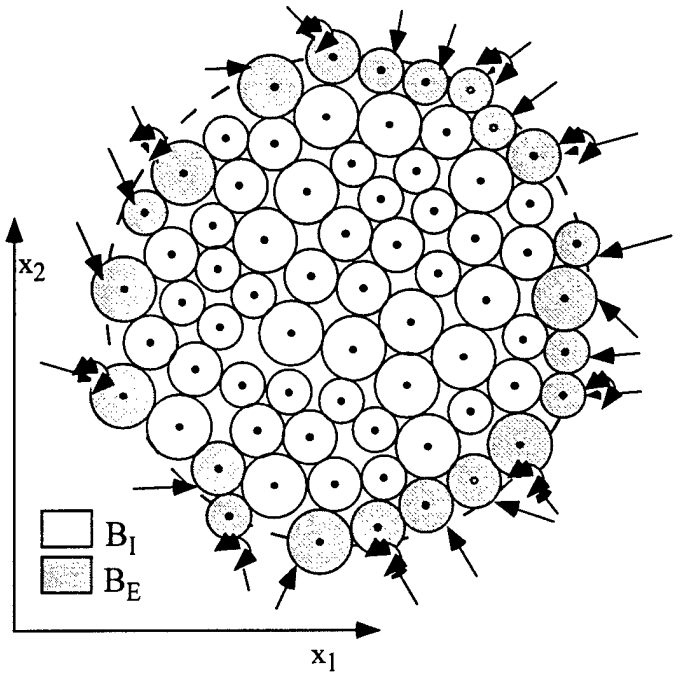

Figure 6. An assembly of discrete particles.

Cylindrical particles are defined by their radius and mass per unit area. Elliptical particles have an additional property to characterize their aspect ratio. The positions of rigid particles, irrespective of their shapes, are defined by the center position and their rotation θ. The motion of set B is therefore characterized by $3N$ independent variables.

The kinematics of the granular media is completely defined by a finite number of degrees of freedom. There is no need to use continuous interpolation functions to represent the kinematics, unlike in finite elements. Indeed, a continuous interpolation between discrete points would be inappropriate for granular media because the displacement is discontinuous at the particle contacts.

Contacts

Contact mechanics (e.g., Johnson, 1985) is a vast subject, which is beyond the scope of this chapter. We will only introduce the basic concepts required in DEM. With the exception of body forces which are applied at the particle contacts, the external and internal forces acting on particles are assumed to be applied at points and not to be distributed on surfaces. There are M contact points belonging to the contact set C, i.e., C=

{1, ..., M}. These contacts can be subdivided between the set I, I= {1, ..., M_I}, which corresponds to contact between particles of B, and the set E, I= { M_{I+1}, ..., M}, which describes the points of application of external concentrated actions. The sets I and E are complementary, i.e., $C = I \cup E = \{1,...,M\}$. By definition, the sets I_a and E_a represent the contact points of I and E on particle a, respectively. The subsets I_a and E_a have the following properties:

$$I = \bigcup_{a \in B} I_a \quad \text{and} \quad E = \bigcup_{a \in B} E_a \tag{1.1}$$

and

$$E_a \cap E_b = \varnothing \quad \text{and} \quad I_a \cap I_b = \{c\} \quad \text{for} \ \forall \ \ a \neq b \in B \tag{1.2}$$

Equation 2 implies that two different sets I_a have at most one point in common. The number of contacts may vary during a deformation process, i. e., I varies depending on the state of B.

Contact detection

In the case of spherical or cylindrical particles, there is a contact between particles a and b when the following criterion is met:

$$\left\| \mathbf{x}_a - \mathbf{x}_b \right\|^2 = \left(x_i^a - x_i^b \right)^2 \leq R_a^2 + R_b^2 \tag{1.3}$$

where x_i^a and x_i^b are the center position of particles a and b, and R_a and R_b their radii, respectively. The contact detection criterion becomes more complicated for elliptical (e.g., Ting, 1992) and polygonal (e.g., Cundall, 1980, 1988) particles.

For large numbers of particles, the detection of contacts becomes a serious computational issue in granular mechanics. The most naive method for detecting contacts consists of applying Eq. 3 N-1 times for each ball of an assembly of N particles. There are therefore Nx(N-1) searches, a task which may rapidly consume a large fraction of the calculation time. For instance, the computer would make 10^6 searches for 10^3 particles, but 10^{12} searches for 10^6 particles, which is an excessively large number of calculations. Several detection algorithms have been proposed. The most efficient ones are $N\,logN$ (e.g.,

Mujinza et al., 1993). We will present one of the most commonly used algorithms (e.g., Cundall and Strack, 1979).

As shown in Fig. 7, the space is divided in a uniform grid forming square boxes. The box size is larger than the diameter of the largest particles, so that no particle covers more than four boxes at once. Assuming that there is a maximum number of M particles per box, the maximum number of searches is $4NM$ as a single particle may cover 4 boxes at once. This search technique requires associating boxes and particles, and updating this association when particles move across the grid.

This simple search technique becomes less efficient when M increases, which is the case when the particles have a wide range of sizes. In these cases, one may consider alternate contact algorithms.

Contact geometry

The contact geometry of rigid cylindrical particles is defined as shown in Fig. 8. In theory, for rigid particles which do not overlap, the contact is reduced to the point of tangency between two particles (Fig. 8a).

$$\mathbf{x}_C = \frac{R_A}{R_A + R_B}\mathbf{x}_A + \frac{R_B}{R_A + R_B}\mathbf{x}_B \tag{1.4}$$

For particles which overlap slightly, the contact geometry is no longer a point but becomes a surface. However, this contact area will be reduced to a point (Fig. 8b) defined as follows:

$$\mathbf{x}_C = \left(\frac{1}{2} - \frac{R_A - R_B}{AB}\right)\mathbf{x}_A + \left(\frac{1}{2} + \frac{R_A - R_B}{AB}\right)\mathbf{x}_B \tag{1.5}$$

For rigid cylindrical particles, the contact point becomes the tangency point (i.e., Eqs. 4 and 5 coincide). In the case of elliptical or polygonal particles, the contact point is more difficult to define as described for elliptical (Ting, 1992) and polygonal particles (Cundall, 1988).

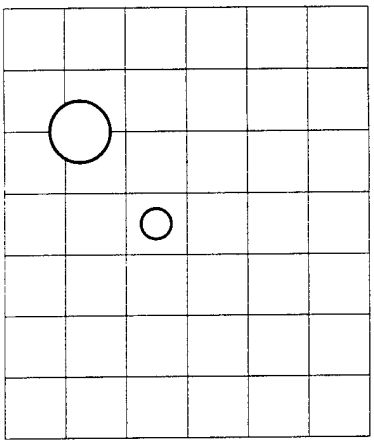

Figure 7. Uniform grid used for detection of contact between two particles.

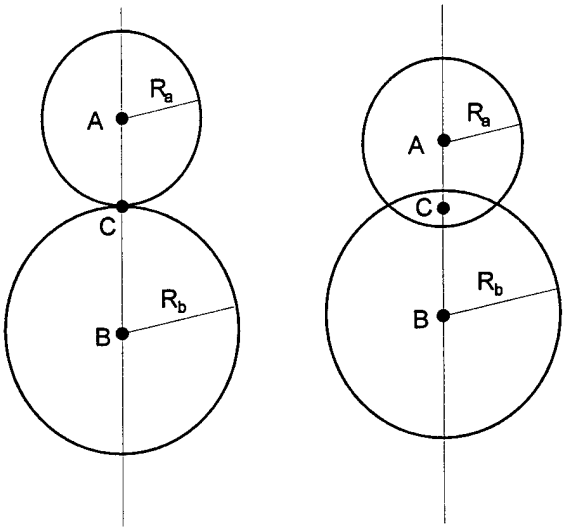

Figure 8. Contact point between two cylindrical particles without and with overlap.

Contact kinematics

The kinematics of the contacts characterizes the relative motion between the particles. As shown in Fig. 9, the relative displacement of particles *a* and *b* at contact point *c* is:

$$\Delta u_i^c = u_i^b - u_i^a + e_{ijk}\left(\omega_j^b r_k^{bc} - \omega_j^a r_k^{ac}\right) \tag{1.6}$$

where u_i^a is the displacement vector of particle center, ω_i^a the rotation of particles located at x_i^a, and

$$r_i^{ac} = x_i^c - x_i^a, \text{ and } \quad r_i^{bc} = x_i^c - x_i^b \tag{1.7}$$

The relative rotation of particles a and b:

$$\Delta\omega_i^c = \omega_i^b - \omega_i^a \tag{1.8}$$

In the case of cylindrical particles,

$$r_i^{ac} = R_a n_i^c,\ r_i^{bc} = -R_b n_i^c,\ \omega_i^a = \omega_a n_3^c,\ \text{and}\ \omega_i^b = \omega_b n_3^c \tag{1.9}$$

where $\mathbf{n}^c$ is the unit vector normal to the contact area:

$$n_i^c = \left(x_i^c - x_i^a\right)/R_a = -\left(x_i^c - x_i^b\right)/R_b \tag{1.10}$$

Equation 6 becomes:

$$\begin{aligned} \Delta u_1^c &= u_1^b - u_1^a - n_2^c\left(\omega_a R_a + \omega_b R_b\right) \\ \Delta u_2^c &= u_2^b - u_2^a + n_1^c\left(\omega_a R_a + \omega_b R_b\right) \end{aligned} \tag{1.11}$$

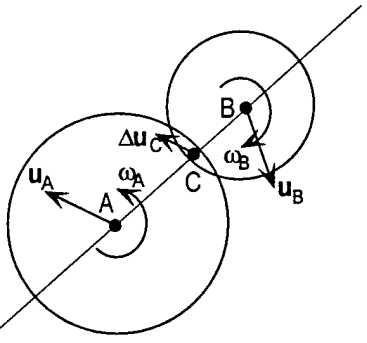

Figure 9. Relative displacement between two particles.

Equation 6 describes exactly the relative displacement between two particles which do not overlap (i.e., $AB = R_a + R_b$). However, Eq. 6 becomes approximate in case of overlap (i.e., $AB < R_a + R_b$). Fortunately, this overlap is usually very small in most cases, and is thought to have no significant consequences.

Contact actions

The actions at contact c are represented by contact forces f_i^{ac} and contact moments m_i^{ac}. Both forces and moments are applied at the contact points. In many instances, the contact moments are neglected, and the contact actions are reduced to forces alone. This assumption may apply to small contact areas between cylindrical and spherical particles,

which cannot transmit significant moments due to their small size. However, this assumption may become questionable for particles of arbitrary shapes and large normal contact forces.

Contact relations

Various types of contact relations between particles were recently reviewed in (Misra, 1995), including contacts between smooth, spherical, non-spherical, cylindrical, and non-cylindrical elastic particles with friction and surface adhesion, rough elastic particles, and viscous bridge. Hereafter, we will only review the normal stiffness between spherical and cylindrical particles, and some findings on contacts with friction.

Elastic contact between smooth particles

The distribution of contact pressure proposed by Hertz (1882)] is:

$$p(r) = p_0\sqrt{1-(r/a)^2} \tag{1.12}$$

where p_0 is the maximum contact pressure, a is the radius of the circular contact area, and r is the polar coordinate. The total load P is related to the contact pressure through:

$$P = \int_0^a p(r)2\pi r dr = \frac{2}{3}p_0\pi a^2 \tag{1.13}$$

Therefore the maximum pressure p_0 is 3/2 times the mean pressure p_m. The radius of the contact area is:

$$a = \pi p_0 R/2E^* = \sqrt[3]{\frac{3PR}{4E^*}} \tag{1.14}$$

where:

$$\frac{1}{E^*} = \frac{1-\nu_1^2}{E_1} + \frac{1-\nu_2^2}{E_2} \quad \text{and} \quad \frac{1}{R} = \frac{1}{R_1} + \frac{1}{R_2} \tag{1.15}$$

In the case of identical elastic properties, $E^*=E/2(1-\nu^2)$. The mutual approach of distant points in the two solids is:

$$\delta = \pi a p_0 / 2E^* = \frac{a^2}{R} = \sqrt[3]{\frac{9P^2}{16RE^{*2}}} \quad \text{or} \quad P = \frac{4}{3} E^* R^2 \left(\delta / R\right)^{3/2} \tag{1.16}$$

The secant normal stiffness k_n is therefore load-dependent:

$$k_n = \frac{P}{\delta} = \frac{4}{3} E^* \sqrt{R} \sqrt{\delta} = \sqrt[3]{\frac{16}{9} E^* P R} \tag{1.17}$$

In the case of cylindrical solids, the half-width of the contact area is:

$$a = \sqrt{\frac{4PR}{\pi E^*}} \tag{1.18}$$

where P is now a force per unit length (i.e. [P] = F L^{-1}). The maximum contact pressure is:

$$p_0 = \frac{2P}{\pi a} = \frac{4}{\pi} p_m = \sqrt{\frac{PE^*}{\pi R}} \tag{1.19}$$

The relative displacement δ is given in (Johnson, 1985):

$$\delta = \frac{P}{\pi E^*} \left(Ln\left(4\pi R E^* / P\right) - 1 \right) \tag{1.20}$$

The secant normal stiffness k_n is therefore load-dependent:

$$k_n = \frac{P}{\delta} = \frac{\pi E^*}{Ln\left(4\pi R E^* / P\right) - 1} \tag{1.21}$$

Figure 10 shows the variation of normal load P with normal relative displacement δ in the case of spherical and cylindrical contact. Figure 11 shows the corresponding secant normal stiffness k_n. The relative displacement δ is normalized with the particle radius R. The normal load P is normalized with RE* for cylindrical particles and RE^{*2} for spherical particles. In the two-dimensional case (i.e., cylinder), [P]= FL^{-1}, and in the three-dimensional case (i.e., sphere) [P]= F.

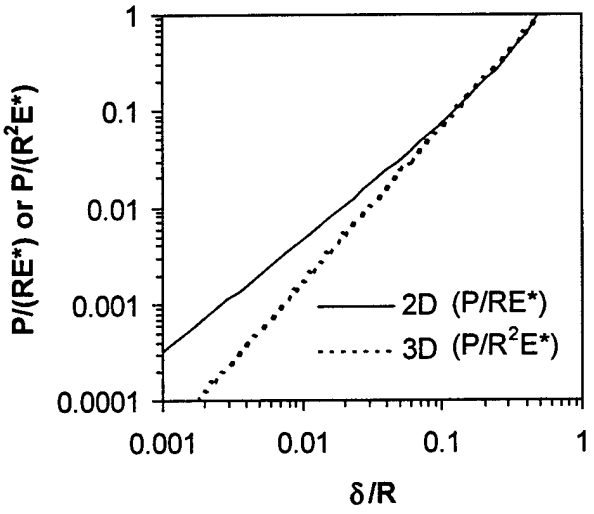

Figure 10. Variation of normal load with relative displacement δ/R for cylindrical (2D) and spherical (3D) particles

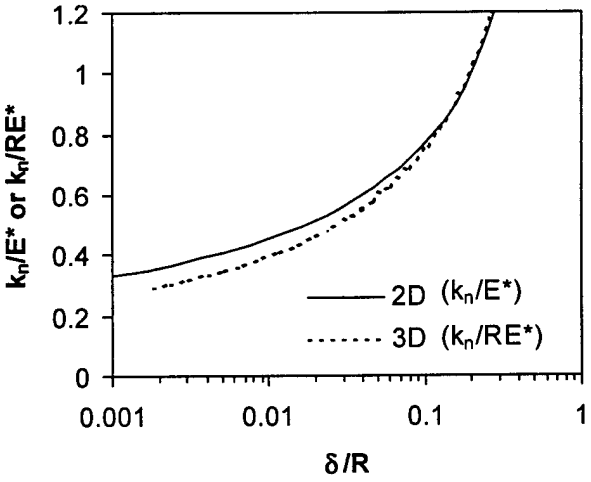

Figure 11. Variation of normal secant stiffness corresponding to Fig. 10.

Table 1 lists typical values of elastic properties for various particle materials. These values are useful to define realistic values of contact stiffness between particles.

Table 1. Elastic properties for particle materials (after (Bardet, 1997; Johnson, 1985).

Material	Young's modulus (Gpa)	Poisson ratio
Perpex	3	0.38
Glass	55	0.25
Steel	200	0.28 - 0.29
Aluminium	55 - 76	0.34 - 0.36
Duraluminium	74	0.32
Cast Iron	113	0.25
Tungsten Carbide	732	0.22
Amphibolite	93 - 121	0.28 - 0.30
Anhydrite	68	0.30
Diabase	87 - 117	0.27 - 0.30
Diorite	75 - 108	0.26 - 0.29
Dolomite	110 - 121	0.30
Dunite	149 - 183	0.26 - 0.28
Feldspathic Gneiss	83 - 118	0.15 - 0.20
Gabbro	89 - 127	0.27 - 0.31
Granite	73 - 86	0.23 - 0.27
Limestone	87 - 108	0.27 - 0.30
Marble	87 - 108	0.27 - 0.30
Mica Schist	79 - 101	0.15 -0.20
Obsidian	65 - 80	0.12 - 0.18
Oligoclasite	80 - 85	0.29
Quartzite	82 - 97	0.12 - 0.15
Rock salt	35	0.25
Slate	79 - 112	0.15 - 0.20
Ice	7.1	0.36

Deformable and rigid particles

As previously mentioned, soil particles were assumed to be rigid and the contact deformable. However, in reality, soil particles are not rigid; they deform when they are

subjected to contact forces. The assumption of rigid particles and deformable contacts is acceptable as long as the contact deformations represent the particle deformations. This condition may be met for particles with simple geometry (e.g., spheres and cylinders) undergoing elastic deformations. However, this condition may not be met for complex deformation patterns and inelastic deformation, and distributed contact loads (e. g., Cundall, 1989). The case of deformable particles is not considered hereafter. One may refer to Cundall (1980) and Shi (1982) to account for elastic deformation of particles.

We will illustrate the fact that the contact deformation may represent the particle deformation in some simple cases. This will be demonstrated by considering the compression of the cylinder of Fig. 12, which is subjected to diametrically opposed concentrated forces.

The stress distribution in the cylinder is given in Timoshenko and Goodier (1951). The stresses at point A are:

$$\sigma_x = \frac{P}{\pi}\left(\frac{1}{R} - \frac{2(a_1^2+2z^2)}{a_1^2\sqrt{a_1^2+z^2}} + \frac{4z}{a_1^2}\right) \text{ and } \sigma_z = \frac{P}{\pi}\left(\frac{1}{R} - \frac{2}{2R-z} - \frac{2}{\sqrt{a_1^2+z^2}}\right) \quad (1.22)$$

In plane strain, the vertical strain is:

$$\varepsilon_z = \frac{1-\nu^2}{E}\left(\sigma_z - \frac{\nu}{1-\nu}\sigma_x\right) \quad (1.23)$$

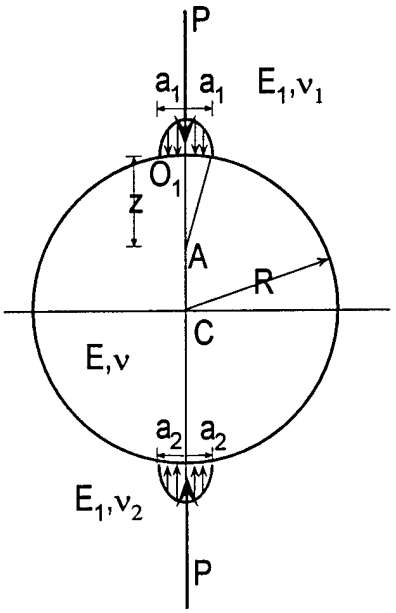

Figure 12. Compression of a cylinder due to diametrically opposed concentrated loads.

The compression of the upper half of the cylinder O_1C is found by integrating ε_z from $z =$ 0 to $z = R$, where $a << R$, to give:

$$\delta_1 = \int_0^R \varepsilon_z dz = \frac{P(1-\nu_1^2)}{\pi E}\left(2Ln(4R/a_1)-1\right) \tag{1.24}$$

A similar expression is obtained for the compression of the lower half of the cylinder so that the total compression of the diameter through the mid-points of the contact areas O_1O_2 is:

$$\delta = \frac{2P(1-\nu^2)}{\pi E}\left(Ln(4R/a_1)+Ln(4R/a_2)-1\right) \tag{1.25}$$

Equation 25 can be used to derive Eq. 20. As clearly indicated by Eqs. 22 to 25, the contact stiffness originates from the particle deformation. In this particular case, the contact deformation accounts for the particle deformation.

Frictional contact

In soil mechanics, the frictional characteristics between two particles is commonly thought to be a basic material property, which can easily be determined from laboratory experiments and tables of physical constants. However, this common belief is

unfortunately unfounded. The determination of friction between two particles is still a complicated problem as described in Singer and Pollock (1992). As shown in Table 2, the values of friction angle ϕ_μ vary not only with mineral type but also on the contact cleanliness, water content, and level of normal load.

Contact models

Several relations were proposed for relating the contact actions and contact kinematics. We will review only two basic ones: the elastic-perfectly plastic relations with and without rotational stiffness and friction.

Elastic-perfectly plastic contact

Figure 13 represents the force-displacement relationship between two cylindrical particles which is used to simulate the intergranular behavior. The contact relationship is activated when two disks overlap. The contact geometry between two disks is characterized by a contact point, and a contact direction which passes through the centers of the particles in contact. N and S denote the projections of the contact force that are respectively tangential and normal to the contact direction. The value of the contact force at time $t+\Delta t$ is calculated from its value at time t by using the following relation

$$\begin{cases} N(t+\Delta t) = N(t) + k_n \Delta n \\ S(t+\Delta t) = S(t) + k_s \Delta s \end{cases} \tag{1.26}$$

where k_n and k_s are the tangential normal and tangential stiffness, respectively, and Δn and Δs are the normal and tangential components of the relative displacement of the contact between time t and $t+\Delta t$. In the case of linear elastic contacts, k_n and k_s are constant. In the case of Hertz contact, k_n and k_s vary with the contact load N and S. In general k_n and k_s are assumed to be equal. More realistic expressions are reported in Misra (1995).

Table 2. Interparticle friction angle ϕ_μ measured from laboratory tests (after Misra, 1995).

Material	Type of test	Conditions	Value ϕ_μ	Reference
Biotite	Along cleavage faces	Dry	14.6-17.2	Horn and Deere, 1962
		Saturated	7.4	—
Calcite	Block on block	Dry	8	—
		Water-saturated	34.2	—
Chlorite	Along cleavage faces	Dry	19.3-27.9	—
		Saturated	12.4	—
Feldspar	Block on block	Dry	6.8	—
		Water-saturated	37.6	—
	Direct shear box, free particles on flat surface		36	El-Sohby, 1969
	Free particle		37	Lee, 1966
	Particle-plane	Saturated	28.9	Procter and Barton, 1974
Feldspar (microline)	Direct shear box, fixed particles on flat surface	Dry	6	Horne, 1965
Feldspar (microline)		Water-saturated	37	—
Glass	Free particles on plate	Dry	10-12	Gray, 1960
		Water-saturated	17	—
	Three balls on glass plate	Dry, Low load	9	—
		Water-saturated and low load	19	—
		After Redrying	16	—
Glass ballotini	Ball on ball	Dry, low load	2	Skinner, 1969
		Dry, high load	4	—
		Flooded, low load	28-40	—
		Flooded, high load	38-40	—
		Dry, low load	3	—
		Dry, high load	7	—
	Direct shear box, free particles on flat surface	Water-saturated	17	Rowe, 1962
		Dry, tested in dry nitrogen	9	Tong, 1970
		Acetone cleaned, tested in dry nitrogen	16	—
		Trichloroethylene, acetone, detergent rinses	21	—
		Water-saturated	15	—
		Cleaned with soap, water and acetone	15	—
		Particles fixed with wax after initial sliding	14-15	—
Muscovite	Along cleavage faces	Dry	16.7-23.3	Horn and Deere, 1962
		Saturated	13	—
Phlogopite	Along cleavage faces	Dry	14-17.2	—
		Saturated	8.5	—
Phosphor-bronze	Ball on ball	Water-saturated	21	Parikh, 1967

Material	Type of test	Conditions	Value ϕ_μ	Reference
Quartz	Block on block	Dependent on surface condition	0-45	Bromwell, 1966
		Dry	7.4	Horn and Deere, 1962
		Water-saturated	24.2	—
	Block over particle set in mortar	Dry	6	Tschebotarioff and Welch, 1948
		Moist	24.25	—
		Water-saturated	24.25	—
	Direct shear box fixed particles on flat surface	Dry	6	—
		Moist and water- saturated	25	—
		Dry	11	Penman, 1953
		Water-saturated	33	—
		High load	19	—
		Low load	29	—
		Air dried	22	Bishop, 1954
		Atmospheric	28	Brogliato, 1996
		Water-saturated	23-30	[175]
		High vacuum	38	Bromwell, 1966
		Water-saturated	26	Tong, 1970
		Moist and water-saturated	28	—
		Dry, tested in dry nitrogen	15	—
	Particle-particle	Saturated	26	Procter and Barton, 1974
	Particle-plane	Saturated	22.2	—
		Dry	7.4	—
	Particles on polished block	Water-saturated	22-31	Rowe, 1962
	Three fixed particles over block	Water-saturated	21-27	Hafiz, 1950
Quartz (clean)	Direct shear box, fixed particles on flat surface	Dry	6	Horn and Deere, 1962
		Water-saturated	23	—
		Amylaraine	31	—
		Carbontetrachloride	11	—
Quartz (milky)		Dry	9	—
		Water-saturated	27	—
Quartz (rose)		Dry	7	—
		Water-saturated	24	—
Steel	Ball on ball	Dry, polished and cleaned with carbontetrachloride	7	Gray, 1960
	Direct shear box, free particles on flat surface	Air	7	Rowe, 1962
		Water-saturated	9	—
	Free particles on plate	Water-saturated, dry and cleaned with carbontetrachloride	8.8	Gray, 1960
	Light load apparatus	Dry, polished	9	—
		Dry, polished and cleaned with carbontetrachloride	9.5-12	—
	Rods on rods	Dry, cleaned with carbontetrachloride	9-14	—
Steel balls	Friction apparatus	Dry	16-32	Skinner, 1969
Zircon	Direct shear box, free particles on flat surface	Water-saturated	23	El-Sohby, 1969

The contact force of Fig. 13 obeys the Coulomb friction law:

$$S(t) \leq \tan\phi_\mu N(t) + c \tag{1.27}$$

where ϕ_μ and c are the friction angle and cohesion between two disks, respectively.

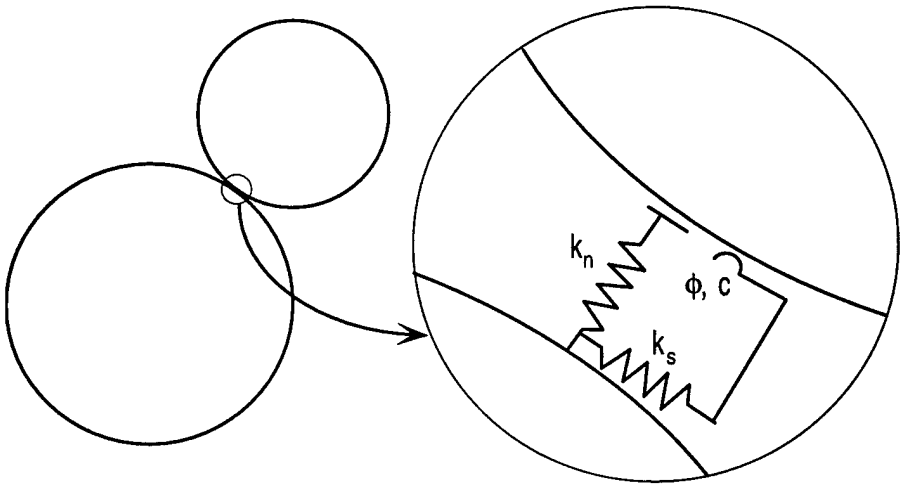

Figure 13. Elastic perfectly-plastic model for contact without rotational stiffness and friction.

Linear-elastic perfectly plastic contact with rolling stiffness and friction

In idealized granular materials, rolling friction is included at the particle contacts by generalizing the elastic perfectly-plastic contact relation. Such a generalized model is schematized in Fig. 14, including its normal, tangential, and rotational stiffnesses, and rolling and sliding frictions. At the particle contacts, the increments of normal force, shear force, and moment are:

$$\Delta F_n = k_n \Delta n, \quad \Delta F_s = k_s \Delta s, \quad \text{and} \quad \Delta M = R k_\theta \Delta\theta \tag{1.28}$$

where k_n, k_s, and k_θ are the normal, tangential, and rotational stiffness of grain contacts, respectively. R is the average particle radius, Δn and Δs are the normal and tangential relative contact displacement, and $\Delta\theta$ is the relative rotation of disks, which is the rotation of the contact surface. Eq. 28 holds provided that the normal and tangential forces, and the moment at contact, obey the following generalized Coulomb friction law:

$$b = -R_2 \left| \Delta\theta_2 - \beta \right| sign\left\{ (\Delta\theta_1 - \beta)(\Delta\theta_2 - \beta) \right\} \tag{1.29}$$

where ϕ_μ is the sliding friction angle, and β the rolling friction angle. The rotational stiffness k_θ is based on an analytical expression derived from the two-dimensional theory of elastic contact (Meftah et al., 1993). k_θ increases proportionally to the cylinder radius and the normal load, which is in agreement with experimental results on hard rubber cylinders (Bardet and Huang, 1993).

Governing equations of statics

The equilibrium of forces on particle a is:

$$\sum_{c \in I_a} f_i^{ac} + \sum_{e \in E_a} f_i^{ae} = 0 \quad i = 1,2,3 \tag{1.30}$$

where f_i^{ac} is the internal force at contact c, and f_i^{ae} the external force at point e. The equilibrium of moments about center of particle a is:

$$\sum_{c \in I_a} \left(m_i^{ac} + e_{ijk} r_j^{ac} f_k^{ac} \right) + \sum_{e \in E_a} \left(m_i^{ae} + e_{ijk} r_j^{ae} f_k^{ae} \right) = 0 \quad i = 1,2,3 \tag{1.31}$$

where m_i^{ac} is the internal moment at contact point c; m_i^{ae} the external moment at point e; e_{ijk} the alternating tensor; $r_j^{ac} = x_j^c - x_j^a$, $r_j^{bc} = x_j^c - x_j^b$; x_j^a and x_j^b the center coordinates of particles a and b; and x_j^c the position of contact point c.

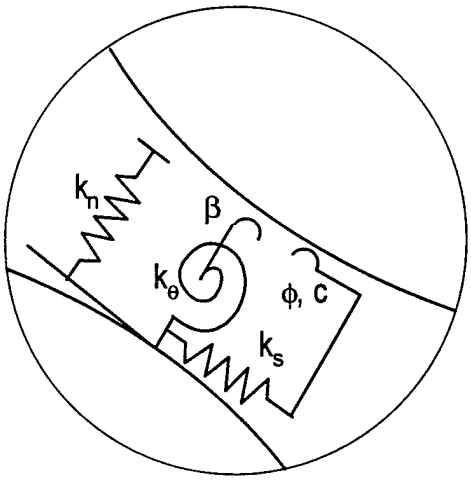

Figure 14. Representation of generalized contact with rotational stiffness and rolling friction.

Boundary conditions

There are several types of boundary conditions, which can be specified on an assembly of particles, including (1) prescribed displacement, velocity, acceleration, and force boundary, (2) periodic boundary, (3) rigid boundary, and (4) flexible boundary.

Prescribed force/displacement

As in the boundary value problems of continuum mechanics, the boundary conditions in granular mechanics can be either prescribed displacement/ velocity/ acceleration, or prescribed force. External forces and moments can be applied to any point of particles.

The motion of a group of particles can conveniently be prescribed by a cluster. Clustered particles are subsets of particles that move as a rigid body and are useful to represent rigid objects. As shown in Fig. 15, the particles may overlap, and move as a solid object. The motion of the a^{th} particle in a cluster is defined by its translation u_i^a and rotation $\Delta\theta_a$ as follows:

$$u_i^a = U_i + e_{ijk}\Delta\theta\,(X_i - x_i^a) \quad \text{and } \Delta\theta_a = \Delta\theta \tag{1.32}$$

where U_i is the translation vector and $\Delta\theta$ is the rotation of a reference point for the cluster.

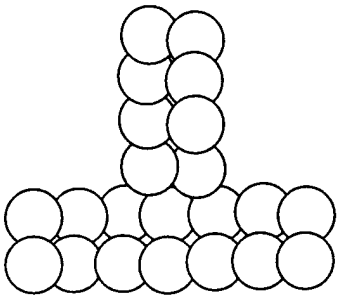

Figure 15. Rigid cluster of particles.

Periodic boundaries

Periodic boundaries are illustrated in Fig. 16. The particles leaving segment AB are reintroduced on segment CD. The periodic boundary conditions can be used in both horizontal and vertical directions, therefore filling the complete space with particles. Periodic boundary conditions have extensively been used for determining average continuum quantities (e.g., stress and strain) free of the heterogeneities caused by rigid boundaries. However, periodic boundaries introduce kinematic constraints in some circumstances. These conditions are met when the deformation patterns have a length scale that is a sub-period of the box. One of these adverse effects is observed for shear bands as explained in Bardet and Proubet (1991).

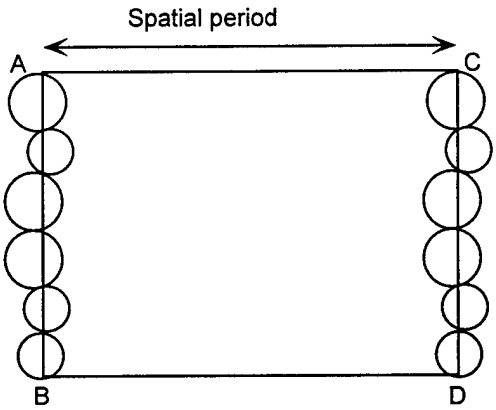

Figure 16. Periodic boundaries.

Rigid walls

Rigid walls simulate the loading platens which transmit loads to laboratory samples. They are usually made of a single segment, but can also be made of several connected

segments for generating various polygonal shapes, such as superficial footings. Displacement, force, or moment can be specified for rigid walls.

Flexible membranes

Flexible membranes were introduced in Bardet and Proubet (1991) to simulate the flexible membranes used in the triaxial test. Forces and moments are externally applied to the boundary particles by specifying the prescribed stress tensor. The forces distributed on the boundary are calculated from the unit vectors normal to the boundary segments and the prescribed stress tensors. For instance in Fig. 17, the force F_i^O applied to the particle center O is:

$$F_i^O = BC\sigma_{ij}n_j^{BC}\,(OC+CB/2)/OA+CD\sigma_{ij}n_j^{CD}+DE\sigma_{ij}n_j^{DE}\,(OD+DE/2)/OF \quad (2.33)$$

where σ_{ij} is the prescribed stress tensor and n_i^{BC}, n_i^{CD}, and n_i^{DE} are the unit vectors normal to segments *BC, CD* and *DE*. The flexible membrane can sustain large deformation. Particles are inserted into the flexible boundary chain as they attempt to force their way between two particles of the flexible boundary.

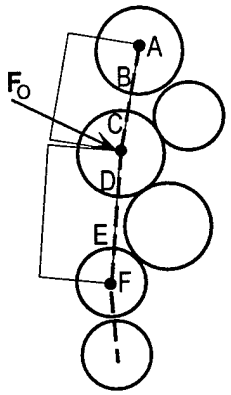

Figure 17. Flexible membrane for stress-controlled boundaries.

PART II. TRANSITION FROM DISCRETE TO CONTINUOUS MEDIA

Background

The definition of stress is one of the critical problems for understanding material instability and the assumptions of higher-order continuum theories. The definition of stress in granular media is a controversial topic in Mechanics. Some researchers (e.g., Bogdanova-Bontcheva and Lippmann, 1975; Chang and Ma, 1991; Kanatani, 1979; and Mülhaus and Vardoulakis, 1987) claim that stress tensor is not symmetric in granular media, and that couple stresses are important to understand material instability such as shear banding. Others (e.g., Christoffersen et al, 1981; and Cundall and Strack, 1978) affirm that the stress asymmetry is absent or negligible for all practical purposes, and unnecessarily complicates the description of the mechanical behavior of granular media.

The controversy about the asymmetry of stress and existence of couple stress is not specific to granular media. Couple stresses were proposed in metals and fracture mechanics to regularize the stress intensity at crack tips (e.g., Sternberg, 1968), but there is not yet a convincing experimental evidence for couple stress (e.g., Diepolder et al., 1991).

Part II re-examines the definition of stress in granular materials, and establishes the conditions under which there may be couple stresses and asymmetric stress. Following the introduction, the second and third sections review the basic equations of granular and equivalent continuous media. The third section re-examines the definition of stress from virtual work and statics. Finally, the last section gives an example illustrating the stress asymmetry in granular media.

Granular medium

Definition

As shown in Fig. 1, the volume V is filled with N particles, some of which are subjected to external forces or moments applied from the exterior of volume V. The particles are grouped in the set $B = \{1,...,N\}$. The forces and moment acting on the particles of B are

concentrated at M points of set $C=\{1,...,M\}$. As shown in Fig. 1, the subset I represents the contact points between two particles of B, whereas the set E denotes the points where external actions are applied:

$$I=\{1,...,M_I\},\quad E=\{M_{I+1},...,M\},\quad \text{and}\quad C=I\cup E=\{1,...,M\} \tag{2.1}$$

The sets I_a, E_a, and C_a denote the contact points on particle a corresponding to internal actions, external actions, and all actions, respectively. The sets C_a, I_a, E_a, I, E, and C are related as follows:

$$C=\bigcup_{a\in B}C_a,\quad C_a=I_a\cup E_a,\quad I=\bigcup_{a\in B}I_a,\quad \text{and}\quad E=\bigcup_{a\in B}E_a \tag{2.2}$$

The intersections of I_a and E_a for two different particles are either empty or reduced to a single point c:

$$E_a\cap E_b=\varnothing\quad \text{and}\ I_a\cap I_b=\{c\}\ \text{ for}\ \forall\ a\neq b\in B \tag{2.3}$$

The particle assembly is in equilibrium when each particle is in equilibrium. The equilibrium of internal and external forces acting on particle a is:

$$\sum_{c\in C_a}f_i^{ac}=0\quad i=1,2,3 \tag{2.4}$$

where f_i^{ac} is the force at contact c. The equilibrium of moments about the center of particle a is:

$$\sum_{c\in C_a}\left(m_i^{ac}+e_{ijk}(x_j^c-x_j^a)f_k^{ac}\right)=0\ \ i=1,2,3 \tag{2.5}$$

where m_i^{ac} represents the internal or external moments at contact point c; e_{ijk} is the permutation symbol used for vector cross product; and x_j^a and x_j^c are the coordinates of particle center a and contact point c, respectively.

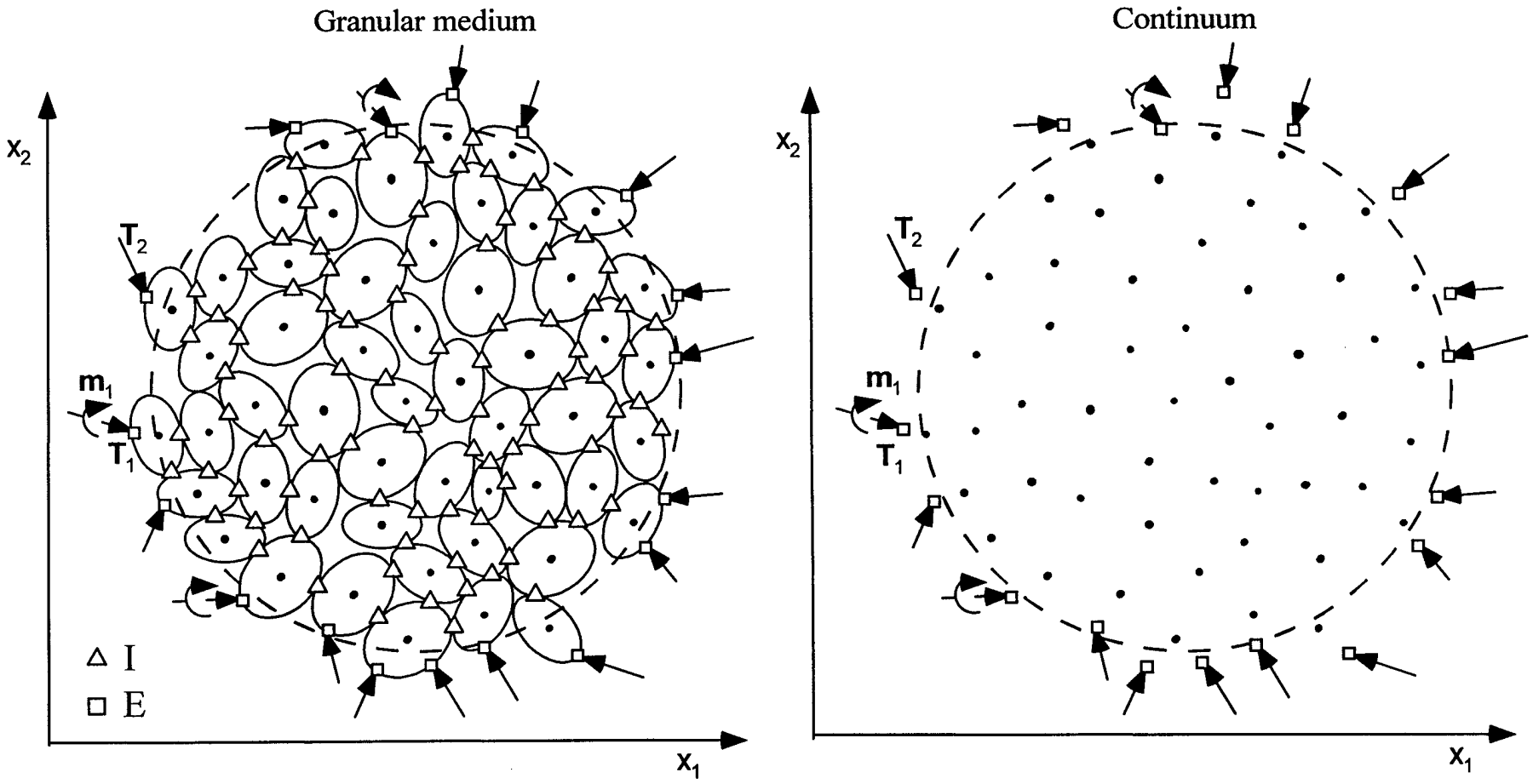

Figure 18. Representation of a granular medium and its equivalent continuum.

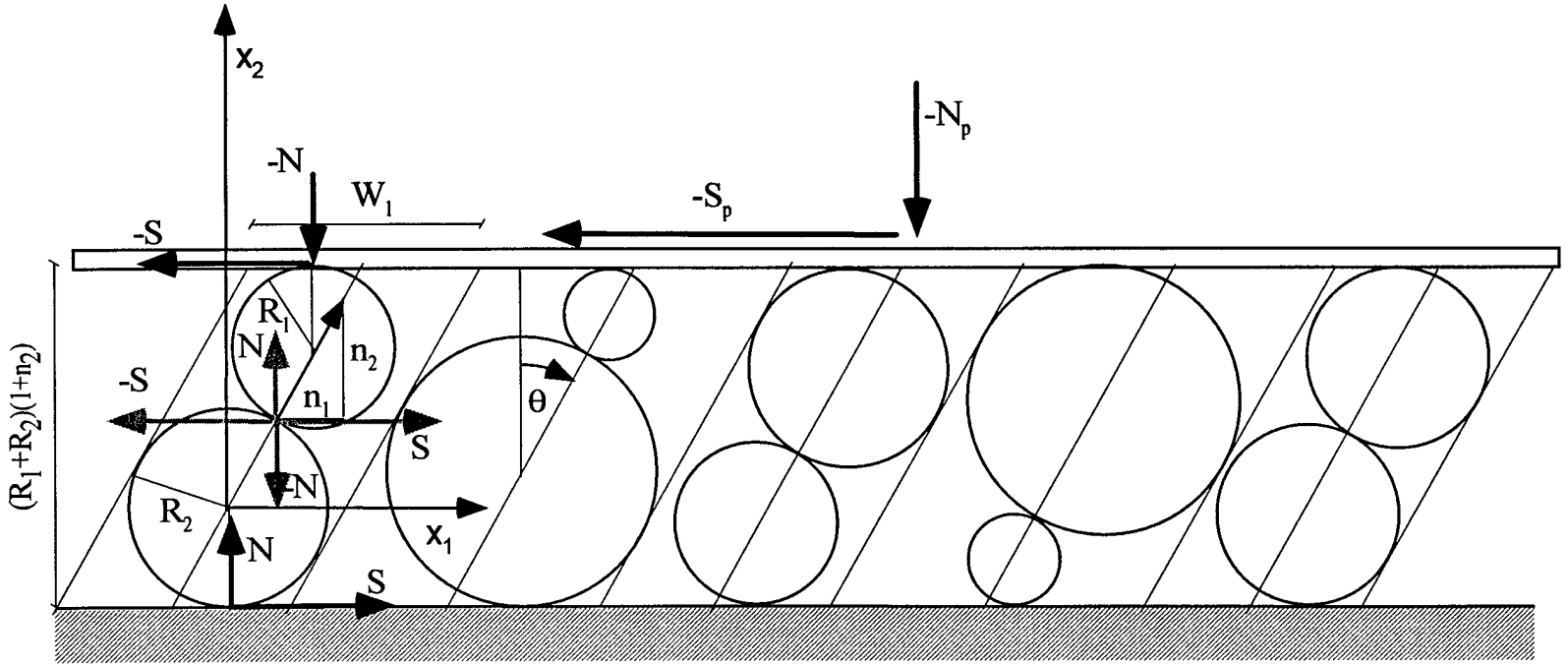

Figure 19. Contact between two particles in a granular medium

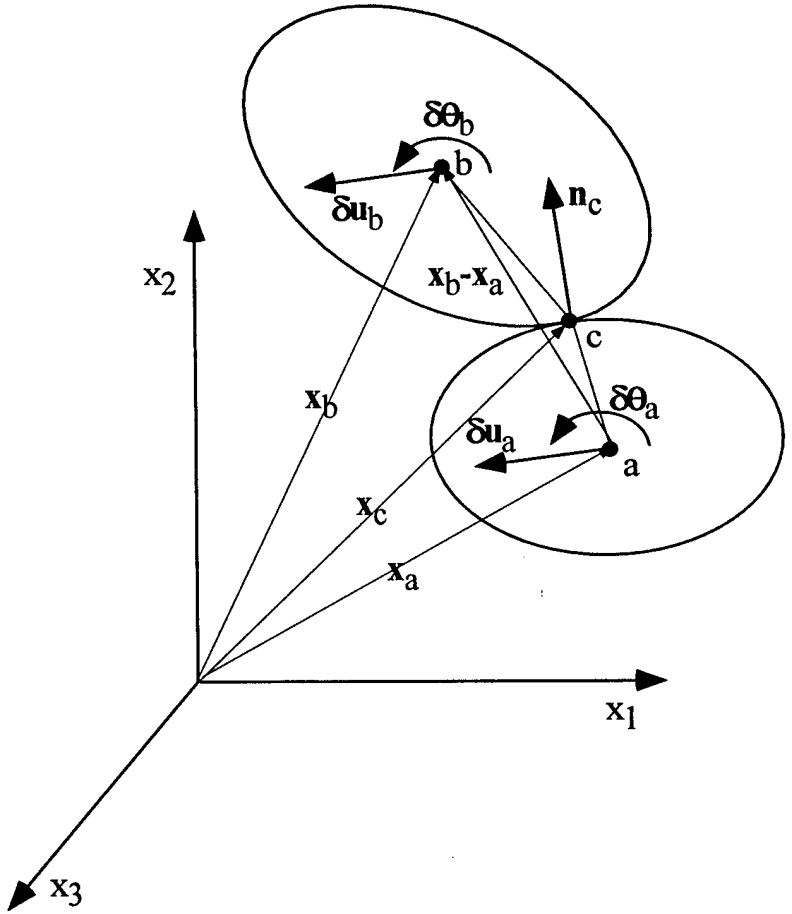

Figure 20. Contact between two idealized particles.

Virtual work in granular media

As shown in Fig. 1, the kinematics of granular media is represented by the displacement δu_i^a of the particle centers, and the particle rotation $\delta\theta_i^a$. After multiplying Eqs. 4 and 5 by any virtual displacement δu_i^a and rotation $\delta\theta_i^a$, and summing for all the particles of volume V, one obtains the following relation:

$$\sum_{a\in B}\sum_{c\in C_a}\left(f_i^{ac}\delta u_i^a+\left(m_i^{ac}+e_{ijk}(x_j^c-x_j^a)f_k^{ac}\right)\delta\theta_i^a\right)=0 \tag{2.6}$$

After transforming the double sum for C_a and B of Eq. 6 into two separate sums for I and E, and noting that contact forces and moments are opposite at internal contact (i.e., $f_i^c=f_i^{ac}=-f_i^{bc}$ and $m_i^c=m_i^{ac}=-m_i^{bc}$), one obtains the principle of virtual work:

$$\delta W_I^D+\delta W_E^D=0 \tag{2.7}$$

where the work δW_E^D done by external forces and moments and the work δW_I^D done by internal forces and moments are:

$$\delta W_I^D=\sum_{c\in I}\left(f_i^c\Delta\delta u_i^c+m_i^c\Delta\delta\theta_i^c\right)\quad\text{and}\quad\delta W_E^D=-\sum_{e\in E}\left(f_i^e\delta u_i^e+m_i^e\delta\theta_i^e\right) \tag{2.8}$$

As shown in Fig. 2, $\Delta\delta u_i^c$ and $\Delta\delta\theta_i^c$ are the relative displacement and rotation of the two particles a and b at their contact point c, respectively:

$$\Delta\delta u_i^c=\delta u_i^b-\delta u_i^a+e_{ijk}\left(\delta\theta_j^b\left(x_k^c-x_k^b\right)-\delta\theta_j^a\left(x_k^c-x_k^a\right)\right)\ \text{and}\ \Delta\delta\theta_i^c=\delta\theta_i^b-\delta\theta_i^a \tag{2.9}$$

δu_i^e and $\delta\theta_i^e$ are the displacement and rotation of the points e of application of external forces and moments. The variational displacements and rotations δu_i^a and $\delta\theta_i^a$ can be selected arbitrarily. In particular, they can be chosen as follows:

$$\delta u_i^a=a_i+b_{ij}x_j^a+c_{ijk}x_j^a x_k^a\quad\text{and}\quad\delta\theta_i^a=\alpha_i+\beta_{ij}x_j^a\quad i=1,2,3 \tag{2.10}$$

where a_i, b_{ij}, c_{ijk}, α_i, and β_{ij} are arbitrary coefficients. By using Eq. 10, $\Delta\delta u_i^c$, $\Delta\delta\theta_i^c$ and δu_i^e become:

$$\Delta\delta u_i^c = b_{ij}\left(x_j^b - x_j^a\right) + c_{ijk}\left(x_j^b x_k^b - x_j^a x_k^a\right) - \alpha_j e_{ijk}\left(x_k^b - x_k^a\right) + \beta_{jl} e_{ijk}\left(x_l^b\left(x_k^c - x_k^b\right) - x_l^a\left(x_k^c - x_k^a\right)\right) \quad (2.11)$$

$$\Delta\delta\theta_i^c = \beta_{ij}\left(x_j^b - x_j^a\right) \quad (2.12)$$

$$\delta u_i^e = \delta u_i^a + e_{ijk}\delta\theta_j^a\left(x_k^e - x_k^{ae}\right) = a_i + b_{ij}x_j^{ae} + c_{ijk}x_j^{ae}x_k^{ae} + e_{ijk}\alpha_j\left(x_k^e - x_k^{ae}\right) + e_{ijk}\beta_{jl}x_l^{ae}\left(x_k^e - x_k^{ae}\right) \quad (2.13)$$

where x^{ae} corresponds to the center of particle a where contact e takes place. By using Eqs. 11 to 13, δW_I^D and δW_E^D become:

$$\begin{aligned}\delta W_I^D = \; & b_{ij}\sum_{c\in I} f_i^c\left(x_j^b - x_j^a\right) + c_{ijk}\sum_{c\in I} f_i^c\left(x_j^b x_k^b - x_j^a x_k^a\right) - \alpha_j\sum_{c\in I} e_{ijk} f_i^c\left(x_k^b - x_k^a\right) \\ & + \beta_{jl}\sum_{c\in I}\left(e_{ijk} f_i^c\left(x_l^b\left(x_k^c - x_k^b\right) - x_l^a\left(x_k^c - x_k^a\right)\right) + m_j^c\left(x_l^b - x_l^a\right)\right)\end{aligned} \quad (2.14)$$

$$\begin{aligned}\delta W_E^D = \; & -a_i\sum_{e\in E} f_i^e - b_{ij}\sum_{e\in E} f_i^e x_j^{ae} - c_{ijk}\sum_{e\in E} f_i^e x_j^{ae} x_k^{ae} - \alpha_j\sum_{e\in E}\left(e_{ijk} f_i^e\left(x_k^e - x_k^{ae}\right) + m_j^e\right) \\ & - \beta_{jl}\sum_{e\in E}\left(e_{ijk} f_i^e\left(x_k^e - x_k^{ae}\right) + m_j^e\right)x_l^{ae}\end{aligned} \quad (2.15)$$

Because Eqs. 7, 14 and 15 hold for arbitrary values of a_i, b_{ij}, c_{ijk}, α_i and β_{ij}, the following relations are obtained:

$$\sum_{e\in E} f_i^e = 0 \qquad i = 1,2,3 \quad (2.16)$$

$$\sum_{c\in I}\left(x_i^b - x_i^a\right) f_j^c = \sum_{e\in E} x_i^{ae} f_j^e \qquad i,j = 1,2,3 \quad (2.17)$$

$$\sum_{c\in I} e_{ijk}\left(x_j^b - x_j^a\right) f_k^c = -\sum_{e\in E} M_i^{ae} \qquad i = 1,2,3 \quad (2.18)$$

$$\sum_{c\in I}\left(e_{ikl} f_l^c\left(x_j^b\left(x_k^c - x_k^b\right) - x_j^a\left(x_k^c - x_k^a\right)\right) + m_i^c\left(x_j^b - x_j^a\right)\right) = \sum_{e\in E} M_i^{ae} x_j^{ae} \quad i,j = 1,2,3 \quad (2.19)$$

$$\sum_{c\in I} f_i^c\left(x_j^b x_k^b - x_j^a x_k^a\right) = \sum_{e\in E} f_i^{ae} x_j^{ae} x_k^{ae} \quad i,j,k = 1,2,3 \quad (2.20)$$

where M_i^{ae} is the external moment acting on particle a about the center of particle a:

$$M_i^{ae} = e_{ijk}\left(x_j^e - x_j^{ae}\right) f_k^e + m_i^e \quad (2.21)$$

Equation 16 translates the equilibrium of external forces applied to the whole assembly of particles. By using Eqs. 17 and 18, one can derive the equilibrium of external moments about the coordinate origin for the assembly of particles, i.e.:

$$\sum_{e\in E}\left(e_{imn}x_m^e f_n^e + m_i^e\right) = 0 \tag{2.22}$$

Therefore, Eq. 18 becomes:

$$\sum_{c\in I} e_{ijk}(x_j^b - x_j^a) f_k^c = -\sum_{e\in E} M_i^{ae} = \sum_{e\in E} e_{imn} x_m^{ae} f_n^e \qquad i = 1,2,3 \tag{2.23}$$

For a volume V to be in equilibrium, the sum of external moments about a common point must vanish (i.e., Eq. 22). However, it is emphasized that the sum of external moments about different particle centers (i.e., $\sum_{e\in E} M_i^{ae}$) is not necessarily equal to zero. M_i^{ae} results from not only contact moments m_i^e but also contact forces f_i^e. It may be different from zero even where there is no contact moment.

Continuum for granular media

In the continuum equivalent for granular media, the traction vector T_i and moment vector m_i acting on the unit surface of unit normal vector n_i is related to the Cauchy stress tensor σ_{ij} and the couple stress tensor μ_{ij} through:

$$T_i = \sigma_{ji} n_j \quad \text{and} \quad m_i = \mu_{ji} n_j \quad i = 1,2,3 \tag{2.24}$$

In the absence of external body force and moment per unit volume, the equations for equilibrium of internal stress and couple stress are:

$$\sigma_{ji,j} = 0 \quad i = 1,2,3 \tag{2.25}$$

$$\mu_{ji,j} + e_{ikl}\sigma_{kl} = 0 \quad i = 1,2,3 \tag{2.26}$$

The kinematics of the equivalent continuum is defined by the fields of displacement vector δu_i and rotation $\delta\theta_l$, which describe the motion of particle centers, i.e.:

$$\delta u_i(x_j^a) = \delta u_i^a, \quad \text{and} \quad \delta\theta_i(x_j^a) = \delta\theta_i^a \quad \forall a \in B \tag{2.27}$$

By multiplying Eqs. 25 and 26 by any variational fields δu_i and $\delta\theta_i$, and integrating over the volume V, one obtains the following relation:

$$\int_V \left(\sigma_{ji,j}\delta u_i + (\mu_{ji,j} + e_{ikl}\sigma_{kl})\delta\theta_i\right) = 0 \tag{2.28}$$

By invoking Gauss theorem, the principle of virtual work is obtained:

$$\delta W_I + \delta W_E = 0 \tag{2.29}$$

where the virtual work δW_E of external forces and moments and the virtual work δW_I of internal stresses are:

$$\delta W_I = \int_V \left(\sigma_{ji}(\delta u_{i,j} + e_{ijk}\delta\theta_k) + \mu_{ji}\delta\theta_{i,j}\right)dV \text{ and } \delta W_E = -\int_S \left(T_i\delta u_i + m_i\delta\theta_i\right)dS \tag{2.30}$$

By choosing δu_i and $\delta\theta_i$ as specified in Eq. 10, Eq. 30 becomes:

$$\delta W_E = -a_i\int_S T_i dS - b_{ij}\int_S T_i x_j dS - c_{ijk}\int_S T_i x_j x_k dS - \alpha_i\int_S m_i dS - \beta_{ij}\int_S m_i x_j dS \tag{2.31}$$

$$\delta W_I = b_{ij}\int_V \sigma_{ji} dV + c_{ijk}\int_V (\sigma_{ji}x_k + \sigma_{ki}x_j)dV - \alpha_i e_{ijk}\int_V \sigma_{jk} dV + \beta_{ij}\int_V \left(\mu_{ji} + e_{ikl}x_j\sigma_{lk}\right)dV \tag{2.32}$$

Because Eqs. 29, 31 and 32 hold for any values of a_i, b_{ij}, c_{ijk},α_i, and β_{ij}, the following relations are obtained:

$$\int_S T_i dS = 0 \quad i = 1,2,3 \tag{2.33}$$

$$\int_V \sigma_{ij} dV = \int_S x_i T_j dS \quad i,j = 1,2,3 \tag{2.34}$$

$$e_{ijk}\int_V \sigma_{jk} dV = -\int_S m_i dS \quad i = 1,2,3 \tag{2.35}$$

$$\int_V \left(\mu_{ij} + e_{jkl}x_i\sigma_{lk}\right)dV = \int_S x_i m_j dS \quad i,j = 1,2,3 \tag{2.36}$$

$$\int_V (\sigma_{ji}x_k + \sigma_{ki}x_j)dV = \int_S T_i x_j x_k dS \quad i,j = 1,2,3 \tag{2.37}$$

Equation 33 implies the equilibrium of external forces. Equation 34 represents the average stress $\overline{\sigma}_{ij}$ in volume V:

$$\overline{\sigma}_{ij} = \frac{1}{V}\int_V \sigma_{ij} dV = \frac{1}{V}\int_S x_i T_j dS \tag{2.38}$$

Equation 35 is useful to examine the symmetry of $\overline{\sigma}_{ij}$:

$$e_{ikj}\overline{\sigma}_{kj} = -\frac{1}{V}\int_S m_i dS \quad i = 1,2,3 \tag{2.39}$$

$e_{ikj}\overline{\sigma}_{kj} = 0$ when the stress tensor is symmetric (i.e., $\overline{\sigma}_{ij} = \overline{\sigma}_{ji}$). However, $\int_S m_i dS$ is not necessarily equal to zero when there are moments at the external boundary. As previously mentioned, these external moments in granular media may result from contact forces without contact moments. Finally, Eq. 36 becomes:

$$\frac{1}{V}\int_V \left(\mu_{ij} + e_{jkl}x_i\sigma_{lk}\right)dV = \overline{\mu}_{ij} + e_{jkl}\overline{\Sigma}_{ilk} \tag{2.40}$$

where $\overline{\Sigma}_{ijk}$ is the average moment of stress:

$$\overline{\Sigma}_{ijk} = \frac{1}{V}\int_V x_i\sigma_{jk}dV \tag{2.41}$$

In summary, the internal work becomes:

$$\delta W_I = V\left(b_{ij}\overline{\sigma}_{ji} + c_{ijk}(\overline{\Sigma}_{kji} + \overline{\Sigma}_{jki}) - \alpha_i e_{ijk}\overline{\sigma}_{jk} + \beta_{ij}(\overline{\mu}_{ji} + e_{ikl}\overline{\Sigma}_{jlk})\right) \tag{2.42}$$

Definition of average stresses in granular media

The average stresses in the equivalent continuum are defined by postulating that the granular and continuous media produce identical internal and external works:

$$\delta W_I^D = \delta W_I \text{ and } \delta W_E^D = \delta W_E \tag{2.43}$$

Average stress

Because Eq. 43 applies to arbitrary values of b_{ij}, the average stress is:

$$\overline{\sigma}_{ij} = \frac{1}{V}\sum_{c\in I}(x_i^b - x_i^a)f_j^c = \frac{1}{V}\sum_{e\in E} x_i^{ae} f_j^e \tag{2.44}$$

Equation 44 is identical to those derived by Weber (1966), Goddard (1977), Christoffersen et al. (1981), and Rosenberg and Selvadurai (1981). In the case of spherical and cylindrical particles *a* and *b*, which are in contact at point *c* with unit

normal vector n_i^c (i.e., $x_i^b - x_i^a = (R_a + R_b)n_i^c$), due to the opposite sign of contact forces and contact normals (i.e., $f_i^{ca} = -f_i^{cb}$ and $n_i^{ca} = -n_i^{cb}$), Eq. 44 becomes:

$$\overline{\sigma}_{ij} = \frac{1}{V}\sum_{c\in I}(R_a + R_b)n_i^c f_j^c = \frac{1}{V}\sum_{a\in B}\sum_{c\in I_a} R_a n_i^{ca} f_j^{ca} \tag{2.45}$$

Symmetry of average stress

Because Eq. 43 applies to arbitrary values of α_j, one obtains:

$$e_{ijk}\overline{\sigma}_{jk} = \frac{1}{V}\sum_{c\in I} e_{ijk}(x_j^b - x_j^a)f_k^c = -\frac{1}{V}\sum_{e\in E} M_i^{ae} = \frac{1}{V}\sum_{e\in E} e_{ijk}x_j^{ae}f_k^e \quad i = 1,2,3 \tag{2.46}$$

Equation 46, which can also be obtained directly from Eq. 44, is useful to determine the amplitude of stress asymmetry. This amplitude can also be characterized by $\overline{\sigma}_{ij} - \overline{\sigma}_{ji}$ as follows:

$$\overline{\sigma}_{ij} - \overline{\sigma}_{ji} = \frac{1}{V}\sum_{e\in E}\left(x_i^{ae}f_j^e - x_j^{ae}f_i^e\right) = -(e_{ijk} - e_{jik})\frac{1}{V}\sum_{e\in E} M_k^{ae} \tag{2.47}$$

Equation 47 implies that the average stress may be asymmetric, even when there is no moment at contacts (i.e., $m_i^e = 0$). The asymmetry results from the sum of the external moments that are created by external forces f_i^e about the particle centers.

The amplitude of stress asymmetry increases with the area S on which the external moments are applied, but decreases with the volume size V. If the external moments are assumed to have bounded values, the amplitude of stress asymmetry decreases with V/S. When $V \to \infty$, the effects of external moments vanish, and the average stress is symmetric. This applies with or without contact moments.

In the case of spherical and cylindrical particles, Eq. 47 becomes:

$$\overline{\sigma}_{ij} - \overline{\sigma}_{ji} = \frac{1}{V}\sum_{a\in B}\sum_{c\in I_a} R_a\left(n_i^{ac}f_j^{ac} - n_j^{ac}f_i^{ac}\right) = \frac{1}{V}\sum_{c\in I}(R_a + R_b)\left(n_i^{ac}f_j^{ac} - n_j^{ac}f_i^{ac}\right) \tag{2.48}$$

Equation 48 shows that $\overline{\sigma}_{ij}$ is not necessarily symmetric when the particles are spheres or cylinders of identical radius. This result, which is in disagreement with Caillerie (1991) and Chang and Liao (1990), will later be verified in a particular example.

Average micropolar stress and first moment of stress

Because Eq. 43 applies to arbitrary values of β_{ij} and c_{ijk}, the following relations are obtained:

$$\overline{\mu}_{ji} + e_{ikl}\overline{\Sigma}_{jlk} = \frac{1}{V}\sum_{c\in I}\left(e_{ikl}f_l^c\left(x_j^b(x_k^c - x_k^b) - x_j^a(x_k^c - x_k^a)\right) + m_i^c(x_j^b - x_j^a)\right) = \frac{1}{V}\sum_{e\in E} M_i^{ae}x_j^{ae}$$

$$i,j = 1,2,3 \tag{2.49}$$

$$\overline{\Sigma}_{kji} + \overline{\Sigma}_{jki} = \frac{1}{V}\sum_{c\in I} f_i^c(x_j^b x_k^b - x_j^a x_k^a) = \frac{1}{V}\sum_{e\in E} f_i^{ae}x_j^{ae}x_k^{ae} \quad i,j,k = 1,2,3 \tag{2.50}$$

Therefore the external moments M_i^{ae}, which result from external contact force f_i^e and/or contact moment m_i^e, generate not only asymmetric stress but also couple stress and first stress moment. This result is in agreement with Eq. 26, which states that couple stresses are required to balance asymmetric stresses. However, the present approach provides only the sums $\overline{\mu}_{ji} + e_{ikl}\overline{\Sigma}_{jlk}$ and $\overline{\Sigma}_{kji} + \overline{\Sigma}_{jki}$, and unfortunately not each term $\overline{\mu}_{ji}$ and $\overline{\Sigma}_{jlk}$.

Alternate definition of average stress

The average stress can also be defined based on statics, instead of virtual work (e.g., Cundall and Strack, 1978). The average stress within volume V is defined as the weighted average of the stress $\overline{\sigma}_{ij}^a$ for each particle a of B:

$$\overline{\sigma}_{ij}^* = \frac{1}{V}\sum_{a\in B}\overline{\sigma}_{ij}^a V_a \tag{2.51}$$

where V_a is the volume of particle a, and:

$$\overline{\sigma}_{ij}^a = \frac{1}{V_a}\int_{V_a}\sigma_{ij}\,dV \tag{2.52}$$

By using Eq. 34, and replacing the traction vector T_i with discrete contact force f_i^c, $\bar{\sigma}_{ij}^a$ becomes:

$$\bar{\sigma}_{ij}^a = \frac{1}{V_a}\int_{S_a} x_i T_j dS = \frac{1}{V_a}\sum_{c\in C_a} x_i^c f_j^c \tag{2.53}$$

Because the contact forces are opposite at internal contacts (i. e., $f_j^{ca} = -f_j^{cb}$), the average stress $\bar{\sigma}_{ij}^*$ is:

$$\bar{\sigma}_{ij}^* = \frac{1}{V}\sum_{a\in B}\sum_{c\in C_a} x_i^c f_j^c = \frac{1}{V}\sum_{c\in I} x_i^c (f_j^{ca} + f_j^{cb}) + \frac{1}{V}\sum_{e\in E} x_i^e f_j^e = \frac{1}{V}\sum_{e\in E} x_i^e f_j^e \tag{2.54}$$

Note that x_i^e in Eq. 54 refers to contact point e, whereas x_i^{ae} in Eq. 44 refers to the center of the particle a where contact e takes place. $\bar{\sigma}_{ij}^*$ and $\bar{\sigma}_{ij}$ are related through:

$$\bar{\sigma}_{ij}^* = \bar{\sigma}_{ij} + \frac{1}{V}\sum_{e\in E}\left(x_i^e - x_i^{ae}\right) f_j^e \tag{2.55}$$

The symmetry of $\bar{\sigma}_{ij}^a$ results from the equilibrium of moments about the coordinate origins for particle a, i.e.:

$$e_{ijk}\bar{\sigma}_{jk}^a = \frac{1}{V_a}\sum_{c\in C_a} e_{ijk} x_j^c f_k^c = 0 \quad i = 1,2,3 \tag{2.56}$$

The stress $\bar{\sigma}_{ij}^*$ is therefore symmetric because it is the weighted sum of symmetric $\bar{\sigma}_{ij}^a$. The symmetry of $\bar{\sigma}_{ij}^*$ can also be shown by using Eq. 54 and invoking the equilibrium of external moments about the coordinate origin (i.e., Eq. 22).

The symmetry of $\bar{\sigma}_{ij}^*$ has significant implications in computational granular mechanics, especially for the computer simulations using dynamic relaxation to solve the equilibrium equations of statics (e.g., Cundall and Strack, 1978; Bardet and Proubet, 1991). When there is no moment at contacts, $\bar{\sigma}_{ij}^*$ should be symmetric, and any computed asymmetry of $\bar{\sigma}_{ij}^*$ should be interpreted as inaccurate calculation and/or lack of static equilibrium.

In the case of spherical and cylindrical particles of radius R_a, $x_i^c = x_i^a + R_a n_i^c$, the average stress $\bar{\sigma}_{ij}^*$ becomes:

$$\bar{\sigma}_{ij}^* = \frac{1}{V}\sum_{a\in B}\frac{1}{V_a}\sum_{c\in C_a}(x_i^a + R_a n_i^c) f_j^c = \frac{1}{V}\sum_{a\in B}\frac{R_a}{V_a}\sum_{c\in C_a} n_i^c f_j^c = \frac{1}{V}\sum_{a\in B} R_a \sum_{c\in C_a} n_i^c f_j^c \qquad (2.57)$$

Equation 57 is the same as that obtained by Cundall and Strack (1979).

Examples

We will illustrate the circumstances of stress asymmetry in the case of double and multiple layer interfaces filled with cylindrical or spherical particles.

Example 1: Double layer interface

The stresses $\bar{\sigma}_{ij}$ and $\bar{\sigma}_{ij}^*$ can be calculated analytically for the particular example of Fig. 3, which represents an interface made of p columns each having two particles. The columns have the same height but are made of particles of various diameters. The particle assembly is subjected to the normal force N_p and shear force S_p, which are assumed to be distributed evenly onto each particle column; the normal and shear forces acting at all contacts are $N = N_p/p$ and $S = S_p/p$, respectively. The contact direction between two particles is identical for all particles in contact. It is characterized by the unit vector **n** of component $n_1 = \sin\theta$ and $n_2 = \cos\theta$. The equilibrium of forces and moments for all particles and the top plate are satisfied when:

$$S = N n_1/(1+n_2) = N\tan(\theta/2) \qquad (2.58)$$

All the contact forces have the same inclination $\theta/2$ relative to the contact direction **n**. The contacts do not slip and the interface remains stable as long as θ remains smaller than 2ϕ, where ϕ is the friction angle between two particles. For the calculation of $\bar{\sigma}_{ij}$, it is convenient to select the coordinate axis at the center of particle 2. In this coordinate system, the center coordinates of particle 1 are:

$$x_1^{1e} = n_1 L \quad \text{and} \quad x_2^{1e} = n_2 L \qquad (2.59)$$

where $L = R_1 + R_2$. By using Eqs. 44 and 59, the stresses $\bar{\sigma}_{ij}$ are:

$$\bar{\sigma}_{11} = -n_1 S/A, \quad \bar{\sigma}_{22} = -\frac{(1+n_2)n_2}{n_1} S/A,$$
$$\bar{\sigma}_{12} = -(1+n_2)S/A, \text{ and } \bar{\sigma}_{21} = -n_2 S/A \tag{2.60}$$

where $A = V/L$, and V is the average volume of particle columns. For interfaces filled with cylindrical or spherical particles, V can be evaluated as follows:

$$V = (1+n_2)LW_1W_2 \tag{2.61}$$

where W_1 is the average width of particle columns in the x_1-direction. For cylindrical particles, W_2 is the particle length. For spherical particles, W_2 is the average width of particle columns in the x_2-direction. Both W_1 and W_2 depend on the density of particles in the interface.

The external moments M_i^{ae} acting on particles 1 and 2 are:

$$M_3^1 = R_1 S \quad \text{and} \quad M_3^2 = R_2 S \tag{2.62}$$

By using Eq. 47 or 60, the amplitude of stress asymmetry is:

$$\bar{\sigma}_{12} - \bar{\sigma}_{21} = -\frac{M_3^1 + M_3^2}{V} = -S/A \tag{2.63}$$

The stress asymmetry vanishes when $S = 0$, i.e., when the particle columns are vertical. As previously stated in Eq. 48, $\bar{\sigma}_{ij}$ is not necessarily symmetric for particles of identical radius (e.g., $R_1 = R_2$). The couple stress and first stress moment is:

$$\bar{\mu}_{13} + \bar{\Sigma}_{121} - \bar{\Sigma}_{112} = R_1 n_1 S/A \quad \text{and} \quad \bar{\mu}_{23} + \bar{\Sigma}_{221} - \bar{\Sigma}_{212} = R_1 n_2 S/A \tag{2.64}$$

For the calculation of $\bar{\sigma}_{ij}^*$, it is convenient to select the coordinate axis at the lowest external contact. The coordinates of the highest contact are therefore:

$$x_1^e = n_1 L \quad \text{and} \quad x_2^e = (1+n_2)L \tag{2.65}$$

and the stress $\bar{\sigma}_{ij}^*$ is:

$$\bar{\sigma}^*_{11} = -n_1 S/A, \quad \bar{\sigma}^*_{22} = -\frac{(1+n_2)^2}{n_1} S/A, \text{ and } \bar{\sigma}^*_{12} = \bar{\sigma}^*_{21} = -(1+n_2)S/A \tag{2.66}$$

As expected, $\bar{\sigma}^*_{ij}$ is symmetric. $\bar{\sigma}^*_{ij}$ and $\bar{\sigma}_{ij}$ are related through:

$$\bar{\sigma}^*_{11} = \bar{\sigma}_{11}, \quad \bar{\sigma}^*_{22} = \bar{\sigma}_{22} - \frac{(1+n_2)}{n_1} S/A, \quad \bar{\sigma}^*_{12} = \bar{\sigma}_{21}, \text{ and } \bar{\sigma}^*_{21} = \bar{\sigma}_{21} - S/A \tag{2.67}$$

Figure 4 compares the normalized variation of $\bar{\sigma}^*_{ij}$ and $\bar{\sigma}_{ij}$ when the angle $\theta = \tan^{-1}(n_1/n_2)$ varies from 0 to 90°. The stress asymmetry (i.e., $\bar{\sigma}_{12} - \bar{\sigma}_{21}$) remains constant and independent from θ.

Example 2: Multi-layer interface

As shown in Fig. 5, the multi-layer interface model is made of p columns of particles, each column i having q_i particles (q_i must be an even number). This multi-layer model is a generalization of the two-layer model, which corresponds to $q_i = 2$ for $i = 1,\ldots,p$. The particle columns have the same height and contact direction **n**, but may have different numbers q_i of particles. All the particles and the top platen are in static equilibrium when Eq. 58 is satisfied; the contact forces are identical to those of the two-layer model. The average stresses in the interface can be determined by averaging the average stresses in each column. Hereafter, we will calculate only the average stresses in a column.

After selecting the coordinate axis at the center of particle q_i, the center coordinates of particle 1 are:

$$x_1 = n_1 L \quad \text{and} \quad x_2 = (1+n_2)L - (R_1 + R_{q_i}) \tag{2.68}$$

where $L = \sum_{j=1}^{q_i} R_j$. The average stresses $\bar{\sigma}_{ij}$ in column i are:

$$\begin{aligned} &\bar{\sigma}_{11} = -n_1 S/A, \quad \bar{\sigma}_{22} = -\frac{(1+n_2)^2}{n_1} S/A + \frac{R_1 + R_{q_i}}{V} \frac{1+n_2}{n_1} S, \\ &\bar{\sigma}_{12} = -(1+n_2)S/A, \text{ and } \bar{\sigma}_{21} = -(1+n_2)S/A + \frac{R_1 + R_{q_i}}{V} S \end{aligned} \tag{2.69}$$

where A and V are defined as for the double layer interface. The values of $\overline{\sigma}_{11}$ and $\overline{\sigma}_{12}$ are identical to those in Eqs. 60, whereas the corresponding values of $\overline{\sigma}_{22}$ and $\overline{\sigma}_{21}$ are different. The differences however vanish when $V \to \infty$. The stresses $\overline{\sigma}^{*}_{ij}$ in the multi-layer are identical to those of the double layer interface (i.e., Eq. 66). As predicted by Eq. 69, $\overline{\sigma}_{ij}$ converges toward $\overline{\sigma}^{*}_{ij}$ when volume V becomes large (i.e., $q \to \infty$). The external moments M_i^{ae} acting on particle 1 and q_i are:

$$M_3^1 = R_1 S \quad \text{and} \quad M_3^{q_i} = R_{q_i} S \tag{2.70}$$

These external moments are responsible for the stress asymmetry as follows:

$$\overline{\sigma}_{12} - \overline{\sigma}_{21} = -S(R_1 + R_{q_i})/V \tag{2.71}$$

The amplitude of stress asymmetry decreases with the number of particles in the columns, and increases with the size of particles at the top and bottom of columns. The stress becomes symmetric when the column height becomes infinite (i.e., $q \to \infty$). The couple stress and first stress moment are:

$$\begin{aligned} \overline{\mu}_{13} + \overline{\Sigma}_{121} - \overline{\Sigma}_{112} &= R_1 n_1 S/A \\ \overline{\mu}_{23} + \overline{\Sigma}_{221} - \overline{\Sigma}_{212} &= R_1(1+n_2)S/A - R_1(R_1 + R_{q_i})S/V \end{aligned} \tag{2.72}$$

In contrast to the asymmetric stress components, $\overline{\mu}_{ij} + e_{ikl}\overline{\Sigma}_{jlk}$ does not decrease when the volume V becomes large (i.e., $q \to \infty$).

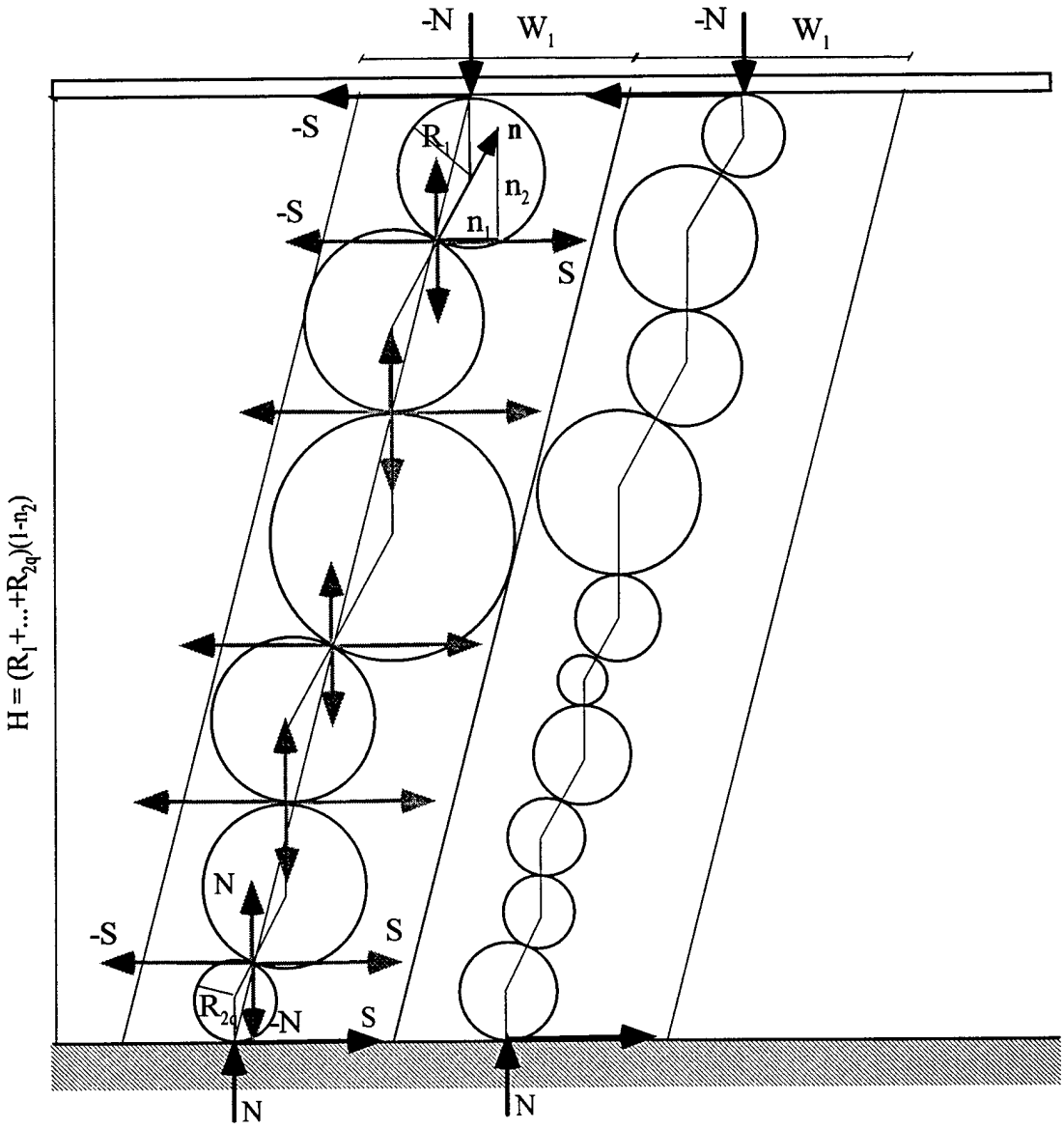

Figure 21. Multi-layer interface model for calculation of average stress.

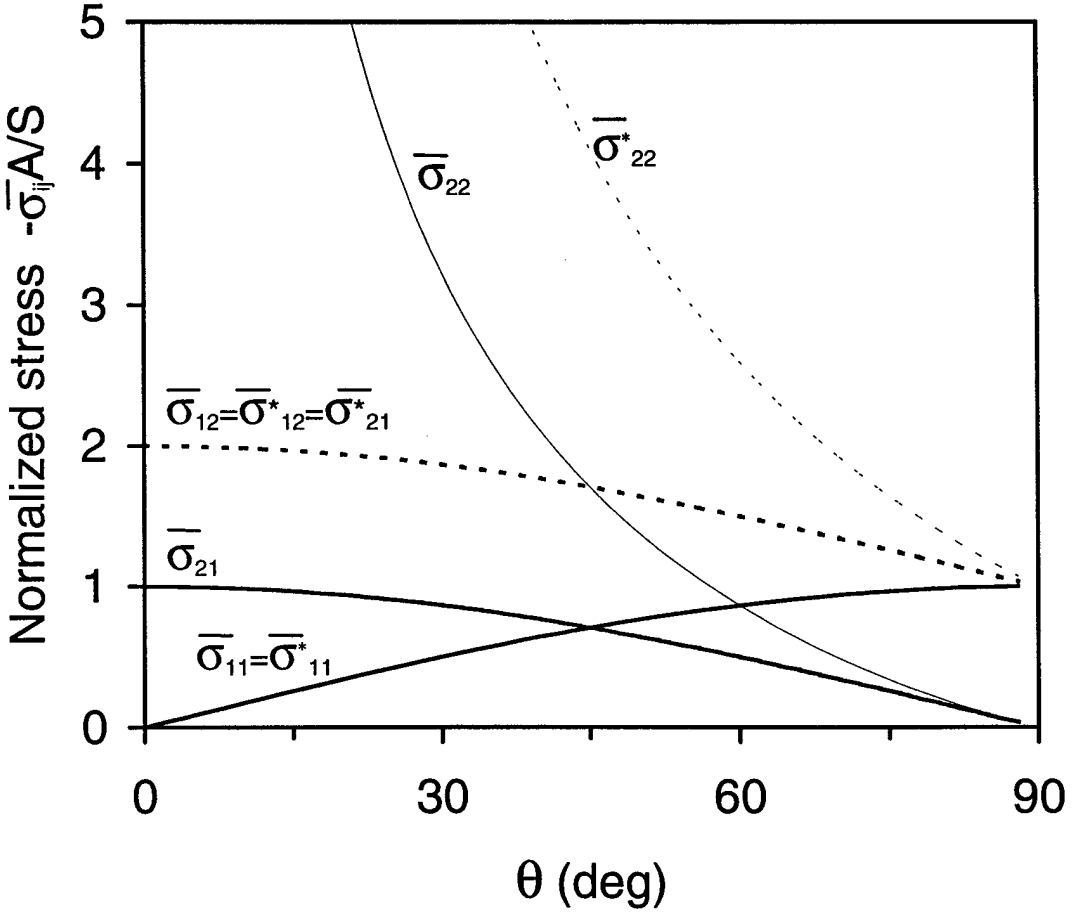

Figure 22. Variation of normalized stresses of $\bar{\sigma}_{ij}A/S$ and $\bar{\sigma}^{*}_{ij}A/S$ with angle θ.

Discussion

The asymmetry of stress depends on the way stresses are defined. Stresses defined by statics are symmetric when there is no contact moment. However stresses defined by virtual work may become asymmetric when there is no contact moment. Our analysis differs from previous ones (e.g., Christoffersen et al., 1981; and Chang and Liao, 1990) because we considered external moments, and established the circumstances and amplitude of stress asymmetry. In agreement with Caillerie (1991), we found that the asymmetry originates from external moments, and that the amplitude of stress asymmetry decreases with the size of the granular volume. The stress asymmetry is therefore more detectable in elongated samples subjected to external moments on their boundary. Bulky samples subjected to small external moments are likely to display negligible stress asymmetry. The stress asymmetry can rightfully be neglected in large masses of granular media far away from boundaries with external moments. However, it may become important in interfaces with significant external moments. There is a need for verifying these findings through computer simulations and laboratory experiments.

Conclusion

We have derived the conditions for the asymmetry of stress in granular materials, and shown that there is asymmetry even when the particle contacts do not transmit moments. This stress asymmetry is obtained when the stress is defined from virtual work, but is lost when the stress is defined from statics. The asymmetry results from external moments applied by external forces. We also show that the amplitude of stress asymmetry decreases with the ratio V/S between surface S and volume V. When V/S becomes very large, the stress asymmetry disappears, with or without external contact moments.

PART III. EXPERIMENTAL INVESTIGATION

Parts I and II of this report covered some of the computational and theoretical approaches for investigating material instability in granular materials. Part III devises an experimental approach to provide these computational and theoretical approaches with relevant and detailed experimental data sets. Specimens of idealized granular media were constructed and tested in the laboratory, and the displacement and rotation of particles were measured using stereophotogrammetry. The laboratory tests were conducted at the University of Southern California; the stereophotogrammetric measurements were carried out at the Joseph Fourier University, in Grenoble, France.

Stereophotogrammetry was found to be the best suited techniques for measuring accurately the displacements and rotations of a large number of nearly identical particles. At the time of this investigation, this optical technique revealed to be more accurate and practical than computer vision methods based on existing digital cameras. The accurate experimental results generated in this study are useful to assess the applicability of higher-order continua to granular behavior, and are therefore instrumental to understand material instabilities within granular media.

The first section of Part III reviews the background that motivated our experimental investigation. The second section describes the experimental set-up and the stereophotogrammetric measurements. The third and last section describes experimental data processing and presents processed results.

Background

Deformations within granular soils are commonly concentrated in narrow zones called shear bands, the thickness of which are 8-10 times the mean grain diameter (Roscoe 1970; Muhlhaus and Vardoulakis 1987). The relation between shear band width and grain size has profound implications in laboratory and centrifuge testing of reduced-scale models. It implies that grain sizes must also be scaled down in laboratory and centrifuge models for simulating the progressive failure of in-situ granular masses.

Hill (1962), Mandel (1963), Rudnicki and Rice (1976) successfully analyzed the emergence and inclination of shear bands, but, since their constitutive theories included no internal length scale, they did not address the problem of shear-band thickness. Aifantis (1984, 1987) and Zbib and Aifantis (1989) introduced an internal length scale by including second- and fourth-order strain gradients into the yield condition of plasticity. The higher-order strain gradients allowed them to account for the thickness, spacing, and velocity of shear bands in metals. Vardoulakis and Aifantis (1989) applied a similar approach to soils by adding second-order strain gradients to the flow rule of plasticity.

As an alternative to higher-order strain gradient theories, Muhlhaus (1986), Muhlhaus and Vardoulakis (1987), and Vardoulakis (1989) introduced an internal length scale by using the micropolar (Cosserat) theory. Although based on different physical assumptions, both micropolar and strain gradient approaches successfully detect the emergence of shear bands and calculate their inclination and thickness. Zbib and Aifantis (1989) also analyzed the evolution of the deformation within the shear bands of metals. They could not apply it to soils due to lack of relevant experiments on soils.

The structure of shear bands in real granular materials is difficult to investigate by using laboratory experiments. The radiographic techniques with lead shots (Roscoe, 1963) estimate the shear band thickness but are not accurate enough to measure the localized field of displacement. The stereophotogrammetric technique of Desrues (1984) measures the displacement but not the rotation of particles. The numerical simulation techniques of Bardet and Proubet (1989, 1991, 1992), and Bardet (1994) provided extensive information on the displacement and rotation of particles but are only numerical substitutes to actual laboratory experiments.

Herein, we present an experimental approach that generates experimental data sets on cylindrical rods and is useful to investigate the application of higher-order continuum theories to granular media. Cylindrical rods, in place of real granular material, are tested under confined axial compression, in an attempt to emulate plane-strain compression tests on real soils. Stereophotogrammetry (Desrues, 1984) are used to determine the displacement and rotation of particles. Stereophotogrammetry was preferred over other

techniques for measuring the displacement of particles. It visualizes displacement fields as a false relief, and automatically tracks particles between two successive photographs. This is a great benefit in the case of large assemblies of nearly identical particles. Stereophotogrammetry automatically digitizes and recognizes individual particles between successive photographs.

Axial compression of idealized granular media

Sample composition and fabrication

As listed in Tables 1 and 2 and shown in Fig. 23, two tests, hereafter referred to as A and B, were carried out; the specimens of tests A and B were made of a total of 1848 cylindrical acrylic rods having for nominal diameter 4, 6 and 8 mm. Specimens A and B had a slightly different slenderness ratio. All rods are made of transparent acrylic material with an average density of 1.3 g/cm^3. The rods were carefully cut to the same length of 10 cm; their faces were perpendicular and transparent as much as possible. Front faces were half painted black in order to track simultaneously rotations and displacements. After a careful inspection, the acrylic rods were found to be slightly imperfect cylinders. Their diameters, as measured with a caliper, slightly vary in the radial and longitudinal directions. Table 3 summarizes average diameter and diameter variation $\Delta\phi$ for a small sample of arbitrarily selected rods. The average diameter is 8.12, 6.19 and 4.22 mm, in comparison to the nominal values of 8 mm, 6 mm and 4 mm. Measured diameters vary typically less than 1%. The black paint was also found not to divide exactly particles in half, and could not be used to determine particle diameters.

Table 1. Particle size distribution for samples A and B of idealized granular material.

Nominal Diameter (mm)	Measured Average Diameter (mm)	Number of Particles		
		Complete Specimen	Stereo Sample A	Stereo Sample B
4.0	4.22	1040	458	419
6.0	6.19	532	243	248
8.0	8.12	266	129	120

Figure 23. Assembly of cylindrical rods subjected to axial compression.

Table 2. Result summary of tests A and B

TEST	Slenderness ratio H/L	Initial Young's Modulus E (MPa)	Ultimate Strength σ_{max} (kPa)	Friction angle at peak failure ϕ_{max} (deg)	Strain at peak failure $\varepsilon_{\phi max}$ (%)	Number of particles digitized
A	2.43	304	84	18.4	3.10	830
B	2.81	574	88	18.3	3.24	787

Table 3. Variation of rod diameters on random samples.

		Diameter ϕ(mm)										
	Trial No.	1	2	3	4	5	Average	Min	Max	$\Delta\phi$ (mm)	$\Delta\phi/\phi$ (%)	Average
8 mm rod	1	8.26	8.18	8.22	8.19	8.23	8.22	8.18	8.26	0.08	0.97	8.12
	2	8.07	8.11	8.15	8.09	8.05	8.09	8.05	8.15	0.10	1.24	
	3	8.04	8.05	8.08	8.07	8.02	8.05	8.02	8.08	0.06	0.75	
6 mm rod	1	6.11	6.08	6.08	6.12	6.07	6.09	6.07	6.12	0.05	0.82	6.19
	2	6.31	6.26	6.27	6.30	6.26	6.28	6.26	6.31	0.05	0.80	
	3	6.20	6.21	6.15	6.20	6.19	6.19	6.15	6.21	0.06	0.97	
4 mm rod	1	4.25	4.25	4.22	4.21	4.24	4.23	4.21	4.25	0.04	0.94	4.22
	2	4.24	4.23	4.22	4.26	4.25	4.24	4.22	4.26	0.04	0.94	
	3	4.19	4.17	4.22	4.19	4.21	4.20	4.17	4.22	0.05	1.19	
									Average $\Delta\phi/\phi$ (%) =		0.96	

Experimental setup for axial compression

Figures 24 shows the experimental set up. The test specimen of Fig. 23 is enclosed in a 0.15 mm thick transparent latex membrane and has circular loading platens at its top and bottom. The membrane is clamped to both platens with compression rings. During the sample fabrication, the membrane is stretched on a rectangular mold, and the rods are manually positioned inside the mold with their axis parallel to one another. Specimens A and B have therefore a different packing, in addition to a different slenderness ratio. Vacuum is applied inside the membrane, which is equivalent to applying an external constant confining pressure to specimens. The equivalent confining pressure was equal to 94.8 kPa. The axial compression is applied by raising the bottom platen at the constant rate of 5.6 mm/min.

As shown in Fig. 24, a light box behind the sample reflects and diffuses the light of a 120 watts bulb through a polished glass. A Nikon FE2 35 mm camera is positioned approximately one meter in front of the specimen. It is equipped with a macrolens to limit optical distortion. The film was a hard contrast, black and white ortho film, 25 ASA, with a fine grain. The camera aperture speed was set to one second.

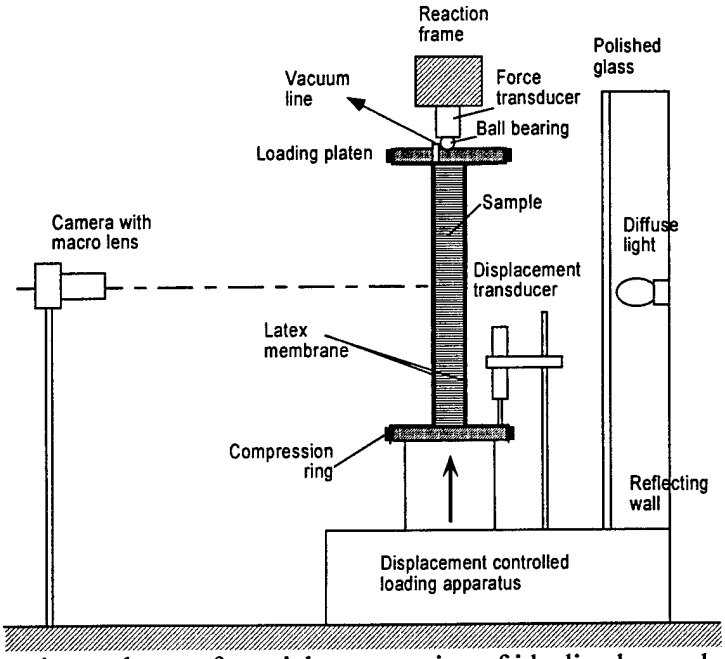

Figure 24. Experimental setup for axial compression of idealized granular materials.

Results

Specimens A and B were tested similarly by increasing the axial force while keeping the confining pressure (i.e., internal vacuum) constant. The stress-strain curves obtained during tests A and B are shown in Fig. 25. The axial strain ε is

$$\varepsilon = \Delta h / h_o \tag{3.1}$$

where Δh is the vertical displacement of the lower platen, and h_o is the initial sample height. The axial stress σ is

$$\sigma = F / A_o \tag{3.2}$$

where F is the measured axial load, and A_o is initial cross-sectional area. Figure 25 shows the stress-train response until 6% axial strain. Both samples failed at approximately at 3% strain. Table 2 summarizes the calculated results for initial Young modulus, peak and residual friction angles, and strain at peak failure for tests A and B. The symbols in Fig. 25 indicate the axial strains at which the photographs were taken.

Eight photographs were digitized in tests A and B. Four photographs were taken at points A1 to A4 during test A, and at points B1 to B4 during test B.

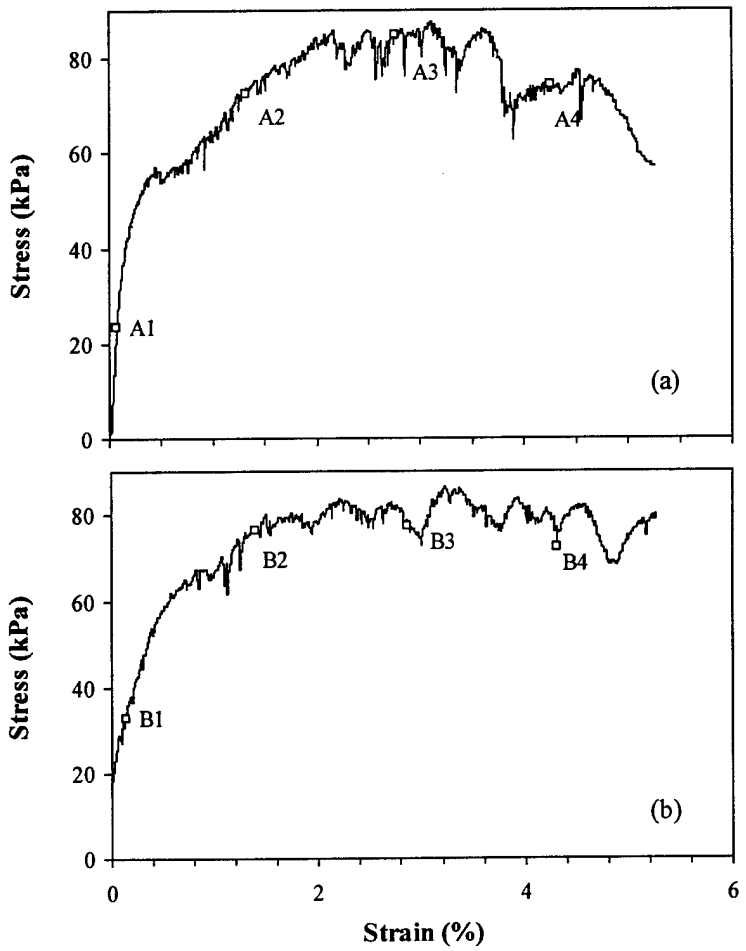

Figure 25. Axial stress-strain response of samples A and B, and location of photographs.

Stereophotogrammetry Measurement

The eight photographs taken during tests A and B were processed by stereophotogrammetry, an optical technique especially suited for tracking the motion of a large number of nearly identical particles.

Principle of stereophotogrammetry for measurement of displacement

The principles of stereophotogrammetric measurement of displacement fields are described in Desrues (1984). The stereophotogrammetry equipment is called stereograph.

The absolute error on measured displacement varies with quality of negatives and operator experiences. In optimum conditions, the stereograph can measure 1 μm at the negative scale, i.e., as small as the grains coating negatives. In our experiment, the absolute error is assumed to be in the order of 10 μm as we used 35 mm negatives, instead of larger negatives.

Application of stereophotogrammetry to kinematics of particles

The 35 mm negatives taken during tests A and B were enlarged to obtain 12.7 x 17.8 cm (5 x 7 inch) negatives, the stereograph using only transparent media. The negatives corresponding to two successive photographs (i.e., A1 and A2) were placed on the stereograph platens. At first, three fixed reference points (F1, F2 and F3 in Fig. 26) were selected close but outside the sample. These three points, which correspond to fixed objects in the laboratory, are references for defining a common coordinate system to all photographs. In principle, the stereograph should indicate that fixed points do not move (i.e., move only within the order of machine accuracy). For experimental reliability, these points are digitized twice. Second, the stereograph software asks to define the area under investigation by selecting four points (see Fig. 26).

Positioning particles requires that three points be digitized for yielding center position and radius of individual particle. Three points are needed because the black paint does not exactly delineate particle diameters. As shown in Fig. 27, points A and B are obvious candidates as they are easily identified. However, point C is a less obvious choice. As explained in a later section on error minimization, point C is chosen as the point farthest away from points *A* and *B*.

ABSTRACT

The research aims at investigating the physical origins of shear band instability in particulate media, and the applicability of higher-order continuum theories for describing material instability in granular media. The particular research objectives are (1) to review the computational tools used for simulating shear bands in idealized granular media, (2) to explore a critical micro-macro transition relevant to material instability (i.e., stress symmetry), and (3) to devise laboratory experiments for generating some experimental data sets useful for numerical and theoretical investigations of material instability in granular media. Our methodology combines computational granular mechanics, higher-order continuum mechanics, and laboratory experiments.

Our comprehensive review of past work on computational granular mechanics reveals the diversity of numerical codes in granular mechanics, and the large number of assumptions entering these codes.

Our theoretical investigation shows that the average stress in granular media, as defined from virtual work, may be asymmetric in the absence of contact moments. We specify the circumstances and amplitude of stress asymmetry, and calculate the corresponding couple stress and first stress moment. We also show that the average stress is always symmetric when it is alternately defined by using statics and no contact moment. The stress asymmetry, which results from external moments, decreases with the volume size. The asymmetric stress, couple stress and first stress moment are analytically calculated in particular examples relevant to shear band instability.

Our experimental methodology is based on the application of stereophotogrammetry to the kinematics of assembly of cylindrical rods, simulating granular media. We are able to measure accurately the kinematics of a large number of nearly identical particles in the laboratory. Our experimental methodology has generated new experimental data sets on granular media useful to re-examine the applicability of higher-order continua to granular media, and are therefore instrumental to understand material instability in granular media.

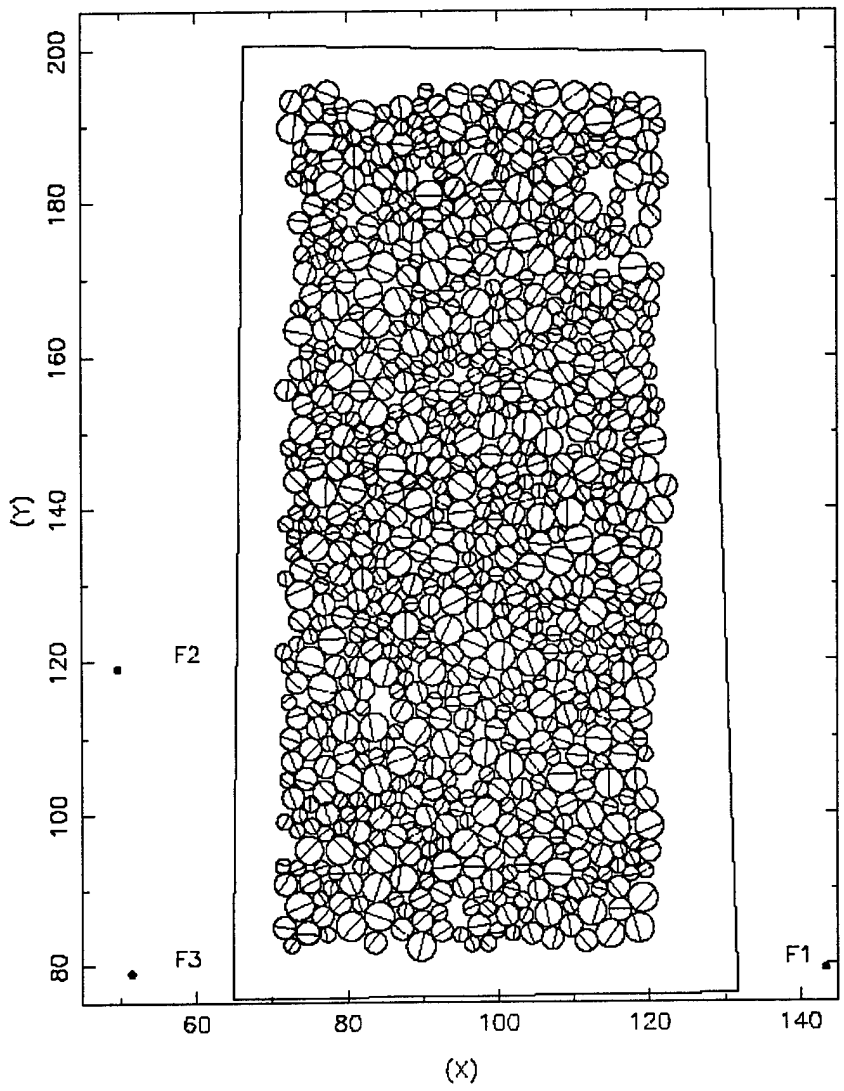

Figure 26. Geometry of sample A, the control points F1 F2 and F3 and the digitizing area.

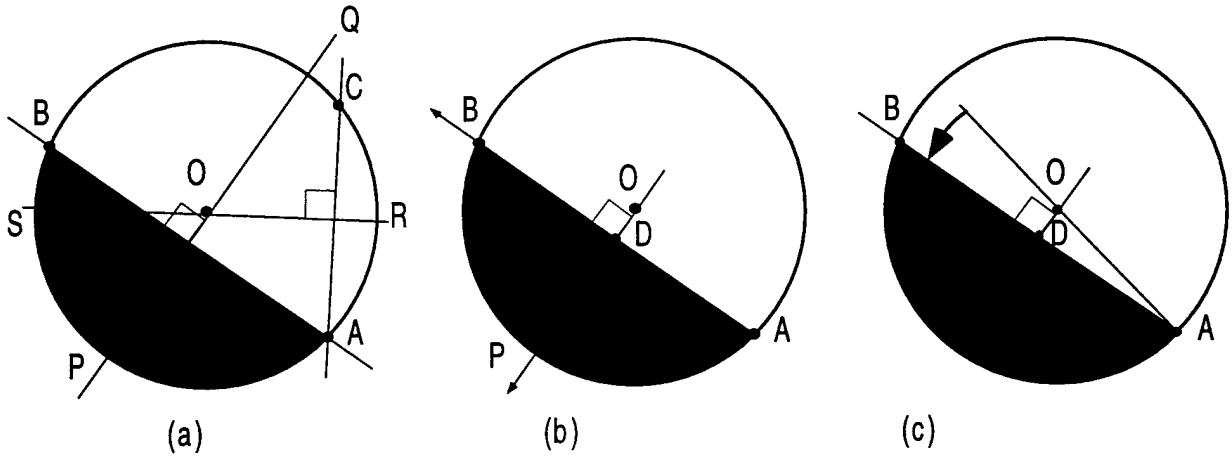

Figure 27. Calculation of center position and radius of particle using three different methods: (a) Method A, (b) Method B, and (c) Method C.

Determination of Assembly Geometry

The stereograph measures the displacement of points A, B and C for individual particles between two successive photographs. As shown in Fig. 27, points A and B are about diametrically opposite, and at the boundary of the painted area. Points A and B are used to track particles between successive photographs. Point C is used to define the center and radius of particles, assuming that particles are perfectly rigid and circular. The stereograph cannot track point C because there is not special mark on particles associated with point C.

Assumption of rigid particles

The assumption of rigid particles was tested by measuring the variation ΔAB of distance AB between the successive steps A1-A2, A2-A3 and A3-A4. In theory, ΔAB should be equal to zero if particles were purely rigid and measurements perfectly accurate. As shown in Fig. 28, the distribution of ΔAB indicates that AB varies less than 1 % between

two successive steps.

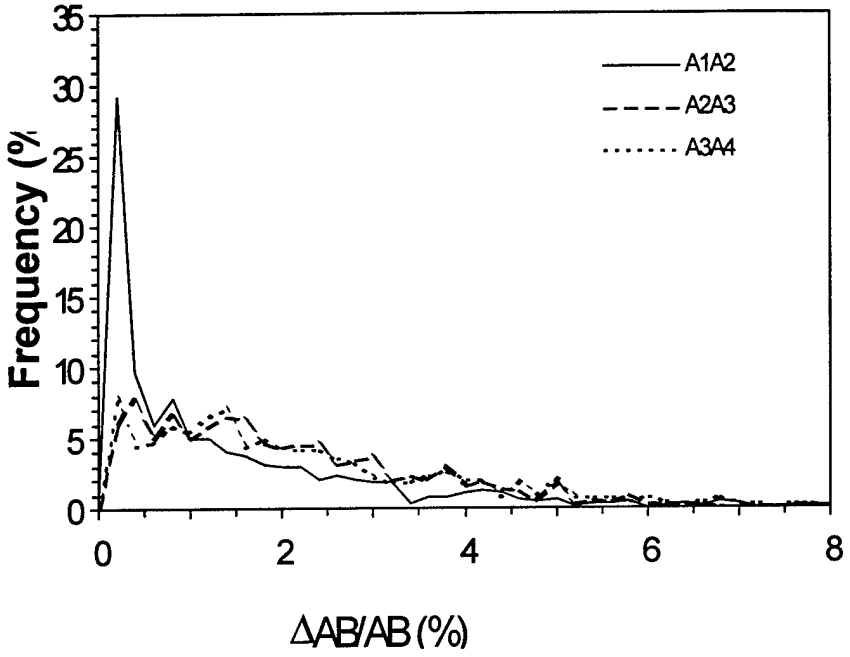

Figure 28. Variation of distance AB at different axial compression of sample A.

Particle center and radius

As shown in Fig. 27, three different methods, labeled A, B and C, were used to calculate the particle center and radius from the raw data measured by the stereograph. The corresponding calculation steps are detailed in the FORTRAN programs GET_AB in APPENDIX.

Method A

Method A calculates the center position and radius of particles, assuming that points A, B and C are on a circle. As shown in Fig. 27a, the circle center O is the intersection of lines PQ and RS passing through the center of segments AB and AC and perpendicular to AB and AC, respectively. Point O, which is the intersection of lines PQ and RS, has the following coordinates (x_0,y_0):

$$\begin{cases} (x_A - x_B)x_0 + (y_A - y_B)y_0 = (x_A^2 - x_B^2)/2 + (y_A^2 - y_B^2)/2 \\ (x_A - x_C)x_0 + (y_A - y_C)y_0 = (x_A^2 - x_C^2)/2 + (y_A^2 - y_C^2)/2 \end{cases} \tag{3.3}$$

where (x_A,y_A), (x_B, y_B) and (x_C,y_C) are the coordinates of points A, B, and C, respectively. Coordinates (x_0,y_0) are always uniquely defined provided that points A, B and C are not aligned. The particle radius R is the distance OA, which is the same as OB and OC.

Methods B and C

As shown in Fig. 27b, Method B assumes that distance OD between segment AB and point O remains constant for a given particle. Method B uses points A and B; it only uses point C at the first step to calculate the initial value of OD.

As shown in Fig. 27c, Method C assumes that angle OAB remains constant for a given particle. Like Method B, Method C uses only point C at the first step to calculate the initial value of angle OAB. Like methods A and B, method C does not fix the distance AB. Methods A, B and C were found to give identical results.

Results on particle diameter

In theory, the measured diameters of rigid particles should remain constant between successive photographs. In practice, the particle diameters, as calculated by methods A, B and C, were found to vary slightly between steps. Figures 29 and 30 show the cumulative distributions of rod diameter, which were calculated from the stereograph at the four stages A1 to A4, and B1 to B4. As shown for sample A in Figs. 29 and 30, the four curves labeled A1 to A4, and B1 to B4, are in good agreement, which establishes that Method A, B and C gives very similar rod diameter between successive photographs.

The staircase line in Figs. 29 and 30, which is labeled "total", represents the cumulative distributions of rod diameter, assuming only three different diameters. The smooth measured distributions indicate that particle diameters vary according to a tri-modal statistical distribution centered about the average values of Table 3. Figures 29 and 30 also show that samples A and B and the complete specimen have slightly different distribution of particles. Not all particles of specimens A and B were digitized. Particles close to the loading caps and close to the lateral boundaries were excluded. As indicated in Table 1, 830 particles were digitized in Specimen A, and 787 particles in Specimen B.

As shown in Table 1, the corresponding number of particles with different diameter in Samples A and B were calculated from Figs. 29 and 30.

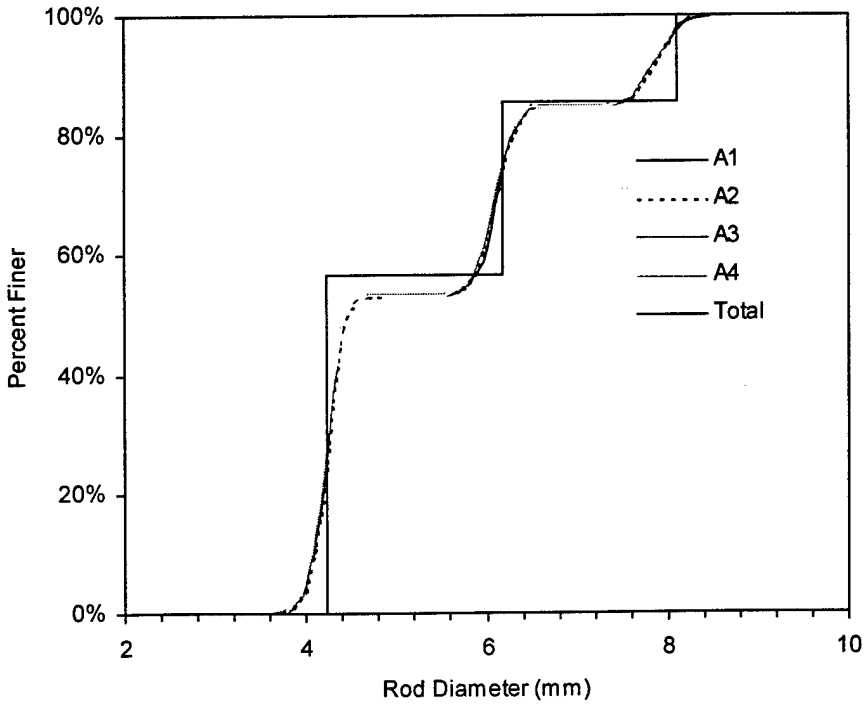

Figure 29. Cumulative rod diameter distribution curves for sample A based (1) on stereo measurement at axial compression stages A1, A2, A3, and A4, and (2) on the complete specimen composition in Table 1.

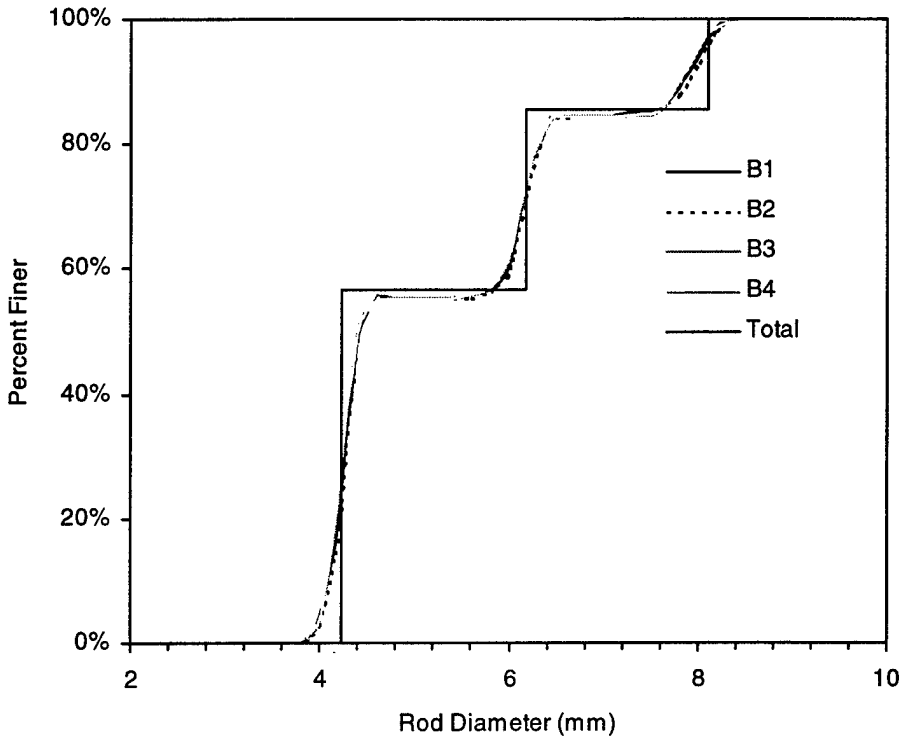

Figure 30. Cumulative rod diameter distribution curves for sample B based (1) on stereo measurement at axial compression stages B1, B2, B3, and B4, and (2) on the complete specimen composition in Table 1.

Figure 31 shows that there is little difference between the cumulative distribution curves for the complete specimen and Samples A and B. Figure 32 shows the variation of particle diameters which is calculated between the axial compression stages A2, A3 and A4 relatively to stage A1. Figure 31 implies that measured particle diameters vary with axial strain. These small variations result from a combination of experimental errors and assumptions on particle rigidity and shape.

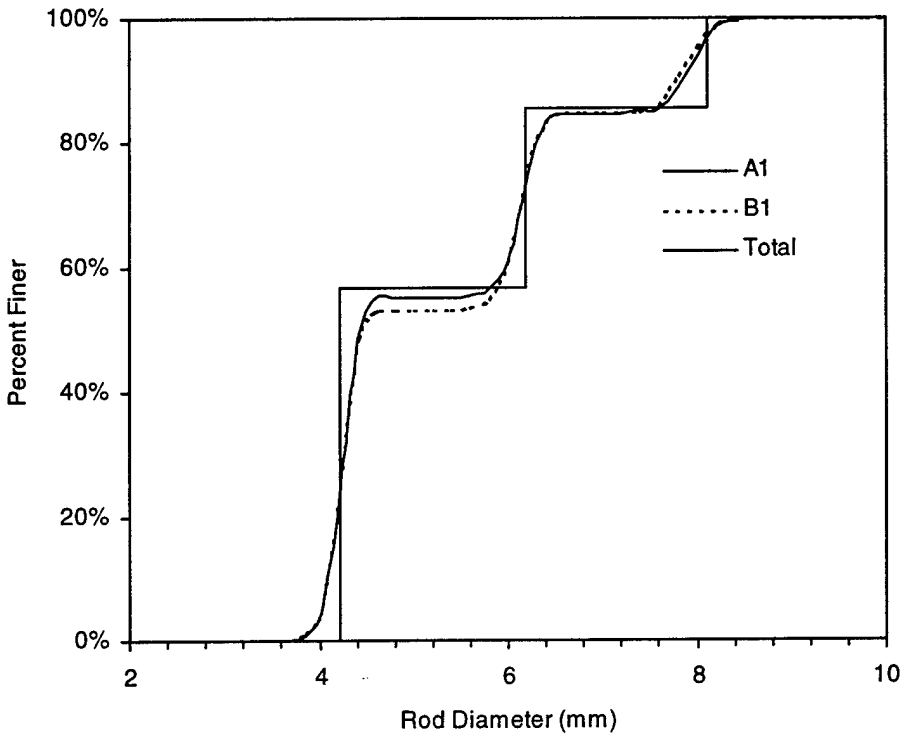

Figure 31. Cumulative rod diameter distribution curves for the complete specimen and Samples A and B.

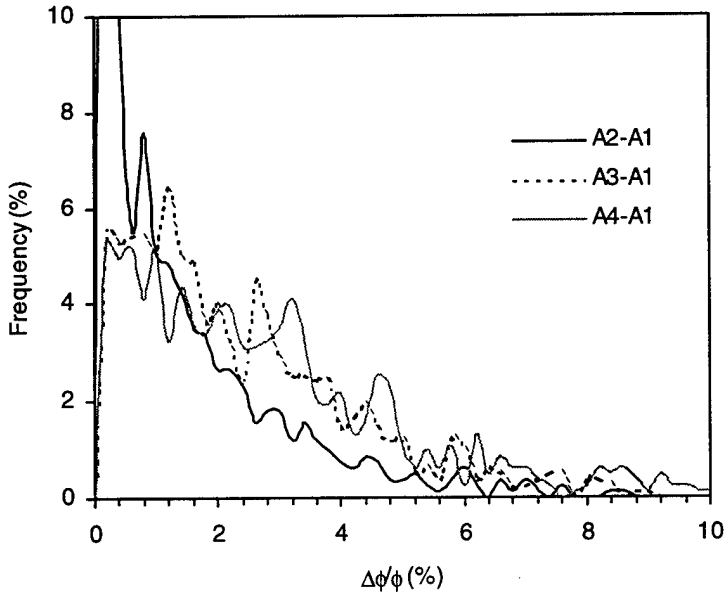

Figure 32. Variation of particle diameter as measured by stereograph at axial compression stages A2, A3, and A4 relatively to stage A1.

Error on center position and radius

Figure 33 shows the graphical determination of errors associated with the determination of particle center O. This graphical construction is more convenient than algebraic derivations of error based on Eq. 3.3. The possible positions of point O is encompassed by the shaded area, which is generated when points A, B and C move independently within the experimental error Δx (i.e., when points A, B and C describe the circles of radius Δx centered about points A, B and C). This graphical construction proves that the error depends of the relative position of points A, B and C. When points A and B are approximately diametrically opposite, the smallest error is obtained when C is the furthest away of points A and B (see Fig. 33a). When point C gets close to point A or B, the shaded area becomes elongated, and the error increases significantly in the direction perpendicular to AB (see Fig. 33b). In summary, an accurate determination of particle center and radius requires to take point C as far as possible from points A and B. In the present investigation, the optimum condition was selected; the error associated with the position of point O is comparable to those of points A and B.

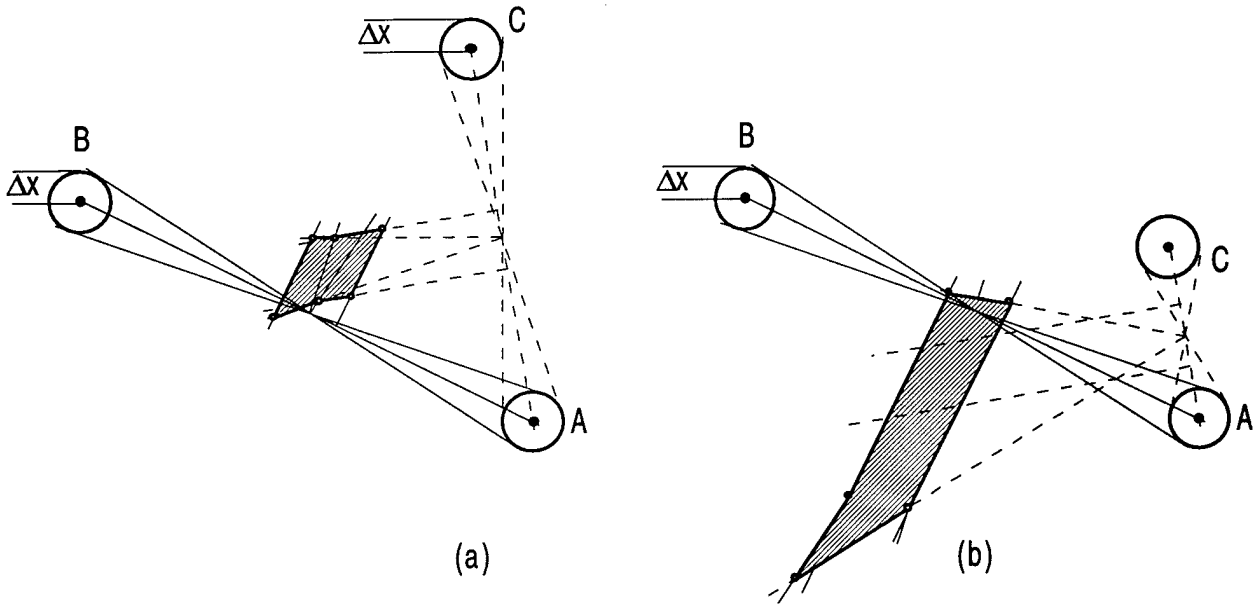

Figure 33. Definition of error for particle center: (a) Point C far away from points A and B, and (b) Point C close to points A or B.

Particle angular position

As sketched in Fig. 34a, when the particle remains rigid, the particle rotation about its center is identical to the rotation of segment AB. Thus, the angular position θ of the particle is:

$$\theta = \tan^{-1}\left(\frac{y_A - y_B}{x_A - x_B}\right) \tag{3.4}$$

The particle and their angular positions for tests A and B are plotted in Figs. 35 and 36. Figure 26 shows a close-up view of sample A.

Error on particle angular position

As shown in Fig. 34b, the error on particle rotation $\Delta\theta$ can be calculated from the error Δx of the position of point *A* and *B*.

$$\Delta\theta = 2\sin^{-1}(2\Delta x/AB) \approx 4\Delta x/AB \tag{3.5}$$

where is it assumed that $\Delta x << AB$. The error $\Delta\theta$ is twice as large for the smallest particles (4 mm) that for the largest particles (8 mm).

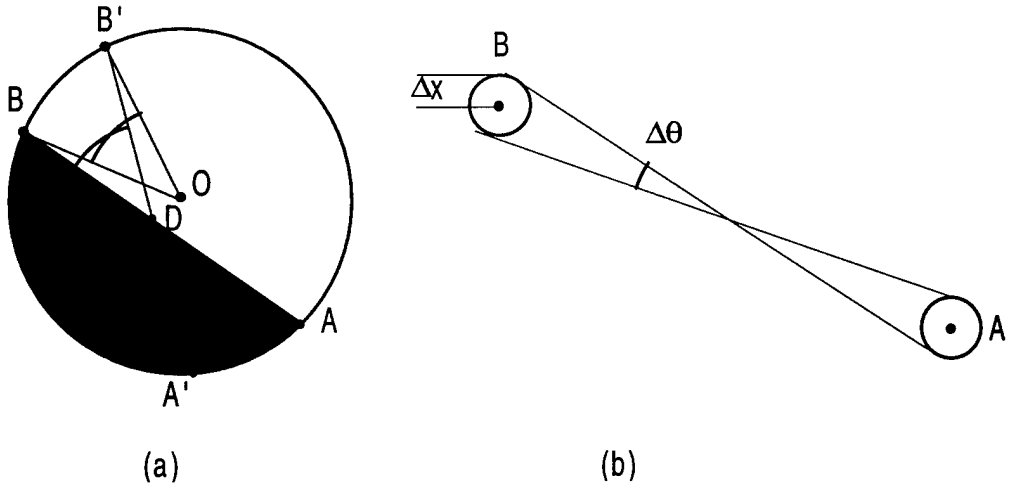

Figure 34. Definition of particle rotation: (a) value of rotation increment and (b) error on determination.

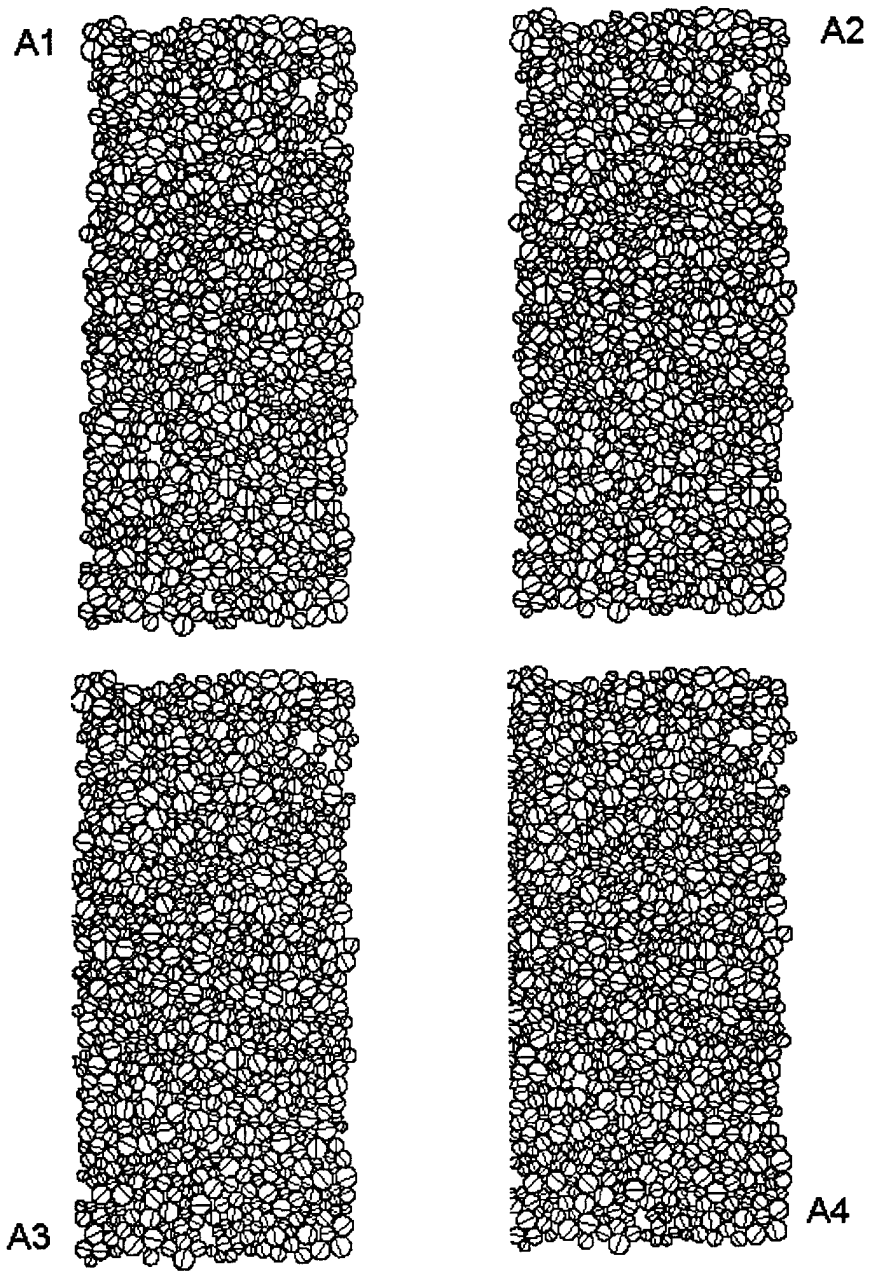

Figure 35. Geometry of sample A at four different stages of axial compression A1-A4.

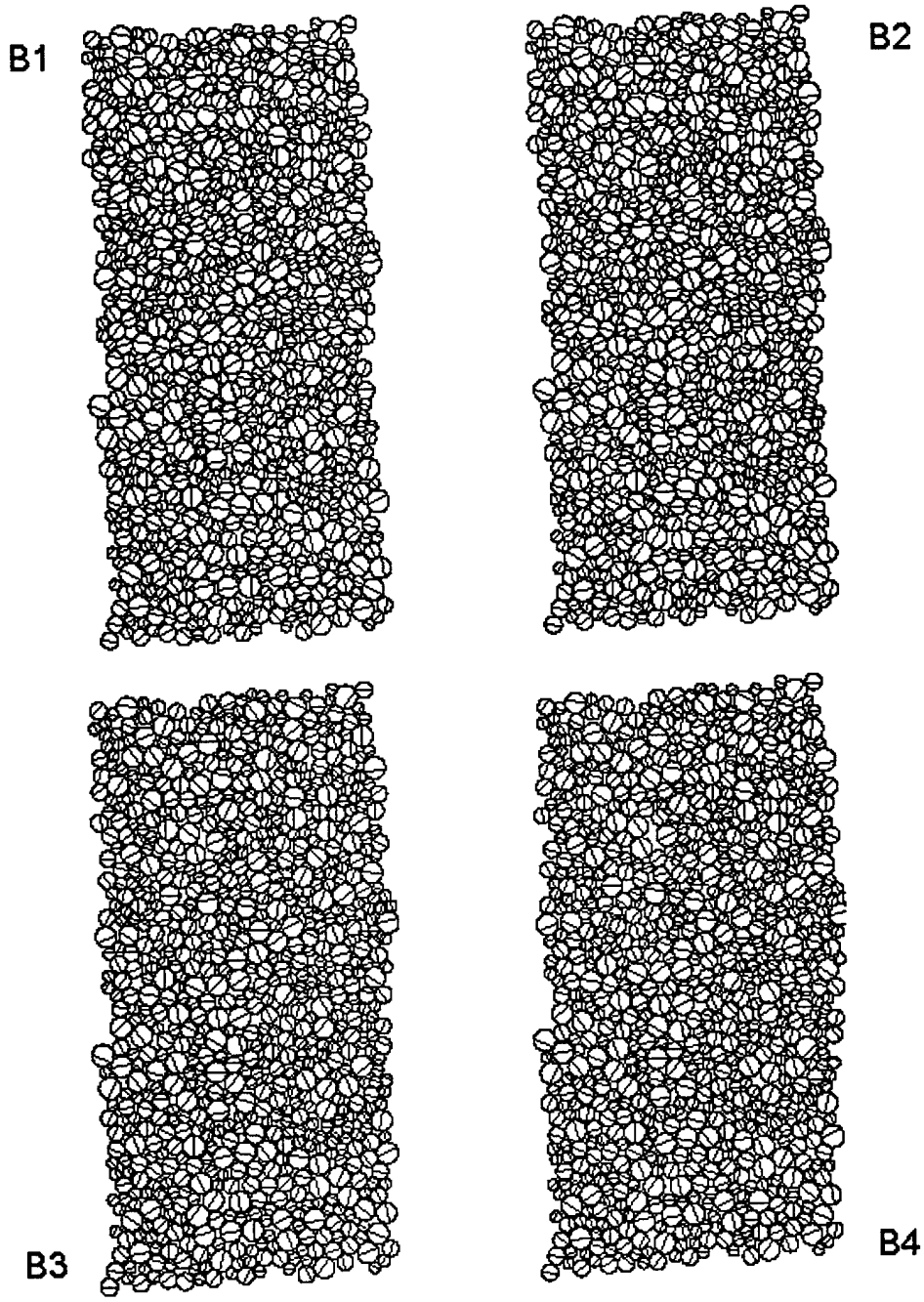

Figure 36. Geometry of sample B at four different stages of axial compression B1-B4.

Interpretation of Results

Once the center, radius and rotation of particles has been determined, various results on the kinematics of granular materials can be investigated in a similar way to previous numerical investigations, but this time based on real experimental measurements instead of numerical simulations.

Stereophotogrammetric visualization

Figure 37 shows a three-dimensional representation of the false relief visualized in the stereograph for assemblies of discrete particles. The rotation of particles are perceived as if the particles where slanted instead of being cut perpendicularly. The abrupt jumps in displacement are perceived as a cliff. Cluster of particles undergoing uniform translation are shown as a flat plateau, while rigid clusters under rotation are represented as inclined plateau.

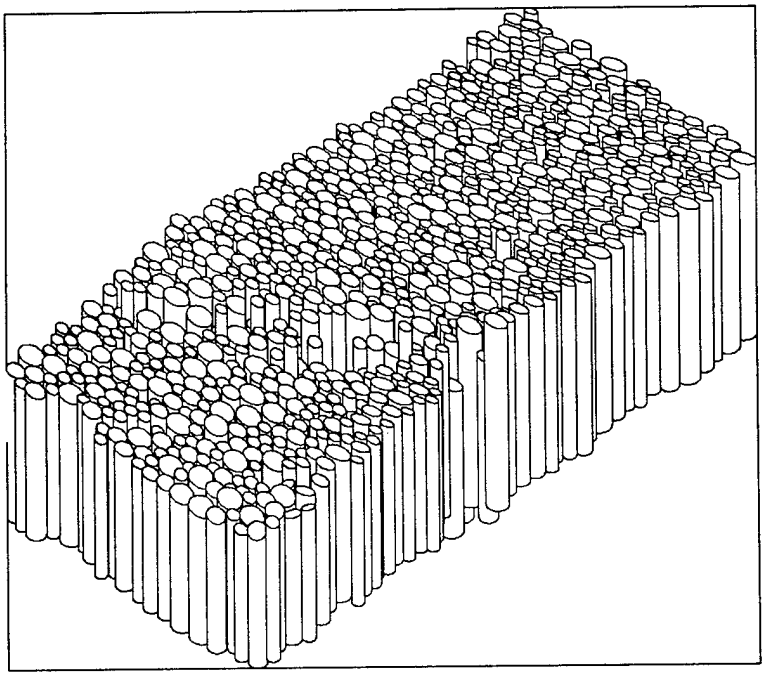

Figure 37. Displacement and rotation of particles visualized by stereophotogrammetry.

Particle displacement

As shown in Figs. 38 and 39, the displacement vectors of particle centers in tests A and B were plotted in two different ways. They were plotted (1) at the particles centers, which are irregularly spaced, and (2) on a regularly spaced grid by interpolating the displacements vectors at the particle centers. The uniform grid displays more clearly strain localization (i.e., shear band). As shown in Fig. 38 for test A, a shear band is formed at stages A2-A3 and A3-A4; it is inclined at about 46° with respect to the horizontal. As shown in Fig. 39 for test B, a shear band is displayed at stages B2-B3 and B3-B4; it is inclined at 42° with respect to the horizontal. Both inclinations are smaller that those predicted by the Mohr-Coulomb theory, i.e., $\theta = \pi/4 + \phi/2$ when ϕ=18° for test A and ϕ=17° for test B.

Shear strain

Figures 40 and 41 display the shear strain next to the incremental displacement vectors at the particle centers. Shear strains were computed using local displacement gradient centered at particle centers, as described in Bardet and Proubet (1991). They are represented by square symbols centered on the particles; their sizes are proportional to shear strain amplitude. As shown in Figs. 40 and 41, shear strains are concentrated in narrow band that coincide with the shear bands of Figs. 38 and 39.

Particle rotation

Figures 42 and 43 display the particle rotation next to incremental displacement vectors. Rotation angles are represented by a pie slice centered at the particle center. The particles rotations are clearly concentrated in the shear bands as the shear strain. It is clear that particle rotation concentrate inside shear band. This result agrees with those of numerical simulation performed by Bardet (1994). Particle rotations have a determinant influence on the localized failure mechanisms of idealized granular media.

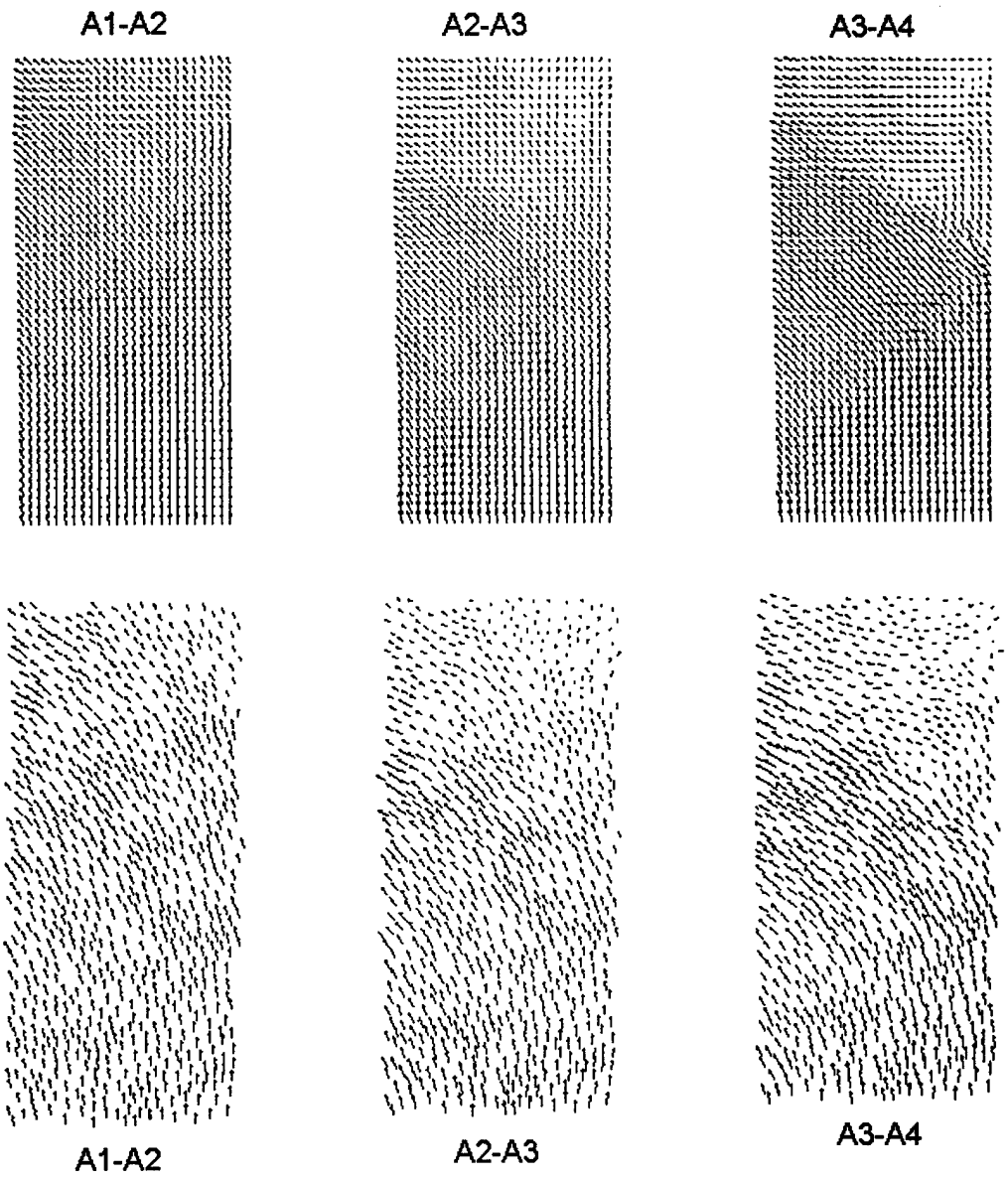

Figure 38. Interpolated displacements on uniform grid (top row) and displacements at particle centers (bottom row) between four successive stages of axial compression A1-A4 of Sample A.

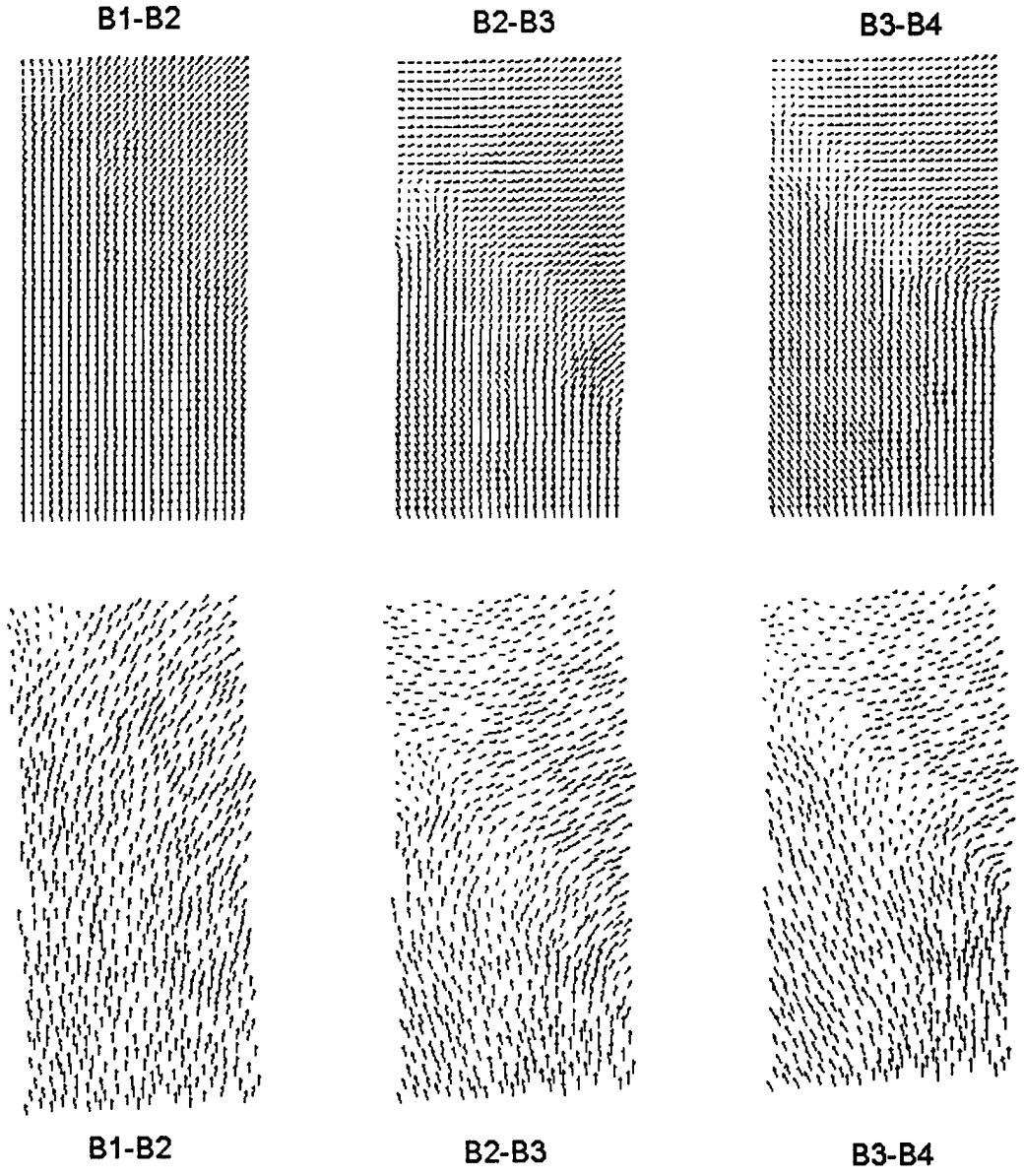

Figure 39. Interpolated displacements on uniform grid (top row) and displacements at particle centers (bottom row) between four successive stages of axial compression B1-B4 of Sample B.

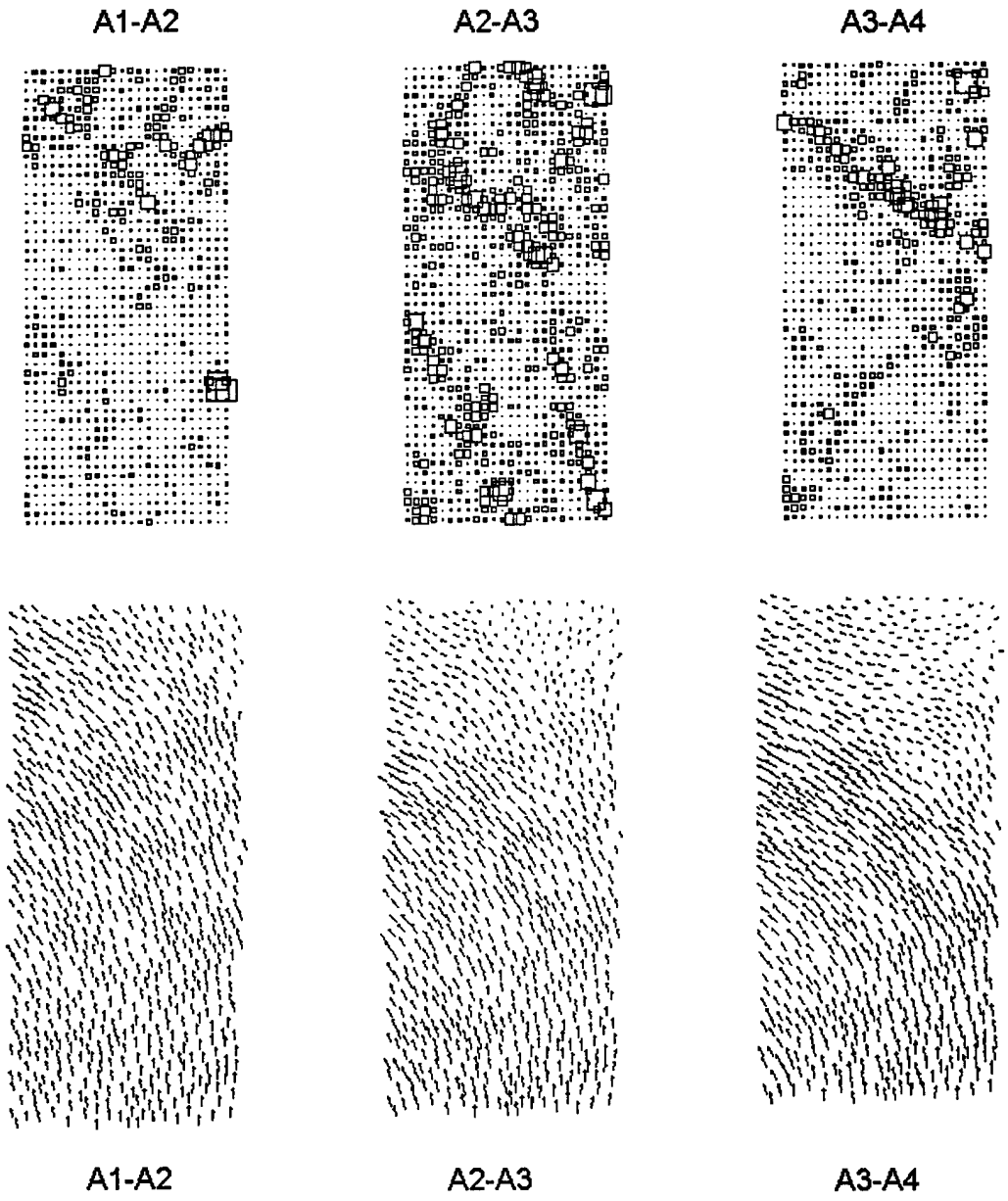

Figure 40. Incremental shear strains (top row) and incremental displacements of particle centers (bottom row) between four successive stages of axial compression A1-A4 of Sample A.

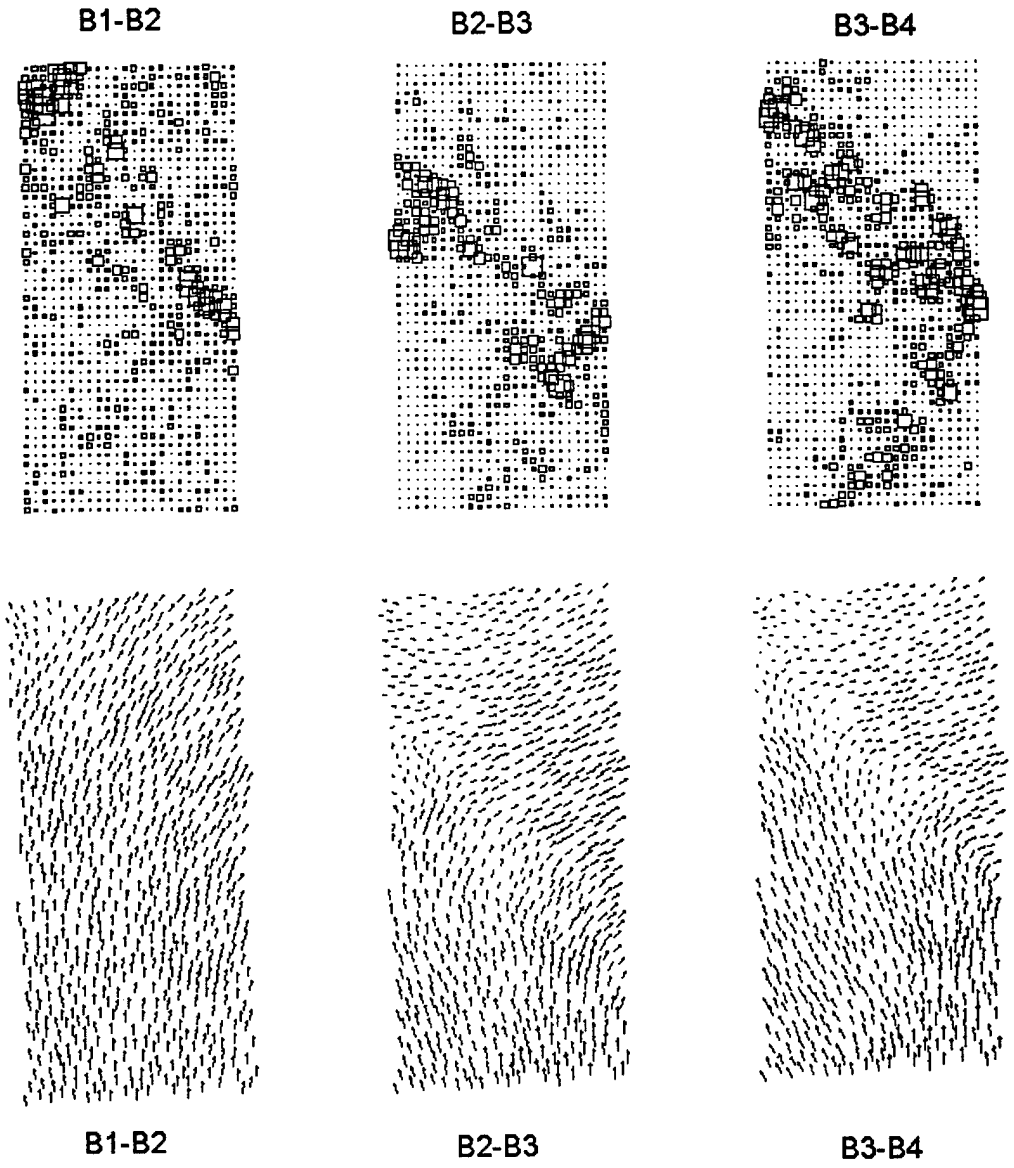

Figure 41. Incremental shear strains (top row) and incremental displacements of particle centers (bottom row) between four successive stages of axial compression B1-B4 of Sample B.

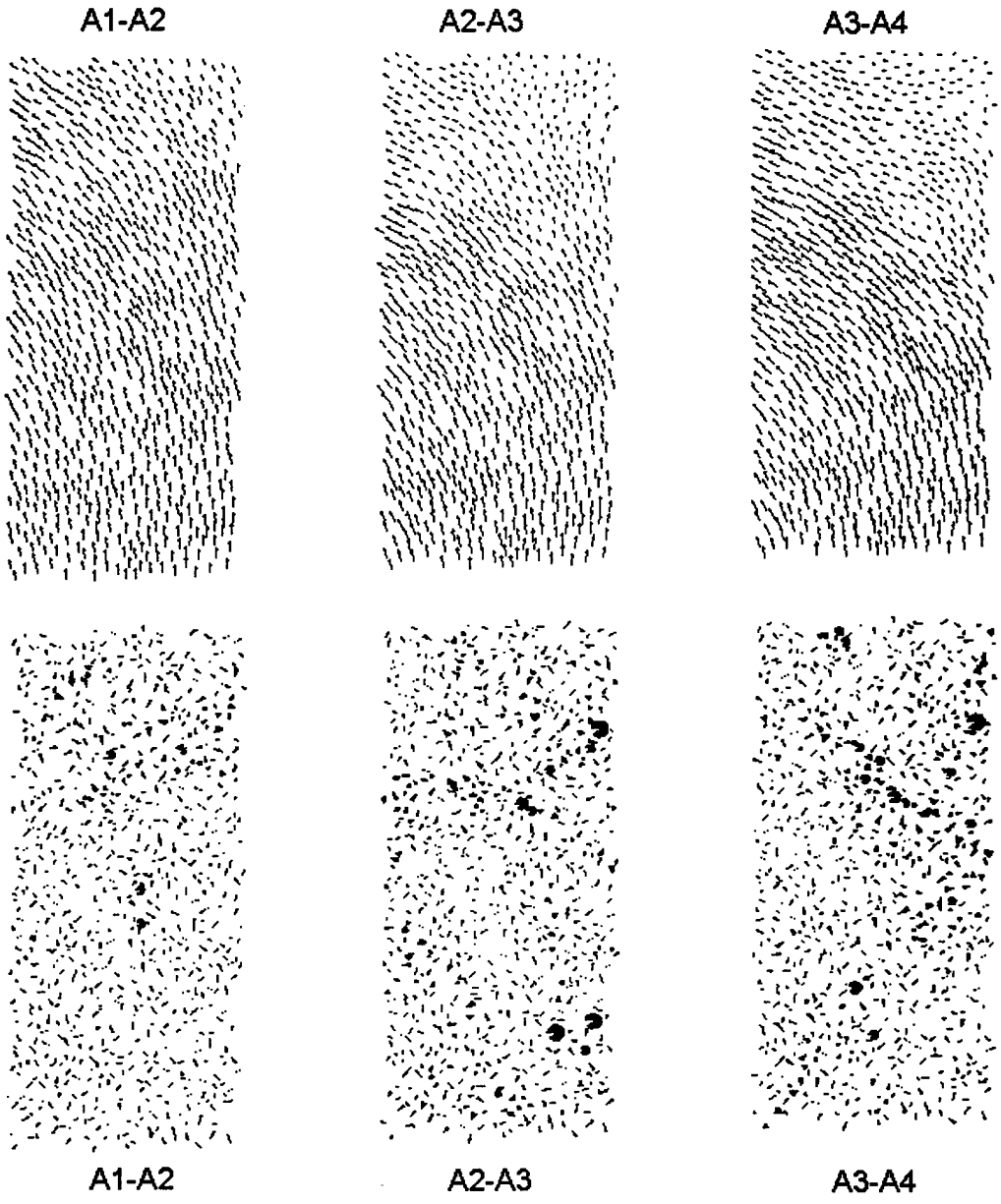

Figure 42. Incremental displacements of particle centers (top row) and particle rotations (bottom row) between four successive stages of axial compression A1-A4 of Sample A.

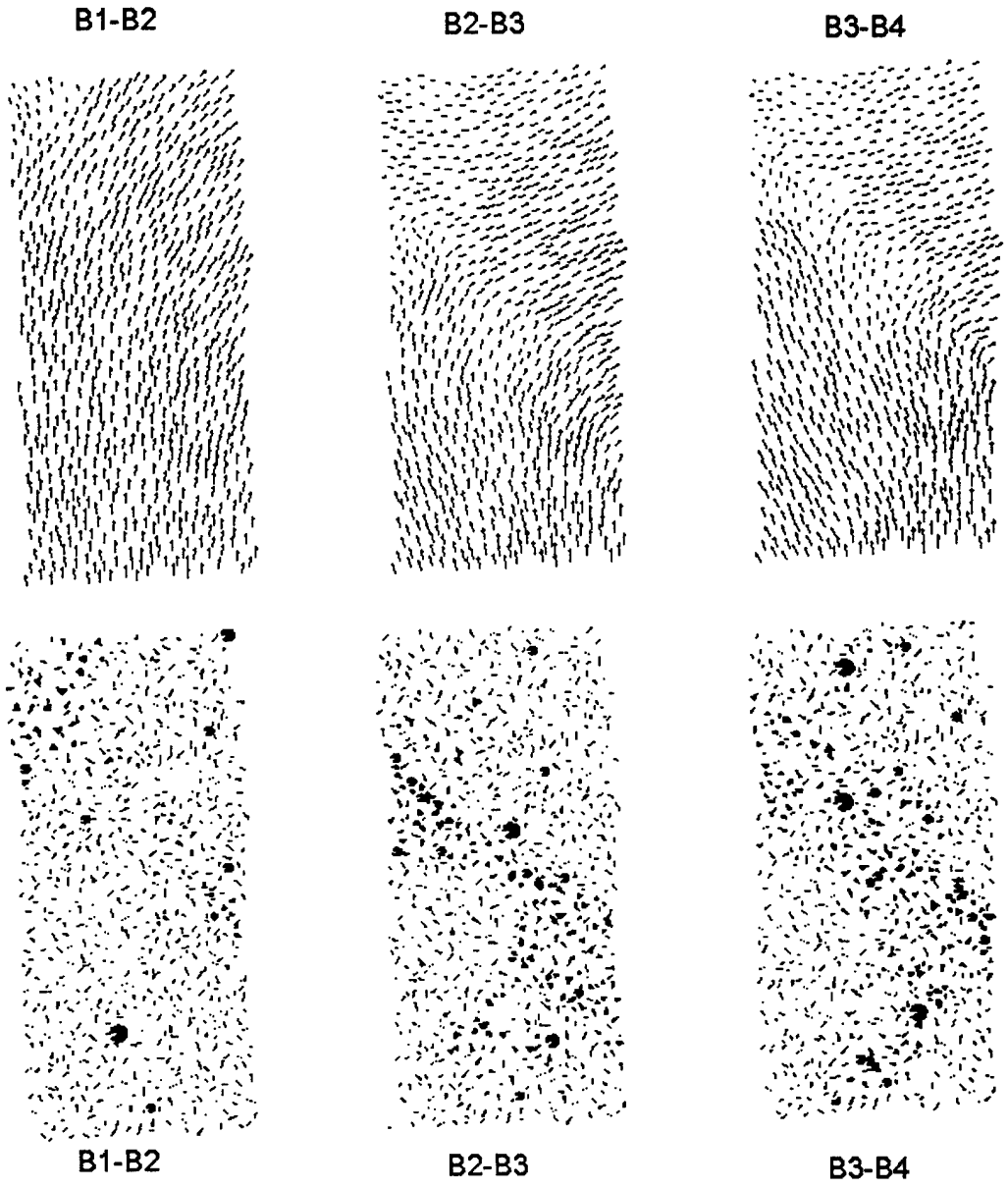

Figure 43. Incremental displacements of particle centers (top row) and particle rotations (bottom row) between four successive stages of axial compression B1-B4 of Sample B.

Discussion

The experimental technique presented above measures successfully the displacement and rotation of idealized granular material, and supports some of the results from past

numerical analyses. However, the present procedure is time consuming for large number of paticles as it requires digitizing three points per particle. More work is required to develop an automatic vision system that retains the advantages of stereophotogrammetry.

CONCLUSION

We have investigated shear band instability in granular media, and some of the higher-order continuum theories proposed to account for instability. We have explored the micro-macro mechanics transition relevant to material instability, and devised laboratory experiments for measuring the kinematics of particles. Our methodology combined computational granular mechanics, higher-order continuum mechanics, and laboratory experiments.

Our comprehensive review of past work on computational granular mechanics reveals the diversity of numerical codes in granular mechanics, and the large number of assumptions entering these codes.

Our theoretical investigation shows that the average stress in granular media, as defined from virtual work, may be asymmetric in the absence of contact moments. We specify the circumstances and amplitude of stress asymmetry, and calculate the corresponding couple stress and first stress moment. We also show that the average stress is always symmetric when it is alternately defined by using statics and no contact moment. The stress asymmetry, which results from external moments, has an amplitude that decreases with the volume size. The asymmetric stress, couple stress and first stress moment are analytically calculated in particular examples relevant to shear band instability.

Our experimental methodology is based on the application of stereophotogrammetry for measuring the kinematics of assembly of cylindrical rods, simulating granular media. We were able to measure the kinematics of a large number of nearly identical particles in the laboratory. Our experimental methodology has generated new experimental data sets on granular media useful to re-examine the applicability of higher-order continua on the response of granular media, and are therefore instrumental to understand material instability in granular media.

REFERENCES

1. **Aifantis, E. C.,** 1984, "On the microstructural origin of certain inelastic models." *Engrg. Mater. Tech. Trans. of ASME*, 16, pp. 326-330.

2. **Aifantis, E. C.,** 1987, "The physics of plastic deformation." *Int. J. Plast.*, 3, pp. 211-247.

3. **Aizawa, T., S. Tamura, Y. Shibata, J. Okuno, and J. Kihara,** 1993, Powder granular modeling and simulation for agglomeration, *Proceedings of the 6th international symposium on agglomeration,* Nagoya, Japan, 70-75.

4. **Anandarajah, A.,** 1994, Micromechanics of clays evaluated by the discrete element methods, *Proceedings of the 8th International Conference on Computer Methods and Advances in Geomechanics, Morgantown,* VA, H. J. Siriwardane, and M. M. Zaman, Balkema, Rotterdam, The Netherlands, 797-802.

5. **Azarkhin, A.,** 1988, Some history dependent problems for dissimilar cylinders with finite friction, *Journal of Applied Mechanics, ASME,* 55, 81-86.

6. **Bardet, J. P.,** 1994, "Observations on the effects of particle rotations on the failure of idealized granular materials," *Mechanics of Materials,* Vol. 18, pp. 159-182.

7. **Bardet, J. P.,** 1994, Numerical simulations of the incremental responses of idealized granular materials, *International Journal of Plasticity,* 10 (8), 879-980.

8. **Bardet, J. P.,** 1997, *Experimental Soil Mechanics*, Prentice-Hall, Upper Saddle River, NJ.

9. **Bardet, J. P., and J. Proubet,** 1989, JP2, a program to simulate the behavior of two-dimensional granular materials, *Civil Engineering Department*, University of Southern California, Los Angeles, CA.

10. **Bardet, J. P., and J. Proubet,** 1991, "A numerical investigation of the structure of persistent shear bands in granular media," *Géotechnique,* Vol. 41, No. 4, pp. 599-613.

11. **Bardet, J. P., and J. Proubet,** 1992, "A shear band analysis in idealized granular materials," *Journal of Engineering Mechanics, ASCE,* Vol. 118, No. 2, pp. 397-415.

12. **Bardet, J. P., and Proubet, J.,** 1991, "An adaptative relaxation technique for the statics of granular materials," *Computers and Structures*, Vol. 39, pp. 221-229.

13. **Bardet, J. P., and Q. Huang,** 1992, Numerical modeling of micropolar effects in idealized granular materials, *in Mechanics of granular materials and powder systems*, M. M. Mehrabadi, ed., *ASME,* 37, 85-92.

14. **Bardet, J. P., and Q. Huang,** 1993, Rotational stiffness of cylindrical particle contacts, *Proceedings of the 2nd International Conference on Micromechanics of Granular Media,* Birmingham, UK, C. Thornton, ed., 39-44.

15. **Bardet, J. P., and R. F. Scott,** 1985, Seismic stability of fractured rock masses with the distinct element method, *Proceedings of the 26th Us Symposium on Rock Mechanics,* Rapid City, SD, E. Ashworth, ed., 139-149.

16. **Bashir, Y. M. and J. D. Goddard,** 1991, A novel simulation method for the quasistatic mechanics of granular assemblages, *J. Rheology,* 35 (5), 849-885.

17. **Bathe, K. J.,** 1996, *Finite element procedures*, Prentice-Hall, Englewood Cliffs, NJ.

18. **Bathurst, R. J., and L. Rothenburg,** 1988, Micromechanical aspects of isotropic granular assemblies with linear contact interactions, *Journal of Applied Mechanics, ASME,* 55, 17-23.

19. **Bathurst, R. J., and L. Rothenburg,** 1988, Note on a random isotropic granular material with negative Poisson's ratio, *International Journal of Engineering Sciences*, 26 (4), 373-383.

20. **Bathurst, R. J., and L. Rothenburg,** 1990, "Observations on stress-force-fabric-relationships in idealized granular materials," *Mechanics of Materials,* Vol. 9, pp. 65-80.

21. **Behringer , R. P., and J. T. Jenkins,** eds., 1997, *Proceedings of the 3rd International Conference on Powders and Grains,* Durham, NC, Balkema, Rotterdam, the Netherlands.

22. **Bentall, R. H., and K. L. Johnson,** 1967 Slip in the rolling contact of two dissimilar elastic rollers, *Int. J. Mech. Sci.,* 9(55), 389-404.

23. **Biarez, J.,** 1962, Contribution à l' étude des propriétés mécaniques des sols et des materiaux pulvérulents, *Ph.D. Thesis, University of Grenoble, France.*

24. **Biarez, J., and R. Gourves,** eds., 1989, *Proceedings of the 1rst International Conference on Powders and Grains,* Clermont-Ferrand, France, Balkema, Rotterdam, the Netherlands.

25. **Bishop, A. W.,** 1954, Correspondence on shear characteristics of a saturated silt measured in triaxial compression, *Géotechnique,* 4 (1), 43-45.

26. **Bogdanova-Bontcheva, N., and H. Lippmann,** 1975, "Rotationssymmetrisches ebenes Fließen eines granularen Modellmaterials, " *Acta Mechanica,* Vol. 21, in German, pp. 93-113.

27. **Bogdanova-Bontcheva, N., and H. Lippmann,** 1975, Rotationssymmetrisches ebenes Fließen eines granularen Modellmaterials, *Acta Mechanica,* 21, in German, 93-113.

28. **Borja, R. I. and J. R. Wren,** 1995a, Micromechanics of granular media, Part I: Generation of overall constitutive equation for assemblies of circular disks, *Comput. Methods Appli. Mech. Engrg.*, 127, 13-36.

29. **Borja, R. I. and J. R. Wren,** 1995b, Micromechanics of continuum models for granular materials, *Proc. 10th Conf. Engineering Mechanics, ASCE,* S. Sture, ed., 11, 497-500.

30. **Brogliato, B.,** 1996, *Nonsmooth Impact Mechanics. Models, Dynamics and Control,* Lecture Notes in Control and Information Sciences, 220, Springer-Verlag,

31. **Bromwell, L. W.,** 1966, The friction of quartz in high vacuum, *M.I.T. Department of Civil Engineering*, Research Report B66-18.

32. **Caillerie, D.,** 1991, "Tenseur des contraintes dans un milieu granulaire," *Proceedings of GRECO Géomateriaux*, Aussoix, Isère, in French, 5 p.

33. **Campbell, C. S., and C. E. Brennen,** 1985, Computer simulation of granular shear flow, *Journal of Fluid Mechanics*, 151, 167-188.

34. **Carter, F.W,** 1926, On the action of a locomotive driving wheel, *Proc. Royal Society,* A112, 151-157.

35. **Chang, C. S.,** 1993, Micromechanical modeling of deformation and failure for granulates with frictional contacts, *Mechanics of Materials,* 16, 13-24.

36. **Chang, C. S., A. Misra, and K. Acheampong,** 1992, Elastoplastic deformation for particulates with frictional contacts, *Journal of Engineering Mechanics, ASCE,* 118 (8), 1692-1707.

37. **Chang, C. S., A. Misra, and S. Sundararam,** 1990, Micromechanical modeling of cemented sands under low amplitude oscillations, *Géotechnique,* 40 (2), 251-263.

38. **Chang, C. S., and A. Misra,** 1989, Computer simulation and modeling of mechanical properties of particulates, *Computers and Geotechnics,* 7 (4), 269-287.

39. **Chang, C. S., and A. Misra,** 1990, Packing structure and mechanical properties of granulates, *Journal of Engineering Mechanics, ASCE,* 116 (5), 1077-1093.

40. **Chang, C. S., and C. L. Liao,** 1990, "Constitutive Relations for a particulate medium with the effect of particle rotation," *International Journal of Solids and Structures,* Vol. 26, No. 4, pp. 437-455.

41. **Chang, C. S., and J. Gao,** 1995, Second-gradient constitutive theory for granular material with random packing structure, *Int. J. Solids and Structures,* 32 (16), 2279-2293.

42. **Chang, C. S., and L. Ma,** 1991, "A micromechanical-based micropolar theory for deformation of granular solids," *International Journal of Solids and Structures,* Vol. 28, No. 1, pp. 67-86.

43. **Chang, C. S., and L. Ma,** 1992, "Elastic material constants for isotropic granular solids with particle rotation," *International Journal of Solids and Structures,* Vol. 29, No. 8, pp. 1001-1018.

44. **Chang, C. S., M. G. Kabir, and Y. Chang,** 1992, Micromechanical modeling for stress-strain behavior of granular soils. II: Evaluation *Journal of Geotechnical Engineering, ASCE,* 118 (12), 1975-1992.

45. **Chang, C. S., S. J. Chao, and Y. Chang,** 1995, Estimates of elastic moduli for granular material with anisotropic random packing structure, *Int. J. Solids and Structures,* 32 (14), 1989-2008.

46. **Chang, C. S., Y. Chang, and M. G. Kabir,** 1992, Micromechanical modeling for stress-strain behavior of granular soils. I: Theory, *Journal of Geotechnical Engineering,* ASCE, 118 (12), 1959-1974.

47. **Chichili, D. R., D. E. Mouton, and M. M. Mehrabadi,** 1993, Simulation of the mechanical behavior of two-dimensional granular assemblies utilizing linear programming, *Mechanics of Materials,* submitted.

48. **Christoffersen, J., M. M. Mehrabadi, S. Nemat-Nasser,** 1981, "A Micromechanical description of granular material behavior," *Journal of Applied Mechanics, ASME,* Vol. 48, pp. 339-344.

49. **Clément, E., J. Duran and J. Rajchenbach,** 1992, Experimental study of heaping in a two-dimensional sandpile, *Physics Review Letters,* 69, 1189-1192.

50. **Cosserat, E., and F. Cosserat,** 1909, "*Théorie de corps déformables*," Hermann, Paris.

51. **Cundall, P. A,** 1982, Adaptative density-scaling for time-explicit calculations, *Proceedings of the 4th International Conference on Numerical methods in geomechanics, Edmonton*, 23-26.

52. **Cundall, P. A.,** 1971, A computer model for simulating progressive large scale movements of blocky rock systems, *Proceedings of the Symposium of the International Society of Rock Mechanics,* Nancy, France, 1, 132-150.

53. **Cundall, P. A.,** 1980, UDEC - A generalized distinct element program for modeling jointed rock, *Final Technical Report to European Research Office,* US Army, Contract No. DAJA 37-79-C-0548, NTIS order No. AD-A087 610/2.

54. **Cundall, P. A.,** 1988, Formulation of a three-dimensional distinct element model - Part I: A scheme to detect and represent contacts in a system composed of many polyhedral blocks, *International Journal of Rock Mechanics,* 25, 107-116.

55. **Cundall, P. A.,** 1989, "Numerical experiments on localization in frictional materials," *Ingenieur-Archiv.* Vol. 59, pp. 148-159.

56. **Cundall, P. A.,** 1989, Numerical modeling of discontinua, *Proceedings of the 1rst US Conference on Discrete Element Methods (DEM),* G. G. W. Mustoe, M. Henriksen, and H. -P. Huttelmaier, eds., Colorado School of Mines Press, Golden, CO, 1-17.

57. **Cundall, P. A., A. Drescher, and O. D. L. Strack,** 1982, "Numerical experiments on granular assemblies ; Measurement and observations," *Proceedings of the IUTAM symposium on deformation and failure of granular materials, Delft,* A. A. Balkema Publishers, P. A. Vermeer & H. J. Luger eds., pp. 355-370.

58. **Cundall, P. A., and O. D. L. Strack,** 1978-1979, "The distinct element method as a tool for research in granular media, Parts I and II," *Report to National Science Foundation, Eng. 76-20711,* Department of Civil and Mineral Engineering, University of Minnesota, Minneapolis, MN.

59. **Cundall, P. A., and O. D. L. Strack,** 1979, "A discrete numerical model for granular assemblies," *Géotechnique,* Vol. 29, pp. 47-65.

60. **Dantu, P.,** 1957, Contribution à l' étude mécanique et géometrique des milieux pulvérulents, *Proceedings of the 4th International Conference of Soil Mechanics and Foundation Engineering*, London, UK.

61. **Daudon, D., J. Lanier, and M. Jean,** 1997, A micromechanical comparison between experimental results and numerical simulation of a biaxial test on 2D granular materials, *Proceedings of the 3rd International Conference on Powders and Grains,* Durham, NC, R. P. Behringer and J. T. Jenkins, eds., Balkema, Rotterdam, the Netherlands, 219-222.

62. **de Josselin de Jong, G.,** 1959, *Statics and kinematics of the failable zone of a granular material,* Vitgeverij Waltman, Delft.

63. **Delassus, E.,** 1917, Mémoire sur la théorie des liaisons finies unilatérales, *Ann. Sci. Ecole Norm. Sup.,* 34, 95-179.

64. **Deresiewicz, H.,** 1958, "Stress-strain relations for a simple model of a granular medium," *Journal of Applied Mechanics, ASME,* September, pp. 403-406.

65. **Deresiewicz, H.,** 1958, Mechanics of granular material, *Advd. Appl. Mech.,* 5, 233-306.

66. **Desrues, J.,** 1984, Localization de la déformation plastique dans les matériaux granulaires, *Thèse d'état, Université de Grenoble..*

67. **Desrues, J., and B. Duthilleul,** 1984, Stereophotogrametric method applied to the determination of plane strain fields, *Journal de Mécanique théorique et appliquée,* 3 (1), 79-103.

68. **Desrues, J., J. Lanier, and P. Stutz,** 1985, Localization of the deformation in tests on sand samples, *Engineering Fracture Mechanics*, 21, 909-921.

69. **Diepolder, W., V. Mannl, and H. Lippman,** 1991, "The Cosserat continuum, a model for grain rotations in metals?," *International Journal of Plasticity,* Vol. 7, pp. 313-328.

70. **Diepolder, W., V. Mannl, and H. Lippman,** 1991, The Cosserat continuum, a model for grain rotations in metals?, *International journal of plasticity,* 7, 313-328.

71. **Dobry, R., and T.-T. Ng,** 1992, Discrete modeling of stress-strain behavior of granular media at small and large strain, *Engineering Computations,* 9, 129-143.

72. **Doménech, A., T. Doménech, and J. Cebrián,** 1987, Introduction to the study of rolling friction, *American Journal of Physics,* 55 (3), 231-235.

73. **Drescher, A.** 1976, An experimental investigation of flow rules for granular materials using optically sensitive glasss particles, *Géotechnique,* 26 (4), 591-601.

74. **Drescher, A. and G. De Josselin de Jong,** 1972, Photoelastic verification of a material model for the flow of a granular material. *J. Mech. Phys. Solids,* 20, 337-351.

75. **Dubujet, P., B. Cambou, F. Dedecker, and F. Emeriault,** 1997, Statistical homogenization for granular media - Application to non linear elastic modeling, *Proceedings of the 3rd International Conference on Powders and Grains,* Durham, NC, R. P. Behringer and J. T. Jenkins, eds., Balkema, Rotterdam, the Netherlands, 199-202.

76. **Duffy, J., and Mindlin, R. D.,** 1957, "Stress-strain relations and vibrations of a granular medium," *Journal of Applied Mechanics, ASME,* Vol. 79, pp. 585-593.

77. **El-Sohby, A. A. K.,** 1969, Deformation of sand under constant stress ratio, *Proceedings of the 7th international conference in Soil Mechanics and Foundation Engineering,* Mexico, 1, 111-119.

78. **Eringen, A. C.,** 1966, "Linear theory of micropolar elasticity," *Journal of Mathematics and Mechanics,* Vol. 15, No. 6, pp. 909-923.

79. **Eringen, A.C.,** 1967, *Mechanics of Continua*, John Wiley, New York, NY.

80. **Fabrikant, V. I.,** 1986, Inclined flat punch of arbitrary shape on an elastic half-space, *Journal of Applied Mechanics, ASME,* 53, 798-806.

81. **Fabrikant, V. I.,** 1988, Elastic field around a circular punch, *Journal of Applied Mechanics, ASME,* 55, 604-605.

82. **Foerster, S., M. Louge, H. Chang and K. Allia,** 1994, Measurements of the collision properties of small spheres, *Phys. Fluids,* 6, 1108-1115.

83. **Frankel, S. P.,** 1950, Convergences rates of iterative treatments of partial differential equations, *Mathl. Tabl. Natn. Res. Coun.,* Washington DC, 4, 65-75.

84. **Germain, P.,** 1973, "The method of virtual power in continuum mechanics. Part 2: Microstructures," *Journal of Applied Mathematics, SIAM,* Vol. 25, No. 3, pp. 556-575.

85. **Germain, P.,** 1973, La méthode des puissances virtuelles en mécanique des milieux continus. Théories due second gradient, *Journal de Mécanique,* 12 (2), 235-274.

86. **Germain, P.,** 1973, The method of virtual power in continuum mechanics. Part 2: Microstructures, *J. of Applied Mathematics, SIAM,* 25 (3), 556-575.

87. **Ghaboussi, J., and R. Barbosa,** 1990, Three-dimensional discrete element method for granular materials, *International Journal for Numerical and Analytical Methods in Geomechanics,* 14, 451-472.

88. **Goddard, J. D.,** 1977, An elastohydrodymanic theory for the rheology of concentrated suspensions of deformable particles, *Journal of Non-Newtonian Fluid mechanics,* 2, 169-189.

89. **Goddard, J. D.,** 1986, Microstructural origins of continuum stress fields - A brief history and some unresolved issues, Chapter 6 in *Recent developments in structured continua*, D. DeKee and P. N. Kaloni, eds., Pitman research notes in mathematics (143, Longman/J. Wiley, p. 179-208.

90. **Goddard, J. D., X. Zhuang, and A. K. Didwania,** 1993, Microcell methods and the adjacency matrix in the simulation of the mechanics of granular media, *Proceedings of the 2nd international conference on discrete element methods,* Massachusetts Institute of Technology, J. R. Williams and G. W. Mustoe, eds., March, 3-14.

91. **Goddard, J.,** 1977, "An Elastohydrodynamics Theory for the Rheology of Concentrated Suspensions of Deformable Particles" *Journal of Non-Newtonian Fluid Mechanics,* Vol. 2, pp. 169-189

92. **Goodman, E. L.,** 1962, "Contact stress analysis of normally loaded rough spheres," *Journal of Applied Mechanics, ASME,* pp. 515-522.

93. **Goodman, E. L.,** 1962, Contact stress analysis of normally loaded rough spheres, *J. of Applied Mech., ASME,* 515-522.

94. **Gray, J. E.,** 1960, The relationship between principal stress dilatancy and friction angle of a granular materials, *M. Sc. Thesis*, University of Manchester, UK.

95. **Greening, D. R., G. G. W. Mustoe, and G. L. DePorter,** 1997, Discrete element modeling of fabrication flaw precursors in the compaction of agglomerated ceramic

powders, *Proceedings of the 3rd International Conference on Powders and Grains,* Durham, NC, R. P. Behringer and J. T. Jenkins, eds., Balkema, Rotterdam, the Netherlands, 113-116.

96. **Hafiz, M. S.,** 1950, Strength characteristics of sands and gravels in direct shear, *PhD thesis*, University of London, UK.

97. **Hahn, J. K.,** 1988, Realistic animation of rigid bodies, *Computer graphics*, 22. (4), 299-308.

98. **Hart, R. D., P. A. Cundall, and J. Lemos,** 1988, Formulation of a three-dimensional distinct element model - Part II: Mechanical calculations for motion and interaction of a system composed of many polyhedral blocks, *International Journal of Rock Mechanics,* 25, 117-126.

99. **Hertz, H.,** 1882, Über die Berührung fester elastische Körper and über die Harte (On the contact of rigid elastic solids and on hardness), *Verhandlungen des Vereins zur Beförderung des Gewerbefleisses*, Leipzig.

100. **Hill, R.,** 1962, "Acceleration waves in solids." *J. Mech. Phys. Solids*, 10, 1-16.

101. **Hill, R.,** 1967, The essential structure of constitutive laws for metal composite and polycrystals, *J. Mech. Physics Solids,* 11, 357-372.

102. **Hocking, G., G. G. W. Mustoe, and J. R. Williams,** 1985, CICE discrete element analysis code - theoretical manual, *Applied Mechanics Inc.,* Lakewood, CO.

103. **Hong, C.-W.,** 1997, Process modeling and design for colloidal powder forming, *Proceedings of the 3rd International Conference on Powders and Grains,* Durham, NC, R. P. Behringer and J. T. Jenkins, eds., Balkema, Rotterdam, the Netherlands, 41-44.

104. **Horn, H. M., and D. V. Deere,** 1962, Frictional characteristics of minerals, *Géotechnique,* 12 (4), 319-335.

105. **Horne, M. R.,** 1965, The behavior of an assembly of rotund, rigid, cohesionless particles (I and II), *Proc. Roy. Soc. London,* A286, 62.

106. **Horne, M. R.,** 1969, The behavior of an assembly of rotund, rigid, cohesionless particles (III), *Proc. Roy. Soc. London,* A310, 21.

107. **Houlsby, G.T.,** 1981, A study of plasticity theory and their applicability to soils, *Ph.D. thesis, University of Cambridge.*

108. **Hughes, T. J. R.,** 1983, Analysis of transient algorithms with particular reference to stability behavior, *Computational methods for transient analysis,* T. Belitschko, and T.J.R. Hughes, eds., North Holland, Amsterdam, Holland, 67-156.

109. **Hughes, T. J. R.,** 1987, *The finite element method,* Prentice-Hall, Englewoods Cliffs, NJ.

110. **Hughes, T. J. R., and T. Belytschko,** 1993, *Nonlinear finite element analysis,* Short course notes, Stanford, CA.

111. **Jagota, A., C. Argento, and S. Mazur,** 1997, Viscoelastic coalescence of spherical particles, *Proceedings of the 3rd International Conference on Powders and Grains,* Durham, NC, R. P. Behringer and J. T. Jenkins, eds., Balkema, Rotterdam, the Netherlands, 31-36.

112. **Jean, M.,** 1995, Frictional contact in collections of rigid or deformable bodies: numerical simulation of geomaterials, in *Mechanics of Geomaterial Interfaces,* eds. A. P. S. Salvadurai and M. J. Boulon, Elsevier Science Publisher, Amsterdam, 463-486.

113. **Jean, M., and J. J. Moreau,** 1996, Numerical treatment of contact and friction: the Contact Dynamics method, *Proc.1996 Engineering Systems Design and Analysis Conference,* eds. A. Lagarde and M. Raous, ASCE, New York, 4, 201-208.

114. **Johnson, D. L., L. M. Schwartz, D. Elata, J. G. Berryman, B. Hornby, and A. N. Norris,** 1997, Linear and nonlinear elasticity of granular media: Stress-induced

anisotropy of a random sphere pack, *Proceedings of the 3rd International Conference on Powders and Grains,* Durham, NC, R. P. Behringer and J. T. Jenkins, eds., Balkema, Rotterdam, the Netherlands, 243-246.

115. **Johnson, K. L.,** 1958, The effect of spin upon the rolling motion of an elastic sphere on a plane, *Journal of Applied Mechanics, September*, 332-338.

116. **Johnson, K. L.,** 1958, The effect of tangential contact force upon the rolling motion of an elastic sphere on a plane, *Journal of Applied Mechanics, September*, 339-346.

117. **Johnson, K. L.,** 1985, "Contact Mechanics," *Cambridge University Press, Cambridge, England,* pp. 306-311.

118. **Johnson, K. L.,** 1985, *Contact Mechanics*, Cambridge University Press, Cambridge, UK.

119. **Kalker, J. J.,** 1970, Transient phenomena in two elastic cylinders rolling over each other with dry friction, *J. of Applied Mech., ASME,* 677-688.

120. **Kalker, J. J.,** 1990, Three-dimensional elastic bodies in rolling contact, *Kluwer Academic Publishers, Dordrecht, The Netherlands,* 59-97.

121. **Kanatani, K.,** 1979, "A micro-polar continuum theory for the flow of granular materials," *International Journal of Engineering Science,* Vol. 17, No. 4, pp. 419-432.

122. **Kawaguchi, T., Y. Yamamoto, T. Tanaka, and Y. Sudji,** 1995, Numerical simulation of a single rising bubble in a two-dimensional fluidized bed, *Proceedings of the 2nd International Conference on Multiphase Flows,* Kyoto, Japan, FB2-17-22.

123. **Ke, T.-C., and J. Bray,** 1995, Modeling of particulate media using discontinuous deformation analysis, *Journal of Engineering Mechanics,* ASCE, 121 (11), 1234-1243.

124. **Kishino, Y.**, 1988, Disc model analysis of granular media, *in Micromechanics of Granular Materials,* M. Satake and J. T. Jenkins, eds., Elsevier Science Publishers, Amsterdam, The Netherlands, 143-152.

125. **Knight, J. B., H. M. Jaeger and S. R. Nagel,** 1993, Vibration-induced size separation in granular media : the convection connection, *Physics Review Letters,* 70, 3728-3731.

126. **Koenders, M. A.,** 1987, The incremental stiffness of an assembly of particles, *Acta Mechanica,* 70, 31-49.

127. **Krawietz, A.,** 1982, Some features of the gross behavior of granular media from micromechanics, *Proceedings of the IUTAM conference on deformation and failure of granular materials, Delft*, Balkema, Rotterdam, The Netherlands, 29-36.

128. **Laalai, K. Sab, and N. Guérin,** 1995, Micromechanical modelling of ballasted tracks, in *Contact Mechanics,* eds. M. Raous et al., Plenum Press, New York, 363-368.

129. **LaBudde, R. A., and D. Greenspan,** 1976, Energy and momentum conserving methods of arbitrary order for the numerical integration of equation of motion, I. Motion of a single particle, II. Motion of a system of particles, *Numerical Mathematics,* 25, 323-346; 26, 1-16.

130. **Lambe, T. W. and R. V. Whitman,** 1979, *Soil Mechanics,* John Wiley and Sons, New York, N.Y.

131. **Lecornu, L.,** 1905, Sur la loi de Coulomb, *Comptes Rendus Acad. Sci. Paris, 140,* 847-848.

132. **Lee, I. K.,** 1966, Stress dilatancy performance of feldspar, *Journal of the Soil Mechanics and Foundations Division*, ASCE, 92, SM2, 79-103.

133. **Lesburg, L., X. Zhang, L. Vu-Quoc, and O. R. Walton,** 1997, Simplified tangential force-displacement models for a discrete element particle flow code,

Proceedings of the 3rd International Conference on Powders and Grains, Durham, NC, R. P. Behringer and J. T. Jenkins, eds., Balkema, Rotterdam, the Netherlands, 243-246.

134. **Lian, G., C. Thornton, and M. J. Adams,** 1997, A microscopic simulation of oblique collision of wet agglomerates, *Proceedings of the 3rd International Conference on Powders and Grains,* Durham, NC, R. P. Behringer and J. T. Jenkins, eds., Balkema, Rotterdam, the Netherlands, 159-162.

135. **Lun, C. K. K., and A. A. Bent,** 1993, Computer simulation of simple shear flow of inelastic frictional spheres, *Proceedings of the 2nd International Conference on Micromechanics of Granular Media,* Birmingham, UK, C. Thornton, ed., Balkema, Rotterdam, 301-306.

136. **Mühlhaus, H. B. and I., Vardoulakis,** 1987, "The thickness of shear bands in granular materials." *Géotechnique*, 37, pp. 271-283.

137. **Mühlhaus, H. B.,** 1986, "Shear-band analysis in granular material by Cosserat-theory." *Ing. Arch.*, Berlin, Germany, 56, 389-399.

138. **Mandel, J.,** 1963, "Propagation des surfaces de discontinuité dans un milieu élasto-plastique." *IUTAM symp. On Stress waves in inelastic solids, Brown University,* Springer-Verlag, Berlin, pp. 331-341.

139. **Manna, S. S., and H. J. Herrmann,** 1991, Precise determination of the fractal dimensions of Appolonian packing and space-filling bearings, *Journal of Physics, A: Math. Gen.,* 24, 481-490.

140. **Matsuoka, H., and S. Yamamoto,** 1994, A microscopic studdy on shear mechanism of granular materials by DEM, *Journal of Geotechnical Engineering, JSCE,* In Japanese, 487, 167-175.

141. **Meakin P., and A. T. Skeltorp,** 1993, Application of experimental and numerical methods to the physics of multiparticle systems, *Advances in Physics,* 42 (1), 1-127.

142. **Meftah, W. P. Evesque, J. Biarez, D. Sornette, and N. E. Abriak,** 1993, Evidence of local 'seisms' of microscopic and macroscopic stress fluctuations during the deformation of packings of grains, in *Powders and Grains,* C. Thornton, ed., Balkema, Rotterdam, 173-178.

143. **Mehrabadi, M. M., B. Loret, and S. Nemat-Nasser,** 1993, Incremental constitutive relations for granular materials based on micromechanics, *Proceedings of the Royal Society,* London, A 441, 443-463.

144. **Mehrabadi, M. M., S. Nemat-Nasser, and M. Oda,** 1982, "On statistical description of stress and fabric in granular materials," *International Journal for Numerical and Analytical Methods in Geomechanics,* Vol. 6, pp. 95-108.

145. **Mindlin, R. D.,** 1949, "Compliance of elastic bodies in contact," *Journal of Applied Mechanics, ASME,* September, pp. 259-268.

146. **Mindlin, R. D., and H. Deresiewicz,** 1953, Elastic spheres in contact under varying oblique forces, *Journal of Applied Mechanics, ASME,* 20, 327-344.

147. **Misra, A.,** 1995, Interfaces in particulate materials, *Mechanics of geomaterial interfaces*, A. P. S. Selvadurai and M. Boulon, eds., Elsevier.

148. **Monteiro Marques, M. D. P.,** 1993, Differential Inclusions, *in Nonsmooth Mechanical Problems: Shocks and Dry Friction,* Berlin, Germany.

149. **Moreau, J. J.,** 1966, Quadratic programming in mechanics: dynamics of one-sided constraints, *SIAM J. Control,* 4, 153-158.

150. **Moreau, J. J.,** 1988, Bounded variation in time, in *Topics in Nonsmooth Mechanics,* J. J. Moreau, P. D. Panagiotopoulos and G. Strang, eds., Berlin, Germany, 1-74.

151. **Moreau, J. J.,** 1988, Unilateral contact and dry friction in finite freedom dynamics, in *Nonsmooth Mechanics and Applications,* J. J. Moreau and P. D. Panagiotopoulos, eds., CISM Courses and Lectures, 302, Springer-Verlag, Wien, New York, 1 - 82.

152. **Moreau, J. J.,** 1993, New computation methods in granular dynamics, *Proceedings of the 2nd International Conference on Micromechanics of Granular Media,* Birmingham, C. Thornton, ed., Balkema, Rotterdam, The Netherlands, 227-232.

153. **Moreau, J. J.,** 1994, Some numerical methods in multibody dynamics: application to granular materials, *Eur. J. Mech. Solids,* 13, 93-114.

154. **Moreau, J. J.,** 1995, Numerical experiments in granular dynamics: vibration-induced size segregation, in *Contact Mechanics,* M. Raous et al., eds., Plenum Press, New York, 347-358.

155. **Moreau, J. J.,** 1996, Numerical investigation, of shear zones in granular materials, *Proceedings of the HLRZ-workshop on Friction, Arching and contact Dynamics,* Jülich, Germany, October.

156. **Mühlhaus, H. B., and I. Vardoulakis,** 1987, "The thickness of shear bands in granular materials," *Géotechnique,* Vol. 37, pp. 271-283.

157. **Mujinza, A., N. Bicanic, and D. R. J. Owen,** 1993, BSD contact detection algorithm for discrete elements in 2D, *Proceedings of the 2nd international conference on discrete element methods,* Massachusetts Institute of Technology, J. R. Williams and G. W. Mustoe, eds., March, 39-52.

158. **Mustoe, G. G. W., M. Henriksen, and H. -P. Huttelmaier,** eds., 1989, *Proceedings of the 1rst US Conference on Discrete Element Methods (DEM),* Colorado School of Mines Press, Golden, CO.

159. **Nakase, H., T. Annaka, F. Katahira, and T. Kyono,** 1992, An application study of the distinct element method to plane strain compression tests, *Soils and Foundations*, in Japanese, 454, 55-64.

160. **Nemat-Nasser, S. and H. J. Herrmann,** 1991, "Precise determination of the fractal dimensions of Appolonian packing and space-filling bearings." *J. Phys. A: Math. Gen.* 24, pp. 481-490.

161. **Nemat-Nasser, S., and M. M. Mehrabadi,** 1983, "Micromechanically based rate constitutive description for granular materials," *Proceedings of Int. Conf. on Constitutive Laws for Engineering Materials; Theory and Applications,* Tucson, A2, Wiley, New York.

162. **Nemat-Nasser, S., and M. M. Mehrabadi,** 1984,Micromechanically based rate constitutive descriptions for granular materials, *Mechanics of Engineering Materials,* C.S. Desai and R.H. Gallagher, eds, John Wiley and Sons, New York, 451-463.

163. **Ng, T. -T. and R. Dobry, R.,** 1994, Numerical simulation of monotonic and cyclic loading of granular soil, *Journal of Geotechnical Engineering, ASCE,* 120 (2), 388-403.

164. **Ng, T. -T.,** 1992, A non-linear numerical model for soil mechanics, *International Journal for Numerical and Analytical Methods in Geomechanics*, 16, 247-263.

165. **Novozhilov, V. V.,** 1961, *Theory of Elasticity*, Pergamon Press, Oxford.

166. **O'connor, R., J. Gill, and J. R. Williams,** 1993, A linear complexity contact detection algorithm for multi-body analysis, *Proceedings of the 2nd international conference on discrete element methods,* Massachusetts Institute of Technology, J. R. Williams and G. W. Mustoe, eds., 53-64.

167. **Oda, M.,** 1972, "The mechanism of fabric changes during compressional deformation of sand," *Soils and Foundations,* Japanese Society of Geotechnical Engineering, Vol. 12, No. 2, p. 1-17.

168. **Oda, M.,** 1972, Deformation mechanism of sand in triaxial compression tests, *Soils and Foundations*, Japanese Society of Soil Mechanics and Foundation Engineering, 12, 45-63.

169. **Oda, M.,** 1972, Initial fabrics and their relations to mechanical properties of granular material, *Soils and Foundations*, Japanese Society of Soil Mechanics and Foundation Engineering, 12, 18-36.

170. **Oda, M.,** 1993, Micro-fabric and couple-stress in shear bands of granular materials, *Proceedings of the 2nd International Conference on Micromechanics of Granular Media,* Birmingham, UK, C. Thornton, ed., 161-166.

171. **Oda, M., and J. Konishi,** 1974, Microscopic deformation mechanism of granular material in simple shear, *Soils and Foundations*, Japanese Society of Soil Mechanics and Foundation Engineering, 14, 25-38.

172. **Oda, M., J. Konishi, and S. Nemat-Nasser**, 1980. Some experimentally based fundamental results on the mechanical behavior of granular materials, *Géotechnique,* 30, 479-495.

173. **Oda, M., J. Konishi, and S. Nemat-Nasser**, 1982, "Experimental micromechanical evaluation of strength of granular materials: effects of particle rolling." *Mech. Mater.* 1, pp. 269-283.

174. **Oda, M., K. Iwashita, and T. Kakiuchi,** 1997, Importance of particle rotation in the mechanics of granular materials, *Proceedings of the 3rd International Conference on Powders and Grains,* Durham, NC, R. P. Behringer and J. T. Jenkins, eds., Balkema, Rotterdam, the Netherlands, 207-210.

175. **Oda, M., Konishi, J, and S. Nemat-Nasser**, 1982, "Experimental micromechanical evaluation of strength of granular materials: effects of particle rolling," *Mechanics of Materials,* Vol. 1, pp. 269-283.

176. **Papadrakakis, M.,** 1981, A method for the automatic evaluation of the dynamic relaxation parameters, *Computer methods in applied mechanics and engineering,* 25, 35-48.

177. **Parikh, P. V.,** 1967, The shearing behavior of sand under axisymmetric loading, *PhD thesis*, University of Manchester, UK.

178. **Park, K. C., and P. Underwood,** 1980, A variable-step central difference method for structural dynamic analysis - Part 1. Theoretical aspects, *Computer methods in applied mechanics and engineering,* 22, 241-258.

179. **Penman, A. D. M.,** 1953, Shear characteristics of saturated silts measured in triaxial compression, *Géotechnique,* 3 (4), 312-328.

180. **Pfeiffer, F., and C. Glocker,** 1966, *Multibody Dynamics with Unilateral Contacts,* John Wiley & Sons, New York.

181. **Procter, D. C., and R. R. Barton,** 1974, Measurement of the angle of interparticle friction, *Géotechnique,* 24 (4), 581-604.

182. **Radjai, F., M. Jean, J. J. Moreau and S. Roux**, 1996, Force distributions in dense two-dimensional granular systems, *Physics Review Letters,* 77, 274.

183. **Reynolds, O.,** 1885, On the dilatancy of media composed of rigid particles in contact, with experimental illustration, *Philosophical Magazine,* Series 5, 20, 469-481.

184. **Reynolds, O.,** 1895, On rolling friction, *Phil. Trans. Royal Society,* 166, 155.

185. **Rice, J. R.,** 1976, The localization of plastic deformation, *Theoretical and Applied Mechanics*, Proceedings of the 14th IUTAM Congress, W.T. Koiter, ed., North Holland, New York, 207-220.

186. **Roscoe, K. H.,** 1970, "Tenth Rankine Lecture: The influence of strains in soil mechanics." *Géotechnique*, 20, pp. 129-170.

187. **Roscoe, K. H., J. R. F. Arthur, and R. G. James**, 1963, "The determination of strains in soils by an X-ray method." *Civ. Eng. Publ. Wks, Rev.,* 58, pp. 873-876.

188. **Roscoe, K.H. and A.N. Schofield,** 1964. Discussion on P.W. Rowe's paper, Stress-dilatancy, earth pressures and slopes (Proc Paper 3507, May 1963), *J. Soil mechanics and Foundation Engineering, ASCE,* 90(1), 136.

189. **Rosenberg, L., and A. P. S. Selvadurai,** 1981, Micromechanical definition of the cauchy stress tensor for particulate media, In *Mechanics of Structured Media,* A. P. S. Selvadurai, ed., Elsevier, Amsterdam, The Netherlands, 469-486.

190. **Rothenberg, L., and A. P. S. Selvadurai,** 1981, "Micromechanical definition of the cauchy stress tensor for particulate media," In Mechanics of Structured Media (edited by A. P. S. Selvadurai), Elsevier, Amsterdam, The Netherlands, pp. 469-486.

191. **Rothenburg, L., and R. J. Bathurst,** 1989, Analytical study of induced anisotropy in idealized granular materials, *Géotechnique,* 39, 601-614.

192. **Rothenburg, L., and R. J. Bathurst,** 1991, Numerical simulation of idealized granular assemblies with plane elliptical particles, *Computers and Geotechnics*, 11, 315-329.

193. **Rothenburg, L., and R. J. Bathurst,** 1992, Micromechanical features of granular assemblies with planar elliptical particles, *Géotechnique,* 42, 79-95.

194. **Rowe, P.W.,** 1962, The stress-dilatancy relation for static equilibrium of an assembly of particles in contact, *Proc. Roy. Soc. London,* A269, 500.

195. **Rudnicki, J. W. and J. R. Rice,** 1975, "Conditions for the localization of deformation in pressure-sensitive dilatant material. *J. Mech. Phys. Solids*, 23, pp. 371-394.

196. **Rudnicki, J.W., and J. R. Rice,** 1975, Conditions for the localization of deformation in pressure-sensitive dilatant materials, *J. Mech. Phys. Solids,* 23, 371-394.

197. **Satake, M.,** 1978, "Constitution of mechanics of granular materials through graph representation," in *Theoretical and Applied Mechanics 26,* University of Tokyo Press, 257 p.

198. **Satake, M.,** 1982, Fabric tensor in granular materials, *Proceedings of the IUTAM symposium on deformation and failure of granular materials, Delft,* Balkema Publishers, P.A. Vermeer & H.J. Luger eds., 63-68.

199. **Savage, S. B., and D. J. Jeffrey,** 1981, The stress tensor in a granular flow at high shear rate, *J. Fluid Mech.,* 110, 255-272.

200. **Schneebli, G.,** 1955, Une analogie mécanique pour les terres sans cohésion, *Proceedings of the Academy of Sciences*, Paris, France, 243, p. 256.

201. **Schofield, A. N., and C. P. Wroth.**, 1968, *Critical State Soil Mechanics.* Mc Graw-Hill, London, UK.

202. **Shi, G. -H,** 1993, Block system modeling by discontinuous deformation analysis, *Topics in engineering Volume 11,* C. A. Brebbia and J. J. Connor, eds., Computational mechanics Publication, Southampton, UK.

203. **Shi, G.-H., and R. E. Goodman,** 1988, Discontinuous deformation analysis - a new method for computing stress, strain and sliding of block systems, in *Key questions in rock mechanics*, Cundall et al., eds., Balkema, Rotterdam, the Netherlands, 381-393.

204. **Shi, G.-H., and R. E. Goodman,** 1989, Generalization of two-dimensional discontinuous deformation analysis for forward modeling, *International Journal for Numerical and Analytical Methods in Geomechanics,* 13(4), 359-380.

205. **Singer I. L., and H. M. Pollock,** 1992, *Fundamentals of friction: Macroscopic and microscopic processes,* Kluwer Academic, Dordrecht, the Netherlands.

206. **Skinner, A. E.,** 1969, A note on the influence of interparticle friction on the shearing strength of a random assembly of spherical particles, *Géotechnique,* 19 (1) 150-157.

207. **Southwell, R. V.** 1940, *Relaxation methods in engineering sciences,* Oxford University Press, Oxford, UK.

208. **Sternberg, E.,** 1968, Couple stress and singular stress concentrations in elastic solid, in Mechanics of generalized continua, *Proceedings of the IUTAM Symposium on the Generalized Cosserat Continuum and the Continuum Theory of Dislocation with Applications,* Edited by E. Kroner, Springer, New York.

209. **Subbash, S. Nemat-Nasser, M. M. Mehrabadi, and H.M. Shodja,** 1991, "Experimental investigation of fabric-stress relations in granular materials," *Mechanics of Materials,* Vol. 11, pp. 87-106.

210. **Sudji, Y., T. Kawaguchi, and T. Tanaka,** 1993, Discrete particle simulation of two-dimensional fluidized bed, *Powder Technology,* 77, 79-87.

211. **Sudji, Y., T. Tanaka, and T. Ishida,** 1992, Lagrangian numerical simulation of plug flow of cohesionless particles in an horizontal pipe, *Powder Technology,* 71, 239-250.

212. **Sukla, A., and H. P. Rossmanith,** 1982, A photoelastic investigation of dynamic load transfer in granular media, *Acta Mechanica*, 42, 211-225.

213. **Sun, G., and C. Thornton,** 1994, Computer simulation of 3D quasi-static shear deformation of particulate media, *Proceedings of 1rst International Particle technology Forum,* American Institute of Chemical Engineers, Denver, CO, 24-29 pp..

214. **Supel, J. A.,** 1985, Local destruction of granular media caused by crushing a single grain, *Archives of Mechanics,* 37 (4-5), 535-548.

215. **Tabor, D.,** 1955, The mechanism of rolling friction: the elastic range, *Proc. Royal Society,* A251, 198-220.

216. **Tamura, S., and T. Aizawa,** 1993, Mechanical behavior of powder particle on the applied vibration, *International journal of modern physics,* 7 (9-10), 1829-1838.

217. **Tatsuoka, F., S. Nakamura, C., Huang, and K. Tani,** 1990, Strength anisotropy and shear band direction in plane strain tests on sand, *Soils and Foundations,* 30, 35-54.

218. **Taylor, R. L.,** 1977, Computer procedures for finite element analysis. Ch. 24, in: O.C. Zienkiewicz, *The finite element method,* 3rd ed., McGraw-Hill Book Co., London, England.

219. **Thornton, C.,** 1979, The conditions of failure of a face-centered cubic array of uniform rigid spheres, *Géotechnique*, 29, pp. 441-459.

220. **Thornton, C.,** 1994, Micromechanics of elastic sphere assemblies during 3D shear, *Proceedings of Mechanics and Statistical Physics of Particulate Materials*, Institute for Mechanics and Materials, La Jolla, CA, June, 64-67.

221. **Thornton, C., and C. W. Randall,** 1988, Applications of theoretical contact mechanics to solid particle system simulation, *in Micromechanics of Granular Materials,* M. Satake and J. T. Jenkins, eds., Elsevier Science Publishers, Amsterdam, Netherlands, pp. 133-142.

222. **Thornton, C., and G. Sun,** 1994, Numerical simulation of general 3D quasi-static shear deformation of granular media, *Proceedings of Numerical Methods in Geotechnical Engineering*, I. M. Smith, ed., Balkema, Rotterdam, Netherlands, 143-148.

223. **Thornton, C.,** ed., 1993, *Proceedings of the 2nd International Conference on Powders and Grains,* Birmingham, UK, Balkema, Rotterdam, the Netherlands.

224. **Thurston, C. W., and H. Deresiewicz,** 1959, Analysis of a compression test of a model of a granular medium, *Journal of Applied Mechanics, ASME,* pp. 251-258.

225. **Timoshenko, S., and J. N. Goodier,** 1951, *Theory of elasticity*, 3rd edition, McGraw-Hill, New York, NY.

226. **Ting, J. M.,** 1992, A robust algorithm for ellipse-based discrete element modeling of granular materials, *Computers and Geotechnics*.

227. **Ting, J. M., and B. T. Corkum,** 1992, A computational laboratory for discrete element geomechanics, *Journal of Computers in Civil Engineering, ASCE,* 6, pp. 129-146.

228. **Ting, J. M., B. T. Corkum, C. R. Kauffman, and C. Greco,** 1989, Discrete numerical model for soil mechanics, *Journal of Geotechnical Engineering*, ASCE, 115, pp. 379-398.

229. **Ting, J. M., M. Khawaja, L. M. Meachum, and J. D. Rowell,** 1993, An ellipse-based discrete element model for granular materials, *International Journal for Numerical and Analytical Methods in Geomechanics,* 17, pp. 603-623.

230. **Tong, P. Y. L.,** 1970, Plane strain deformation of sands, *PhD thesis*, University of Manchester, UK.

231. **Trent, B. C. and L. G. Margolin,** 1992, A numerical laboratory for granular solids, *Engineering Computations,* 9, pp. 191-197.

232. **Truesdell, C.,** 1985, *The Elements of Continuum Mechanics,* Springer-Verlag, Berlin, Germany.

233. **Tschebotarioff, G. P., and J. D. Welch,** 1948, lateral earth pressures and friction between soil minerals, *Proceedings of the 2nd International Conference on Soil Mechanics and Foundations,* Rotterdam, VII, pp. 135-138.

234. **Tsuji, Y.,** 1997, Discrete particle simulation of dispersed gas-solid flows, *Proceedings of the 3rd International Conference on Powders and Grains,* Durham, NC, R. P. Behringer and J. T. Jenkins, eds., Balkema, Rotterdam, the Netherlands, pp. 25-30.

235. **Underwood, P.,** 1983, Dynamic relaxation, in *Computational methods for transient analysis,* T. Belitschko and T.J.R. Hughes, eds., North Holland, Amsterdam, Holland, pp. 245-265.

236. **Underwood, P., and K. C. Park,** 1980, A variable-step central difference method for structural dynamic analysis, Part 2. Implementation and performance evaluation, *Computer methods in applied mechanics and engineering,* 23, pp. 259-279.

237. **Vardoulakis, I. and B. Graf,** 1985, Calibration of constitutive models for granular materials using data from biaxial experiments, *Géotechnique,* 35, pp. 299-317.

238. **Vardoulakis, I. and E. C. Aifantis,** 1989, "Gradient dependent dilatancy and its implicaitons in shear banding and liquefaction." *Ingenieur-Archiv*, 59, pp. 197-208.

239. **Vardoulakis, I.,** 1988, Theoretical and experimental bounds for shear-band bifurcation strain in biaxial tests on dry sand, *Res Mechanica*, 23, pp. 239-259.

240. **Vardoulakis, I.,** 1989, "Shear-banding and liquefaction in granular materials on the basis of a Cosserat continuum theory." *Ing. Arch.*, Berlin, Germany, 59(2), pp. 106-114.

241. **Vardoulakis, I., and J. Sulem,** 1995. *Bifurcation analysis in geomechanics*, Chapman & Hall, Glasgow, UK, pp. 211 and 342.

242. **Vermeulen, P. J., and K. L. Johnson,** 1964, Contact of nonspherical elastic bodies transmitting tangential forces, *Journal of Applied Mechanics,* June, pp. 338-340.

243. **Walton, O. R.,** 1980, Particle dynamics modeling of geological materials, *Lawrence Livermore National Laboratory*, Report UCRL-52915.

244. **Walton, O. R.,** 1993, Numerical simulation of inelastic, frictional particle-particle interactions, in *Particulate two-phase flow,* M. C. Roco, ed., Butterworth Heinemann, Boston, pp. 884-910.

245. **Walton, O. R., and R. L. Braun**, 1986, Stress calculations for assemblies of inelastic spheres in uniform shear, *Acta Mechanica*, 63, 73-86.

246. **Walton, O. R., and R. L. Braun**, 1986, Viscosity, granular-temperature, and stress calculations for shearing assemblies of inelastic, frictional disks, *Journal of Rheology*, 30, pp. 949-980.

247. **Walton, O. R., R. L. Braun, R. G. Mallon, and D. M. Cervelli,** 1988, Particle-dynamics calculations of gravity flows of inelastic, frictional sphere, *Micromechanics of granular materials*, M. Satake and J. T. Jenkins, eds., Elsevier Science Publishers, Amsterdam, pp. 153-161.

248. **Weber, J.,** 1966, "Recherche concernant le contraintes intergranulaires dans les milieux pulvérulents," *Bulletin de Liaison des Ponts et Chausées*, No. 20, Paris, France.

249. **Weber, J.,** 1996, Recherches concernant les contraintes intergranulaires dans les milieux pulvérulents, *Cahiers du Groupe Français de Rhéologie,* 2, 161-170 (see also *Bulletin de Liaison des Ponts et Chaussées* 20, pp. 3-1 to 3-20).

250. **Wells, J. C.,** 1997, Contact of rough elastic spheres: a simplified analysis, *Proceedings of the 3rd International Conference on Powders and Grains,* Durham, NC, R. P. Behringer and J. T. Jenkins, eds., Balkema, Rotterdam, the Netherlands, pp. 311-314.

251. **Williams, J. R., and G. G. W. Mustoe,** 1987, Modal methods for the analysis of discrete systems, *Computers and Geotechnics,* 4, pp. 1-19.

252. **Williams, J. R., and G. G. W. Mustoe,** eds., 1993, *Proceedings of the 2nd International Conference on Discrete Element Methods (DEM),* The Massachusetts

Institute of Technology, Intelligent Engineering System Laboratory Publication, Cambridge, MA.

253. **Witters, J., and D. Duymelinck,** 1986, Rolling and sliding resistive forces on balls moving on a flat surface, *American Journal of Physics,* 54 (1), pp. 80-83.

254. **Zbib, H. M. and E. C. Aifantis,** 1989, "A gradient-dependent flow theory of plasticity: Application to metal and soil instabilities." *App. Mech. Review, Pan-American Congress of Applied Mechanics*, 42, pp. 295-304.

255. **Zhuang, X. and J. D. Goddard,** 1993, Computer simulation and experiments on the quasi-static mechanics and transport properties of granular materials, *Res. Rep. GR 93-01,* University of California, San Diego, CA, October.

256. **Zhuang, X., K. Didwania, and J. D. Goddard,** 1995, Simulation of the quasi-static mechanics and scalar transport properties of ideal granular assemblages, *Journal of computational physics,* 121, pp. 331-346.

257. **Zienkiewicz, O. C., and R. L. Taylor,** 1991, *The finite element method,* Vol. 2, McGraw-Hill, London, UK.

APPENDIX

Listing of stereophotgrammetric data processing programs used in Part III.

```
C=====================================================================
C   GET_AB calculates of particle center and radius by three
C   different methods, and calculates particle rotation
C
C   INPUT FILES:  C1C2.ORI,C2C3.ORI,C3C4.ORI
C
C   OUTPUT FILES:  BALL_A.OUT,BALL_B.OUT,BALL_C.OUT
C                  AB.OUT
C                  DIAMETER_A.OUT
C=====================================================================
      PARAMETER(M=2000)
      REAL FX1(2,3),FY1(2,3),FX2(2,3),FY2(2,3),FX3(2,3),FY3(2,3)
      REAL AX1(2,M),AY1(2,M),BX1(2,M),BY1(2,M),CX1(2,M),CY1(2,M),
     &     AX2(2,M),AY2(2,M),BX2(2,M),BY2(2,M),CX2(2,M),CY2(2,M),
     &     AX3(2,M),AY3(2,M),BX3(2,M),BY3(2,M),CX3(2,M),CY3(2,M)
      REAL X1(2,M),Y1(2,M),R1(2,M),X2(2,M),Y2(2,M),R2(2,M),
     &     X3(2,M),Y3(2,M),R3(2,M)
      REAL D0(M),TA(M),T1(M),T2(M),T3(M),T4(M),D1(2,M),D2(2,M),D3(2,M)
           CHARACTER*80 NAME,DIR1,DIR2,T

C     Work directory
      WRITE(*,'(A,$)') ' Enter Test A or B: '
      READ(*,'(A)') T
      DIR1='F:\WORK\AFOSR\Processing\TEST'//TRIM(T)//'\Raw\'
      DIR2='F:\WORK\AFOSR\Processing\TEST'//TRIM(T)//'\Processed\'

C     Read data from files
      NAME=TRIM(DIR1)//'C1C2.ORI'
      OPEN(1, FILE=NAME,STATUS='OLD')
      CALL READ_DATA(FX1,FY1,AX1,AY1,BX1,BY1,CX1,CY1,N1,1)
      CLOSE(1)
      NAME=TRIM(DIR1)//'C2C3.ORI'
      OPEN(1, FILE=NAME,STATUS='OLD')
      CALL READ_DATA(FX2,FY2,AX2,AY2,BX2,BY2,CX2,CY2,N2,2)
      CLOSE(1)
      NAME=TRIM(DIR1)//'C3C4.ORI'
      OPEN(1, FILE=NAME,STATUS='OLD')
      CALL READ_DATA(FX3,FY3,AX3,AY3,BX3,BY3,CX3,CY3,N3,2)
      CLOSE(1)

C     Check data
      WRITE(6,*) 'Fixed points 1'
      WRITE(6,*) 'D12 =',DIST(FX1(1,1),FY1(1,1),FX1(1,2),FY1(1,2))
      WRITE(6,*) 'D23 =',DIST(FX1(1,3),FY1(1,3),FX1(1,2),FY1(1,2))
      WRITE(6,*) 'Fixed points 2'
      WRITE(6,*) 'D12 =',DIST(FX2(1,1),FY2(1,1),FX2(1,2),FY2(1,2))
      WRITE(6,*) 'D23 =',DIST(FX2(1,3),FY2(1,3),FX2(1,2),FY2(1,2))
      WRITE(6,*) 'Fixed points 3'
      WRITE(6,*) 'D12 =',DIST(FX3(1,1),FY3(1,1),FX3(1,2),FY3(1,2))
      WRITE(6,*) 'D23 =',DIST(FX3(1,3),FY3(1,3),FX3(1,2),FY3(1,2))
      WRITE(6,*) 'Number of particles',N1,N2,N3
```

```
C   Calculate particle rotation
    DO I=1,N1
     T1(I)=ATAN2(BY1(1,I)-AY1(1,I),BX1(1,I)-AX1(1,I))
     T2(I)=ATAN2(BY1(2,I)-AY1(2,I),BX1(2,I)-AX1(2,I))
     T3(I)=ATAN2(BY3(1,I)-AY3(1,I),BX3(1,I)-AX3(1,I))
     T4(I)=ATAN2(BY3(2,I)-AY3(2,I),BX3(2,I)-AX3(2,I))
    END DO

C   Calculate particle center and radius by Method A
    CALL PARCEN_A(X1,Y1,R1,AX1,AY1,BX1,BY1,CX1,CY1,N1)
    CALL PARCEN_A(X2,Y2,R2,AX2,AY2,BX2,BY2,CX2,CY2,N2)
    CALL PARCEN_A(X3,Y3,R3,AX3,AY3,BX3,BY3,CX3,CY3,N3)

C   Write ouput results
    NAME=TRIM(DIR2)//'BALL_A.OUT'
    OPEN(4,FILE=NAME,STATUS='UNKNOWN')
    CALL WRITE_BALL(X1,Y1,R1,X3,Y3,R3,T1,T2,T3,T4,N1)
    CLOSE(4)
    NAME=TRIM(DIR2)//'DIAMETER_A.OUT'
    OPEN(4,FILE=NAME,STATUS='UNKNOWN')
    WRITE(4,'(6(5X,A4))') 'D1','D2','D2','D3','D3','D4'
    DO I=1,N1
     WRITE(4,'(6F12.5)') 2.*R1(:,I),2.*R2(:,I),2.*R3(:,I)
    END DO
    CLOSE(4)

C   Calculate particle center and radius by Method B
    DO I=1,N1
     AB=DIST(AX1(1,I),AY1(1,I),BX1(1,I),BY1(1,I))
     D0(I)=(-(X1(1,I)-AX1(1,I))*(BY1(1,I)-AY1(1,I))+
    &       (Y1(1,I)-AY1(1,I))*(BX1(1,I)-AX1(1,I)) )/AB
    END DO
    CALL PARCEN_B(X1,Y1,R1,AX1,AY1,BX1,BY1,D0,N1)
    CALL PARCEN_B(X2,Y2,R2,AX2,AY2,BX2,BY2,D0,N2)
    CALL PARCEN_B(X3,Y3,R3,AX3,AY3,BX3,BY3,D0,N3)

C   Write ouput results
    NAME=TRIM(DIR2)//'BALL_B.OUT'
    OPEN(4,FILE=NAME,STATUS='UNKNOWN')
    CALL WRITE_BALL(X1,Y1,R1,X3,Y3,R3,T1,T2,T3,T4,N1)
    CLOSE(4)

C   Calculate particle center and radius by Method C
    DO I=1,N1
     TA(I)=D0(I)/DIST(AX1(1,I),AY1(1,I),BX1(1,I),BY1(1,I))
    END DO
    CALL PARCEN_C(X1,Y1,R1,AX1,AY1,BX1,BY1,TA,N1)
    CALL PARCEN_C(X2,Y2,R2,AX2,AY2,BX2,BY2,TA,N2)
    CALL PARCEN_C(X3,Y3,R3,AX3,AY3,BX3,BY3,TA,N3)

C   Write ouput results
    NAME=TRIM(DIR2)//'BALL_C.OUT'
    OPEN(4,FILE=NAME,STATUS='UNKNOWN')
    CALL WRITE_BALL(X1,Y1,R1,X3,Y3,R3,T1,T2,T3,T4,N1)
    CLOSE(4)

C   Calculate distance AB and diameter
    DO I=1,N1
     DO J=1,2
      D1(J,I)=DIST(AX1(J,I),AY1(J,I),BX1(J,I),BY1(J,I))
      D2(J,I)=DIST(AX2(J,I),AY2(J,I),BX2(J,I),BY2(J,I))
      D3(J,I)=DIST(AX3(J,I),AY3(J,I),BX3(J,I),BY3(J,I))
```

```
      END DO
      END DO
      NAME=TRIM(DIR2)//'AB.OUT'
      OPEN(4,FILE=NAME,STATUS='UNKNOWN')
      WRITE(4,'(6(5X,A4))') 'AB1','AB2','AB2','AB3','AB3','AB4'
      DO I=1,N1
       WRITE(4,'(6F12.5)') D1(:,I),D2(:,I),D3(:,I)
      END DO
      CLOSE(4)
      END


C=====================================================================
      SUBROUTINE PARCEN_A(X,Y,R,AX,AY,BX,BY,CX,CY,N)
      INTEGER N
      REAL X(2,N),Y(2,N),R(2,N),AX(2,N),AY(2,N), BX(2,N),BY(2,N),CX(2,N),CY(2,N)
C PARCEN_A calculate the center and radius of particles with 3 points
C  Input
C    N:                      total number of particles
C    AX,AY,BX,BY,CX,CY:  coordinates of points A, B and C
C  Output
C    X,Y:            center position
C    R:              radius
C=====================================================================
      DO I=1,N
      DO J=1,2
       A=AX(J,I)-BX(J,I)
       B=AY(J,I)-BY(J,I)
       E=(AY(J,I)**2-BY(J,I)**2+AX(J,I)**2-BX(J,I)**2)/2.
       C=AX(J,I)-CX(J,I)
       D=AY(J,I)-CY(J,I)
       F=(AY(J,I)**2-CY(J,I)**2+AX(J,I)**2-CX(J,I)**2)/2.
       X(J,I)=(E*D-B*F)/(A*D-B*C)
       Y(J,I)=(A*F-E*C)/(A*D-B*C)
       R(J,I)=DIST(X(J,I),Y(J,I),AX(J,I),AY(J,I))
      END DO
      END DO
      END


C=====================================================================
      SUBROUTINE PARCEN_B(X,Y,R,AX,AY,BX,BY,D0,N)
      INTEGER N
      REAL X(2,N),Y(2,N),R(2,N),AX(2,N),AY(2,N),BX(2,N),BY(2,N),D0(N)
C PARCEN_B calculate the center and radius of particles
C with constant vector D0
C  Input
C    N:                  total number of particles
C    AX,AY,BX,BY   coordinates of points A and B
C    D0                  constant length D0
C  Output
C    X,Y:        center position
C    R:          radius
C=====================================================================
      DO I=1,N
       DO J=1,2
       XX=BX(J,I)-AX(J,I)
       YY=BY(J,I)-AY(J,I)
       X(J,I)=(AX(J,I)+BX(J,I))/2.-YY*D0(I)/SQRT(XX**2+YY**2)
       Y(J,I)=(AY(J,I)+BY(J,I))/2.+XX*D0(I)/SQRT(XX**2+YY**2)
       R(J,I)=DIST(X(J,I),Y(J,I),AX(J,I),AY(J,I))
      END DO
```

```
      END DO
      END

C=======================================================================
      SUBROUTINE PARCEN_C(X,Y,R,AX,AY,BX,BY,TA,N)
      INTEGER N
      REAL X(2,N),Y(2,N),R(2,N),AX(2,N),AY(2,N),BX(2,N),BY(2,N),TA(N)
C PARCEN_C calculate the center and radius of particles with method C
C with constant angle ALPHA
C  Input
C     N:              total number of particles
C     AX,AY,BX,BY     coordinates of points A and B
C     ALPHA           constant angle
C  Output
C     X,Y:        center position
C     R:          radius
C=======================================================================
      DO I=1,N
       DO J=1,2
        X(J,I)=(AX(J,I)+BX(J,I))/2.-TA(I)*(BY(J,I)-AY(J,I))
        Y(J,I)=(AY(J,I)+BY(J,I))/2.+TA(I)*(BX(J,I)-AX(J,I))
        R(J,I)=DIST(X(J,I),Y(J,I),AX(J,I),AY(J,I))
       END DO
      END DO
      END

C=======================================================================
      SUBROUTINE READ_DATA(FX,FY,AX,AY,BX,BY,CX,CY,N,K)
      REAL FX(2,1),FY(2,1),
     &     AX(2,1),AY(2,1),BX(2,1),BY(2,1),CX(2,1),CY(2,1)
C=======================================================================
      REAL CNX(2,4),CNY(2,4)

C  read rotation D and translation (DX,DY) of global data
      READ(1,*) D1,DX1,DY1
      IF(K==2) THEN
        READ(1,*) D2,DX2,DY2
      ELSE
       D2=D1
       DX2=DX1
       DY2=DY1
      ENDIF
C  read XMIN,XMAX,YMIN,YMAX of global data
      READ(1,*) XMIN,XMAX,YMIN,YMAX
C  read fixed points
      DO I=1,3
       CALL READ_PT(FX(1,I),FY(1,I),DX1,DY1,D1,DX2,DY2,D2,K)
      END DO
C  read coordinates of corners
      DO I=1,4
       CALL READ_PT(CNX(1,I),CNY(1,I),DX1,DY1,D1,DX2,DY2,D2,K)
      END DO
C  read all points A, B and C
C  and select origin at third fixed point
      READ (1,*) N
      DO I=1,N
       CALL READ_PT(AX(1,I),AY(1,I),DX1,DY1,D1,DX2,DY2,D2,K)
       CALL READ_PT(BX(1,I),BY(1,I),DX1,DY1,D1,DX2,DY2,D2,K)
       CALL READ_PT(CX(1,I),CY(1,I),DX1,DY1,D1,DX2,DY2,D2,K)
       AX(:,I)=AX(:,I)-FX(:,3)
       AY(:,I)=AY(:,I)-FY(:,3)
```

```
      BX(:,I)=BX(:,I)-FX(:,3)
      BY(:,I)=BY(:,I)-FY(:,3)
      CX(:,I)=CX(:,I)-FX(:,3)
      CY(:,I)=CY(:,I)-FY(:,3)
     END DO
     CLOSE(1)
     END

C=======================================================================
      SUBROUTINE READ_PT(X,Y,DX1,DY1,D1,DX2,DY2,D2,K)
      REAL X(2),Y(2)
C=======================================================================
      PARAMETER(S=2.1)
      READ(1,*) X1,Y1,X2,Y2
      IF(K==1) THEN
       X(1)=X1
       Y(1)=Y1
      ELSE
       X(1)=(X1-DX1)*COS(D1)-(Y1-DY1)*SIN(D1)
       Y(1)=(Y1-DY1)*COS(D1)+(X1-DX1)*SIN(D1)
      ENDIF
      X(2)=(X2-DX2)*COS(D2)-(Y2-DY2)*SIN(D2)
      Y(2)=(Y2-DY2)*COS(D2)+(X2-DX2)*SIN(D2)
C   scale length to obtain mm
      X=S*X
      Y=S*Y
      END

C=======================================================================
      REAL FUNCTION DIST(X1,Y1,X2,Y2)
C=======================================================================
      DIST=SQRT((X1-X2)**2+(Y1-Y2)**2)
      END

C=======================================================================
      SUBROUTINE WRITE_BALL(X1,Y1,R1,X3,Y3,R3,T1,T2,T3,T4,N)
      REAL X1(2,N),Y1(2,N),R1(2,N),X3(2,N),Y3(2,N),R3(2,N),
     &    T1(N),T2(N),T3(N),T4(N)
C=======================================================================
     WRITE(4,*) N
     WRITE(4,'(16(5X,A5))') 'X1','Y1','R1','T1','X2','Y2','R2','T2',
     &                 'X3','Y3','R3','T3','X4','Y4','R4','T4'
     DO I=1,N
      WRITE(4,'(16(1X,F9.4))')X1(1,I),Y1(1,I),R1(1,I),T1(I),
     &                 X1(2,I),Y1(2,I),R1(2,I),T2(I),
     &                 X3(1,I),Y3(1,I),R3(1,I),T3(I),
     &                 X3(2,I),Y3(2,I),R3(2,I),T4(I)
     END DO
     END
```

```
C=============================================================
C   DISP_ROT plots displacement vector and rotation of particles
C   INPUT FILE: BALL_A.OUT
C=============================================================
      PARAMETER (M=2000)
      CHARACTER*256 LABEL
      REAL X1(M),Y1(M),R1(M),T1(M),X2(M),Y2(M),R2(M),T2(M),
     &     X3(M),Y3(M),R3(M),T3(M),X4(M),Y4(M),R4(M),T4(M)
      CHARACTER*80 NAME,DIR2,T

      SCALE=5.

C  Work directory
      WRITE(*,'(A,$)') ' Enter Test A or B: '
      READ(*,'(A)') T
      DIR2='F:\WORK\AFOSR\Processing\TEST'//TRIM(T)//'\Processed\'

C  Read center position and radius
      NAME=TRIM(DIR2)//'BALL_A.OUT'
      OPEN(1,FILE=NAME,STATUS='OLD')
      READ(1,*) N1
      READ(1,'(A)') LABEL
      DO I=1,N1
        READ(1,*) X1(I),Y1(I),R1(I),T1(I),X2(I),Y2(I),R2(I),T2(I),
     &          X3(I),Y3(I),R3(I),T3(I),X4(I),Y4(I),R4(I),T4(I)
      END DO
      CLOSE(1)

C  Plotting extrema
      XMIN=MINVAL(X1(1:N1))
      XMAX=MAXVAL(X1(1:N1))
      YMIN=MINVAL(Y1(1:N1))
      YMAX=MAXVAL(Y1(1:N1))
       W=ABS(XMIN-XMAX)
       H=ABS(YMIN-YMAX)
       XMIN=XMIN-0.05*W
       XMAX=XMAX+0.05*W
       YMIN=YMIN-0.05*H
       YMAX=YMAX+0.05*H

C  Draw displacement vectors
      NAME=TRIM(DIR2)//'DISP_ROT.GIF/GIF'
      CALL PGBEGIN(0,NAME,1,1)
      CALL PGSCR(0, 1., 1., 1.)    !black becomes white
      CALL PGSCR(1, 0., 0., 0.)    !white becomes black
      CALL PGQVP(0,XP1,XP2,YP1,YP2)
      CALL PGVPORT(0.1,0.3,0.5,0.9)
      CALL PGWNAD(XMIN,XMAX,YMIN,YMAX)
      DO I=1,N1
       CALL ARROW(X1(I),Y1(I),X2(I),Y2(I))
      END DO
      CALL PGVPORT(0.3,0.5,0.5,0.9)
      CALL PGWNAD(XMIN,XMAX,YMIN,YMAX)
      DO I=1,N1
       CALL ARROW(X2(I),Y2(I),X3(I),Y3(I))
      END DO
      CALL PGVPORT(0.5,0.7,0.5,0.9)
      CALL PGWNAD(XMIN,XMAX,YMIN,YMAX)
      DO I=1,N1
       CALL ARROW(X3(I),Y3(I),X4(I),Y4(I))
      END DO
```

```
C  Draw rotation
      CALL PGVPORT(0.1,0.3,0.1,0.5)
      CALL PGWNAD(XMIN,XMAX,YMIN,YMAX)
      DO I=1,N1
       CALL PIE(X1(I),Y1(I),R1(I),T1(I),T2(I),SCALE)
      END DO
      CALL PGVPORT(0.3,0.5,0.1,0.5)
      CALL PGWNAD(XMIN,XMAX,YMIN,YMAX)
      DO I=1,N1
       CALL PIE(X2(I),Y2(I),R2(I),T2(I),T3(I),SCALE)
      END DO
      CALL PGVPORT(0.5,0.7,0.1,0.5)
      CALL PGWNAD(XMIN,XMAX,YMIN,YMAX)
      DO I=1,N1
       CALL PIE(X3(I),Y3(I),R3(I),T3(I),T4(I),SCALE)
      END DO
      CALL PGEND
      END


C=======================================================================
C*ARROW
C+
      SUBROUTINE ARROW(X0,Y0,X1,Y1)
C
C  ARROW plots a vector from (x0,y0) to (x1,y1)
C--
C=======================================================================
      REAL X(3),Y(3)
      PARAMETER (ANG=0.44,TIP=0.2,ZMIN=0.1)
      Z=SQRT((X1-X0)**2+(Y1-Y0)**2)
      IF(Z<ZMIN) RETURN
      X(1)=X0
      Y(1)=Y0
      X(2)=X1
      Y(2)=Y1
      CALL PGLINE(2,X,Y)
      ALF=ATAN2(Y1-Y0,X1-X0)
      X(1)=X(2)-Z*COS(ALF-ANG)*TIP
      Y(1)=Y(2)-Z*SIN(ALF-ANG)*TIP
      X(3)=X(2)-Z*COS(ALF+ANG)*TIP
      Y(3)=Y(2)-Z*SIN(ALF+ANG)*TIP
      CALL PGLINE(3,X,Y)
      END


C=======================================================================
C*PIE
C+
      SUBROUTINE PIE(X0,Y0,R,T0,T1,S)
C
C  PIE plot a pie of radius R at (X0,Y0) starting from angle T0 to T1
C  with a scale S
C--
C=======================================================================
      PARAMETER (N=11)
      REAL X(N),Y(N)
      PI=ATAN(1.)*4.
      IF(ABS(T1-T0)<0.001) RETURN
      X(1)=X0
      Y(1)=Y0
      DT=S*(T1-T0)/FLOAT(N-2)
```

```
IF(S*ABS(T1-T0)>2.*PI)DT=2.*PI/FLOAT(N-2)
DO I=2,N-1
  T=T0+FLOAT(I-1)*DT
  X(I)=X(1)+R*COS(T)
  Y(I)=Y(1)+R*SIN(T)
END DO
X(N)=X(1)
Y(N)=Y(1)
CALL PGSFS(1)
CALL PGPOLY(N,X,Y)
END
```

```
C=============================================================
C   STRAIN plots strain field (Desrues' technique)
C
C   INPUT FILE: BALL_A.OUT
C=============================================================
      USE MSIMSL
      PARAMETER (M=2000)
      CHARACTER*256 LABEL
      REAL X1(M),Y1(M),R1(M),T1(M),X2(M),Y2(M),R2(M),T2(M),
     &     X3(M),Y3(M),R3(M),T3(M),X4(M),Y4(M),R4(M),T4(M)
      CHARACTER*80 NAME,DIR2,T

      SCALE=5.

C     Work directory
      WRITE(*,'(A,$)') ' Enter Test A or B: '
      READ(*,'(A)') T
      DIR2='F:\WORK\AFOSR\Processing\TEST'//TRIM(T)//'\Processed\'

C     Read center position and radius
      NAME=TRIM(DIR2)//'BALL_A.OUT'
      OPEN(1,FILE=NAME,STATUS='OLD')
      READ(1,*) N1
      READ(1,'(A)') LABEL
      DO I=1,N1
        READ(1,*) X1(I),Y1(I),R1(I),T1(I),X2(I),Y2(I),R2(I),T2(I),
     &          X3(I),Y3(I),R3(I),T3(I),X4(I),Y4(I),R4(I),T4(I)
      END DO
      CLOSE(1)

C     Plotting extrema
      XMIN=MINVAL(X1(1:N1))
      XMAX=MAXVAL(X1(1:N1))
      YMIN=MINVAL(Y1(1:N1))
      YMAX=MAXVAL(Y1(1:N1))
      W=ABS(XMIN-XMAX)
      H=ABS(YMIN-YMAX)
      XMIN=XMIN-0.05*W
      XMAX=XMAX+0.05*W
      YMIN=YMIN-0.05*H
      YMAX=YMAX+0.05*H

C     Plot shear strain at centers of grid
      NAME=TRIM(DIR2)//'Strain.gif/GIF'
      CALL PGBEGIN(0,NAME,1,1)
      CALL PGSCR(0, 1., 1., 1.)    !black becomes white
      CALL PGSCR(1, 0., 0., 0.)    !white becomes black
      CALL PGQVP(0,XP1,XP2,YP1,YP2)
      CALL PGVPORT(0.1,0.3,0.5,0.9)
      CALL PGWNAD(XMIN,XMAX,YMIN,YMAX)
      CALL STRAIN(X1,Y1,X2,Y2,N1,XMIN,XMAX,YMIN,YMAX)
      CALL PGVPORT(0.3,0.5,0.5,0.9)
      CALL PGWNAD(XMIN,XMAX,YMIN,YMAX)
      CALL STRAIN(X2,Y2,X3,Y3,N1,XMIN,XMAX,YMIN,YMAX)
      CALL PGVPORT(0.5,0.7,0.5,0.9)
      CALL PGWNAD(XMIN,XMAX,YMIN,YMAX)
      CALL STRAIN(X3,Y3,X4,Y4,N1,XMIN,XMAX,YMIN,YMAX)

C     Plot displacement vectors
      CALL PGVPORT(0.1,0.3,0.1,0.5)
      CALL PGWNAD(XMIN,XMAX,YMIN,YMAX)
      DO I=1,N1
```

```
      CALL ARROW(X1(I),Y1(I),X2(I),Y2(I))
     END DO
     CALL PGVPORT(0.3,0.5,0.1,0.5)
     CALL PGWNAD(XMIN,XMAX,YMIN,YMAX)
     DO I=1,N1
      CALL ARROW(X2(I),Y2(I),X3(I),Y3(I))
     END DO
     CALL PGVPORT(0.5,0.7,0.1,0.5)
     CALL PGWNAD(XMIN,XMAX,YMIN,YMAX)
     DO I=1,N1
      CALL ARROW(X3(I),Y3(I),X4(I),Y4(I))
     END DO
     CALL PGEND
     END


C=======================================================================
C*STRAIN
C+
     SUBROUTINE STRAIN(X1,Y1,X2,Y2,N1,XMIN,XMAX,YMIN,YMAX)

          REAL X1(N1),Y1(N1),X2(N1),Y2(N1),XMIN,XMAX,YMIN,YMAX
C
C  STRAIN plots a square symbol to represent shear strain
C--
C=======================================================================
     PARAMETER (NX=25,NY=50)
     REAL XL(2,4),VL(2,4),XG(NX),YG(NY),EPS(3)
     REAL DET,SHL(3,4),SHG(3,4),B(3,8)
     REAL,ALLOCATABLE:: XY(:,:),WX(:),WY(:),VX(:,:),VY(:,:),GAM(:,:)

C  Define local shape functions
     CALL QUAD_SHL(SHL)

C  Define grid points
     XXMAX=XMAX-0.1*(XMAX-XMIN)
     XXMIN=XMIN+0.1*(XMAX-XMIN)
     DO I=1,NX
      XG(I)=XXMIN+(XXMAX-XXMIN)*(I-1)/FLOAT(NX-1)
     END DO
     YYMAX=YMAX-0.1*(YMAX-YMIN)
     YYMIN=YMIN+0.1*(YMAX-YMIN)
     DO I=1,NY
      YG(I)=YYMIN+(YYMAX-YYMIN)*(I-1)/FLOAT(NY-1)
     END DO

C  Calculate displacement at grid points
      IF(ALLOCATED(XY)) DEALLOCATE(XY,WX,WY,VX,VY,GAM)
     ALLOCATE(XY(2,N1),WX(N1),WY(N1),VX(NX,NY),VY(NX,NY))
     ALLOCATE(GAM(NX-1,NY-1))
     XY(1,:)=X1(:N1)
     XY(2,:)=Y1(:N1)
     WX=X2(:N1)-X1(:N1)
     WY=Y2(:N1)-Y1(:N1)
     CALL SURF(N1,XY,WX,NX,NY,XG,YG,VX,NX)
     CALL SURF(N1,XY,WY,NX,NY,XG,YG,VY,NX)

C  Calculate strain at grid points
     DO I=1,NX-1
      DO J=1,NY-1
       XL(1,1)=XG(I)
       XL(1,2)=XG(I+1)
```

```
      XL(1,3)=XG(I+1)
      XL(1,4)=XG(I)
      XL(2,1)=YG(J)
      XL(2,2)=YG(J)
      XL(2,3)=YG(J+1)
      XL(2,4)=YG(J+1)
      CALL QUADSHG(XL,SHL,SHG,DET)
      B=0.
      B(1,1::2)=SHG(1,:)
      B(2,2::2)=SHG(2,:)
      B(3,1::2)=SHG(2,:)
      B(3,2::2)=SHG(1,:)
      VL(1,1)=VX(I,J)
      VL(1,2)=VX(I+1,J)
      VL(1,3)=VX(I+1,J)
      VL(1,4)=VX(I,J)
      VL(2,1)=VY(I,J)
      VL(2,2)=VY(I,J)
      VL(2,3)=VY(I,J+1)
      VL(2,4)=VY(I,J+1)
      EPS=MATMUL(B(:,:),RESHAPE(VL,(/8/)))
      GAM(I,J)=SQRT((EPS(1)-EPS(2))**2+EPS(3)**2)
     END DO
    END DO

C   Plot square symbol at center of grid
    SMAX=10.
    GMAX=MAXVAL(GAM)
    DO I=1,NX-1
     DO J=1,NY-1
      XX=(XG(I)+XG(I+1))/2.
      YY=(YG(J)+YG(J+1))/2.
      CALL PLOT_SQUARE(XX,YY,GAM(I,J),GMAX,SMAX)
     END DO
    END DO
    END


C=====================================================================================
    SUBROUTINE QUADSHG(XL,SHL,SHG,DET)

    REAL XL(2,4),DET,SHL(3,4),SHG(3,4)

C   QUADSHG calculates global derivatives of shape functions and
C   jacobian determinant for a four node quadrilateral element
C         XL(J,I)              global coordinate
C         DET                  jacobian determinant
C         SH(1,I)      local XI derivative of shape function
C         SH(2,I)      local ETA derivative of shape function
C         SH(3,I)      local shape function
C         SHG(1,I)x derivative of shape function
C         SHG(2,I)y derivative of shape function
C         SHG(3,I)shape function
C         I                    local node number or global coordinate number
C         J                    global coordinate number
C=====================================================================================
    REAL XS(2,2),TEMP
    SHG=SHL
    XS=MATMUL(SHG(1:2,:),TRANSPOSE(XL(1:2,:)))
    DET=XS(1,1)*XS(2,2)-XS(1,2)*XS(2,1)
    XS=XS/DET
    DET=4.*DET
```

```
      DO I=1,4
       TEMP=XS(2,2)*SHG(1,I)-XS(2,1)*SHG(2,I)
       SHG(2,I)=-XS(2,1)*SHG(1,I)+XS(1,1)*SHG(2,I)
       SHG(1,I)=TEMP
      END DO
      END

C=======================================================================
C*QUAD_SHL
C+
      SUBROUTINE QUAD_SHL(SHL)

      REAL SHL(3,4)

C  QUAD_SHL calculates shape functions and local derivatives for element QUAD
C         SHL(1,I) local XI derivative of shape function
C         SHL(2,I) local ETA derivative of shape function
C         SHL(3,I) local shape function
C         I                       local node number
C---
C=======================================================================
      REAL RG(4),SG(4)
      DATA RG/-0.5, 0.5,0.5,-0.5/
      DATA SG/-0.5,-0.5,0.5, 0.5/
      DO I=1,4
       SHL(1,I)=0.5*RG(I)
       SHL(2,I)=0.5*SG(I)
       SHL(3,I)=0.25
      END DO
      END


C=======================================================================
C*PLOT_SQUARE
C+
      SUBROUTINE PLOT_SQUARE(X,Y,V,VMAX,SMAX)

C  PLOT_SQUARE plots a square at position (X,Y) proportional to V
C
C  Input
C    X,Y     location where to center square
C    V       value
C    VMAX    maximimum value corresponding to maximum size SMAX
C    SMAX    maximum size for square
C
C---
C=======================================================================
      REAL XR(5),YR(5)
C  define square
      D=V/VMAX*SMAX
      XR(1)=X-D/2.
      YR(1)=Y-D/2.
      XR(2)=XR(1)+D
      YR(2)=YR(1)
      XR(3)=XR(2)
      YR(3)=YR(2)+D
      XR(4)=XR(3)-D
      YR(4)=YR(3)
      XR(5)=XR(1)
      YR(5)=YR(1)
C  full for V>0, hollow for V<0
```

```
      CALL PGSCI(1)
      CALL PGSFS(2)
      CALL PGPOLY(5,XR,YR)
      RETURN
      END


C=======================================================================
C*ARROW
C+
      SUBROUTINE ARROW(X0,Y0,X1,Y1)
C
C  ARROW plots a vector from (x0,y0) to (x1,y1)
C--
C=======================================================================
     REAL X(3),Y(3)
      PARAMETER (ANG=0.44,TIP=0.2,ZMIN=0.1)
      Z=SQRT((X1-X0)**2+(Y1-Y0)**2)
      IF(Z<ZMIN) RETURN
      X(1)=X0
      Y(1)=Y0
      X(2)=X1
      Y(2)=Y1
      CALL PGLINE(2,X,Y)
      ALF=ATAN2(Y1-Y0,X1-X0)
      X(1)=X(2)-Z*COS(ALF-ANG)*TIP
      Y(1)=Y(2)-Z*SIN(ALF-ANG)*TIP
      X(3)=X(2)-Z*COS(ALF+ANG)*TIP
      Y(3)=Y(2)-Z*SIN(ALF+ANG)*TIP
      CALL PGLINE(3,X,Y)
      END
```

ACKNOWLEDGMENT

This document reports on the research sponsored by the AFOSR grant (F49620–93–1–0295) augmented by the AASERT extension (F49620–95–1–0420). This work has been partially supported by the Air Force Office of Scientific Research, the National Science Foundation, and by the ALERT program of the European Community. The AFOSR grant (F49620–93–1–0295) was augmented by an AASERT grant (F49620–95–1–0420) to support Julie Young, who subsequently to this award was granted a NSF fellowship in 1998. The authors are thankful to I. Vardoulakis of the National Technical University of Athens, Greece, and J. Desrues and D. Caillerie of the University Joseph Fourier of Grenoble, France, for valuable comments. The authors also thanks Dr. Nakase of the EPRI, Japan, for making available its discrete materials.

TABLE OF CONTENTS

INTRODUCTION

Among engineering materials, granular materials experience the most complicated and diversified types of instabilities, owing to their particulate and multiphase structures. These instabilities include surface instability (e.g., rockburst and exfoliation), volume instability (e.g., buckling and arching), localized instability (e.g., shear bands), and fluid-grain interaction instability (e.g., liquefaction). These various types of instability have been observed in the field, in association with global and/or local failures of geomaterials. They have been reproduced and studied in the laboratory, and analyzed by using continuum mechanics. However, the physical origins of instabilities in geomaterials are still poorly understood.

The present research is focused on shear band instability in granular media, and especially on the physical origins of these instabilities. In the following review of past work, we intend to show that past continuum theories are based on diverse assumptions, and rely on semi-intuitive arguments not necessarily founded on physical observations.

Shear band instability

Most constitutive models for geomaterials describe their mechanical behavior through stress-strain relationships, which have no internal characteristic length specific to materials. This macro-description postulates that the responses of small laboratory specimens are the scaled responses of larger granular masses in the field. In the absence of instability, macro-continuum mechanics has been successfully used to calculate stresses and strains in solids. It has also been successful to explain some aspects of the unstable behavior of geomaterials, such as surface and volume instability (Hill and Hutchinson, 1974; Vardoulakis, 1979, 1981, and 1988; Vardoulakis and Graf, 1985; Bardet, 1991) and the inclination of shear bands (Rudnicki and Rice, 1975; Rice, 1976; Vardoulakis, 1980; Bardet, 1991). However, without an internal length, macro- theories simply fail to describe the thickness of shear bands, which was found to be about eight times the mean grain size in granular materials (e.g., Mühlhaus and Vardoulakis, 1987). The thickness of shear bands is an internal length that does not scale with the specimen

size. When a continuum theory ignores this internal length, the numerical solution of boundary value problems leads to strain-softening response and localized deformation that strongly depend on mesh sizes (e.g., de Borst and Sluys, 1992).

Four alternate types of continuum theory with an internal length have been proposed to describe shear band instability in geomaterials. These approaches are: 1) higher order strain gradient theory, 2) micropolar theory, 3) nonlocal theory, and 4) viscous regularization.

Higher order strain gradient approach

Zbib and Aifantis (1989) introduced higher order strain gradients into continuum models to ascribe an internal length to materials and to capture the thickness of shears bands. Zbib and Aifantis (1988) derived analytical solutions for the post-bifurcation structures of shear bands, which are in agreement with experimental observations on metals. Vardoulakis and Aifantis (1989) investigated the effects of gradient dependent dilatancy on shear bands and liquefaction instabilities within saturated sands. Their assumption of gradient dependent dilatancy invokes basic microscopic considerations for two-dimensional materials. Their theory produces the thickness of shear bands, and creates liquefying strips in saturated sand specimens. However, in their dilatancy relationship, they replaced a factor 1/2 by an "unspecified dimensionless coefficient to be determined from experiment." They did not clearly explain the physical origins of gradient dependent dilatancy and liquefaction patterns either.

The gradient effects on yield and plastic potential surfaces are difficult to exhibit and calibrate by experiments on geomaterials. Oka et al. (1991) applied the higher order gradient approach to clays. Oka calibrated the coefficients of higher order effects by trial and error to produce the desirable shear band thickness. There is a definite need for developing a approach for investigating the physical justification of higher order gradients in particulate media.

Micropolar approach

The micropolar theory (Eringen, 1966, 1968) is a continuum version of the structural theory of Cosserat (1909). It enriches the kinematics and kinetics of continua by adding material rotations and couple stresses. Using a micropolar approach similar to Kanatani (1979), Mühlhaus and Vardoulakis (1986) explained the emergence, orientation and thickness of shear bands in granular materials. Bardet and Proubet (1992a) used a similar linear stability analysis and micropolar description, and investigated the structure of persistent shear bands in idealized granular media. They successfully described the thickness of shear bands and the relation between particle rotation and displacement within persistent shear bands. However, the coefficients of their micropolar models, based on the flow or deformation theory of plasticity, had to be set to unrealistic values to reproduce the observations.

Chang et al. (1990, 1991, 1992) developed micropolar theories for granular materials based on microscopic models. They derived the micropolar constants in terms of the inter-particle stiffness, and investigated the micropolar effects on the solution of selected boundary value problems. Chang derived stress-strain relationships without examining their effects on material instability. He did not investigate the problem of strain localization as De Borst and Sluys (1992).

Dietsche et al (1991) examined the micropolar effects on bifurcation, without justifying the physical origins of their continuum assumptions. Their study assesses only the micropolar effects on the uniqueness of boundary value problems.

Like the higher order gradient theory, the micropolar theory introduces an internal length in boundary value problems. However, there is still need for establishing the physical relevance of the micropolar theory for the instability in particulate media.

Nonlocal continuum approach

Nonlocal continuum mechanics (Bazant, 1991 and 1992; Eringen, 1992; Valanis, 1992) is especially suited for investigating material instability and strain softening. Nonlocal continuum mechanics replaces the local stress by an average stress, which is the integral

of the weighted local stress over a material volume. Nonlocal models possess an internal length that relates to the thickness of shear bands (Bazant and Pijaudier-Cabot, 1988). Nonlocal models have been especially designed to assess damage in brittle materials (e.g., concrete) with cohesive granular bonds (Ju, 1991). Recently, Bazant (1992) introduced a new concept of nonlocal damage based on the micromechanics of crack interaction, and therefore established the physics for the spatial averaging integral and weight function employed in nonlocal models. However, the concept of crack interaction and propagation does not apply to a random packing of particulate media with cohesionless contacts. The damage concept seems more applicable to cemented or overconsolidated soils, for which cohesive bonds can be damaged and broken. However, the damage concept appeals for describing the strain softening of dense sands, which is attributed to stress-dilatancy.

Viscous regularization

The dissipative properties of physical viscosity introduce an internal length, which relates to the thickness of shear bands in metals under dynamic loads (e.g., Perzyna, 1991). Artificial viscosity, referred to as viscous regularization, was first introduced for capturing shock waves (Lapidus, 1967). Loret and Prevost (1990) adapted it for geomaterials to capture the thickness of shear bands. However, the viscosity measured for granular materials in the laboratory is much smaller than the artificial viscosity required for capturing the thickness of shear bands. The diffusion of pore-water generates viscous effects (Bardet, 1992) that are also too small for explaining shear bands. The introduction of artificial viscosity in geomaterials seems to be a numerical expedient deprived of physical justification. This numerical artifice requires an excessively large artificial viscosity which unrealistically attenuates waves and accelerations within boundary value problems.

The continuum theories - higher order gradient theory, micropolar theory, nonlocal theory, and viscous regularization - agree on the necessity of introducing an internal length. They justify their assumptions by the need to limit localization in the numerical solution of boundary value problems. Their diverse assumptions rely on semi-intuitive arguments not necessarily founded on microscopic observations for particulate media.